

Hydrate occurrence in Europe: a review of available evidence

Timothy A. Minshull^{a*}, Hector Marín-Moreno^b, Peter Betlem^c, Joerg Bialas^d, Stefan Buenz^e, Ewa Burwicz^d, Alejandra L. Cameselle^{f, r}, Gunay Cifci^g, Michela Giustiniani^h, Jess I. T. Hillmanⁱ, Sebastian Hölz^d, John R. Hopper^j, Gabriel Ion^k, Ricardo León^l, Vitor Magalhaes^m, Yizhaq Makovskyⁿ, Maria-Pilar Mata^l, Michael D. Max^o, Ilia Ostrovsky^p, Tove Nielsen^j, Seda Okay^g, Nick O'Neill^q, Luis M. Pinheiro^f, Andreia A. Plaza-Faverola^e, Daniel Rey^r, Srikumar Roy^s, Katrin Schwalenberg^t, Kim Senger^c, Sunil Vadakkepuliambatta^e, Atanas Vasilev^u and Juan-Tomás Vázquez^v

^a School of Ocean and Earth Science, National Oceanography Centre Southampton, University of Southampton, European Way, Southampton SO14 3ZH, UK; tmin@noc.soton.ac.uk

^b National Oceanography Centre, European Way, Southampton SO14 3ZH, UK; hector.marin.moreno@noc.ac.uk

^c Department of Arctic Geology, The University Centre in Svalbard, P.O. Box 156, 9171 Longyearbyen, Norway; Peter.Betlem@unis.no; Kim.Senger@unis.no

^d Geomar Helmholtz Centre for Ocean Research Kiel, Marine Geodynamics, 24148 Kiel, Germany; jbialas@geomar.de; eburwicz@geomar.de; shoelz@geomar.de

^e CAGE-Center for Arctic Gas Hydrate, Environment and Climate, Department of Geosciences, UiT-The Arctic University of Norway, 9037 Tromsø, Norway; stefan.buenz@uit.no;

andreaia.a.faverola@uit.no; sunil.vadakkepuliambatta@uit.no

^f University of Aveiro, Geosciences Department and CESAM, Campus Santiago, 3810-193 Aveiro, Portugal; lmp@ua.pt

^g Institute of Marine Sciences and Technology, Dokuz Eylul University, Inciralti, Izmir, Turkey; Gunay.cifci@deu.edu.tr

^h National Institute of Oceanography and Applied Geophysics, 1-34010 Sgonico, Italy; mgiustiniani@inogs.it

ⁱ GNS Science, 1, Fairway Drive, Avalon 5010, New Zealand; j.hillman@gns.cri.nz

^j Geological Survey of Denmark and Greenland, Department of Geophysics, DK-1350 Copenhagen, Denmark; jrh@geus.dk; tni@geus.dk;

^k National Institute of Marine Geology and Geoecology, RO-024053 Bucharest, Romania; gion@geoecomar.ro

^l Geological Survey of Spain, C/Rios Rosas 23, Madrid 28003, Spain; r.leon@igme.es; p.mata@igme.es

^m Portuguese Institute for Sea and Atmosphere, Marine Geology and Georesources Division, Rua C Aeroporto, P-1749077 Lisbon, Portugal; vitor.magalhaes@ipma.pt

ⁿ Dr Moses Strauss Department of Marine Geosciences, Leon H. Charney School of Marine Sciences, University of Haifa, Haifa, Israel; yizhaq@univ.haifa.ac.il

^o MaxSystems LLC, Washington D.C., USA; michael.max@icrag-centre.org

^p Israel Oceanographic and Limnological Research, Kinneret Limnological Laboratory, P. O. Box 447, Migdal 1495001, Israel; ostrovsky@ocean.org.il

^q Irish Shelf Petroleum Studies Group (ISPSG), PIP Secretariat, 7 Dundrum Business Park, Windy Arbour, Dublin 14 N2Y7, Ireland; noneill@pip.ie

^r Department of Marine Geosciences and Territorial Planning, University of Vigo, CP.36.310 Vigo (Pontevedra), Spain; danirey@uvigo.es; acamaselle@uvigo.es

^s Irish Centre for Research in Applied Geosciences, School of Earth Sciences, University College Dublin, Belfield, Dublin 4, Ireland; srikumar.roy@icrag-centre.org

48 t Federal Institute for Geosciences and Natural Resources, Hannover, Germany;
49 katrin.schwalenberg@bgr.de
50 u Institute of Oceanology, Varna, Bulgaria; gasberg@mail.bg
51 v Spanish Institute of Oceanography, Spain; juantomas.vazquez@ieo.es
52
53 * Corresponding author
54
55 Declarations of interest: none

56 **Abstract**

57 Large national programs in the United States and several Asian countries have defined and characterised
58 their marine methane hydrate occurrences in some detail, but European hydrate occurrence has received
59 less attention. The European Union-funded project “Marine gas hydrate – an indigenous resource of
60 natural gas for Europe” (MIGRATE) aimed to determine the European potential inventory of
61 exploitable gas hydrate, to assess current technologies for their production, and to evaluate the
62 associated risks. We present a synthesis of results from a MIGRATE working group that focused on
63 the definition and assessment of hydrate in Europe. Our review includes the western and eastern margins
64 of Greenland, the Barents Sea and onshore and offshore Svalbard, the Atlantic margin of Europe,
65 extending south to the northwestern margin of Morocco, the Mediterranean Sea, the Sea of Marmara,
66 and the western and southern margins of the Black Sea. We have not attempted to cover the high Arctic,
67 the Russian, Ukrainian and Georgian sectors of the Black Sea, or overseas territories of European
68 nations. Following a formalised process, we defined a range of indicators of hydrate presence based on
69 geophysical, geochemical and geological data. Our study was framed by the constraint of the hydrate
70 stability field in European seas. Direct hydrate indicators included sampling of hydrate; the presence of
71 bottom simulating reflectors in seismic reflection profiles; gas seepage into the ocean; and chlorinity
72 anomalies in sediment cores. Indirect indicators included geophysical survey evidence for seismic
73 velocity and/or resistivity anomalies, seismic reflectivity anomalies or subsurface gas escape structures;
74 various seabed features associated with gas escape, and the presence of an underlying conventional
75 petroleum system. We used these indicators to develop a database of hydrate occurrence across Europe.
76 We identified a series of regions where there is substantial evidence for hydrate occurrence (some areas
77 offshore Greenland, offshore west Svalbard, the Barents Sea, the mid-Norwegian margin, the Gulf of
78 Cadiz, parts of the eastern Mediterranean, the Sea of Marmara and the Black Sea) and regions where
79 the evidence is more tenuous (other areas offshore Greenland and of the eastern Mediterranean, onshore
80 Svalbard, offshore Ireland and offshore northwest Iberia). We provide an overview of the evidence for
81 hydrate occurrence in each of these regions. We conclude that around Europe, areas with strong
82 evidence for the presence of hydrate commonly coincide with conventional thermogenic hydrocarbon
83 provinces.

84

85 *Keywords:* methane hydrate; Europe

86

87 **1. Introduction**

88 Gas hydrate is an ice-like, crystalline solid comprising a hydrogen-bonded water lattice with trapped
89 gas molecules that is stable at high pressures and low temperatures (e.g., Sloan and Koh, 2008). In
90 nature the most common hydrate-forming gas is methane. Methane hydrate is widespread in seafloor
91 sediments and as such may provide a useful energy resource. Because, for equivalent energy production,
92 burning methane generates significantly less greenhouse gases than burning coal, the energy mix

93 required to satisfy the target of keeping the average global temperature rise below 2°C during the 21st
94 century may involve substantial gas production, including from undiscovered sources (e.g., McGlade
95 and Ekins, 2015). Methane hydrate could be one such source, providing a transition fuel to a low-carbon
96 energy system that compliments intermittent renewable energy generation and supports energy security.
97 Hydrate-bearing sands have been identified as a key target for production (Boswell and Collett, 2011).
98 Hydrate is also of interest because hydrate dissociation might be triggered by global ocean warming,
99 potentially leading to further greenhouse warming (e.g., Archer et al., 2009; Ruppel and Kessler, 2017),
100 and because of their role as a potential geohazard for offshore operations and infrastructure.

101

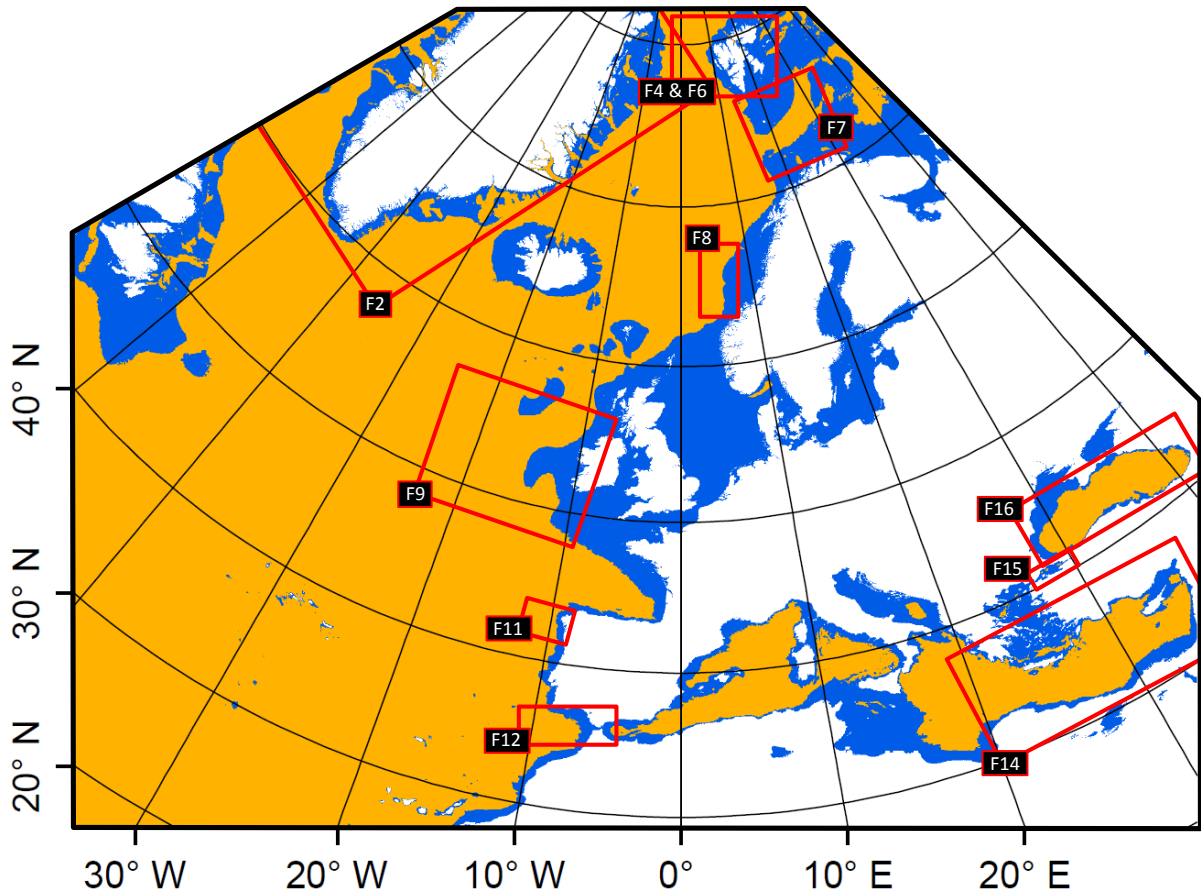
102 Driven by high demand for energy and limited conventional hydrocarbon resources, several nations,
103 including the USA, Japan, China, Korea and India, have developed large national hydrate research and
104 exploration programmes (e.g., Gabitto, 2010; Oyama and Masutani, 2017; Song et al., 2014). In Europe,
105 however, there has been less investment in hydrate research. Gas demand declined in Europe during the
106 first half of this decade, but is likely to show a modest increase in the next decade, despite increasing
107 development of renewables (Honoré, 2014). Thus there is a continuing need to better understand hydrate
108 potential in Europe, and the original motivation for this study was to provide a foundation for future
109 hydrate exploration in Europe. However, for many European nations, imported shale gas is now seen
110 as a more cost-efficient route to supplement conventional gas supplies, and hydrate exploration is not
111 seen as a priority. Therefore our study has expanded beyond a focus on hydrate in sands, to cover all
112 forms of hydrate occurrence around Europe and some adjacent areas. Our goal is to review the current
113 state of knowledge of hydrate occurrence within this area.

114

115 Our study is framed by the offshore stability field for pure methane hydrate in seawater around Europe,
116 estimated from global databases (Fig. 1). The region of stability is most poorly constrained offshore
117 Greenland, where few constraints are available on the geothermal gradient, but is likely to include many
118 of the deeper fjords. The limit of stability lies at varying distances from the coast on the northwest
119 European margin, and hydrate is stable in parts of the Barents Sea and a small part of the Skagerrak.
120 Hydrate is stable in large areas of the western and eastern Mediterranean basins, the Tyrrhenian Sea
121 and the Black Sea, and in small areas of the Adriatic and Aegean Seas and the Sea of Marmara. Hydrate
122 also can be stable beneath permafrost and beneath ice sheets. These settings require more complex
123 hydrate stability calculations that depend on often poorly known parameters. Therefore we have not
124 attempted to carry out such calculations for the whole of our study area. However, in section 4 below
125 we discuss the possibility of hydrate stability beneath permafrost and ice caps onshore Svalbard.

126

127 We first describe the methods that we used to identify areas where the presence of hydrate was
128 indicated. Then we describe in a series of sections the evidence for hydrate occurrence within these
129 areas. Finally we synthesise the available evidence on hydrate occurrence in Europe.



130

131 Figure 1: Pure methane hydrate stability zone around Europe (orange area). Blue marks offshore areas
 132 where pure methane hydrate is not stable, but other forms of hydrate may be stable. The limit of
 133 stability is estimated using the 30 arc-second bathymetry grid from the General Bathymetric Chart of
 134 the Oceans, GEBCO (https://www.gebco.net/data_and_products/gridded_bathymetry_data/), the
 135 0.25° seabed temperature grid from the National Oceanic and Atmospheric Administration, NOAA
 136 (<https://www.nodc.noaa.gov/cgi-bin/OC5/SELECT/woaselect.pl>), a salinity of 3.5% wt, and the
 137 Moridis (2003) phase boundary for Structure I hydrate. Seabed temperature data were interpolated to
 138 match the resolution of the bathymetric grid. Red boxes mark the areas shown in other figures.
 139

140 **2. Methods**

141 To frame our study, we developed a list of hydrate indicators and a workflow for scientific exploration
 142 of marine hydrate; our workflow is adapted from the hydrate petroleum system approach of Max and
 143 Johnson (2014). For a detailed hydrate assessment from an energy resource perspective, readers are
 144 referred to Boswell et al. (2016), and for a complete review on the hydrate systems concept we refer to
 145 Collett et al. (2009).

146

147 2.1 Hydrate indicators

148 We define hydrate indicators as geological, geophysical and geochemical observations that either
 149 provide strong evidence to confirm the current presence of hydrate, or simply suggest that hydrate might
 150 be present. We considered two categories of hydrate indicators, based on their confidence in confirming
 151 the hydrate presence: (i) direct indicators and (ii) indirect indicators. Direct indicators include sampling

152 of hydrate, and observations of hydrate bottom simulating reflectors (BSRs), gas seepage and pore
153 water chlorinity anomalies. Indirect indicators include gas chimneys, anomalies in seismic velocity and
154 electrical resistivity, zones of anomalous reflectivity, the presence of a conventional petroleum
155 province, and various seabed features (cold seeps without gas, backscatter anomalies, mud volcanoes,
156 pockmarks and pingos). Except for the sampling of hydrate, all the other indicators are not only found
157 in hydrate systems and should be considered as hydrate indicators only if they are inferred within or
158 close to the hydrate stability zone (HSZ). In marine settings, the HSZ is the region with appropriate
159 sub-seafloor pressure and temperature conditions to form hydrate. Its thickness is given by the distance
160 between the seabed and the intersection of the thermal structure (obtained using the seabed temperature
161 and geothermal gradient) with a hydrate phase boundary (e.g., Marín-Moreno et al., 2016).

162

163 A hydrate BSR is a seismic reflector with opposite polarity to the seafloor that generally mimics the
164 seafloor at a depth consistent with the expected base of the HSZ. The presence of a continuous BSR
165 may be an indication of dispersed gas being present in pore water below it rather than being an indicator
166 of the presence of significant hydrate above (e.g., Max and Johnson, 2014). Also, other geological
167 phenomena can create BSRs at different depths (e.g., Berndt et al., 2004). Nevertheless, the presence
168 of a hydrate BSR allows us to constrain the extent of the HSZ (Boswell et al., 2016) and likely requires
169 the presence of at least some hydrate, so we consider it as a direct indicator for hydrate. Hydrate
170 accumulations often have been identified without associated BSRs, for example in the Gulf of Mexico
171 (Majumdar et al., 2016).

172

173 Pore water chlorinity anomalies can arise from dissociation of hydrate during the ascent of a core from
174 the seabed to the surface vessel. Gas seeps from the seabed within the HSZ indicate that pore waters
175 are saturated with gas and therefore hydrate is very likely to be present. Gas escape structures such as
176 pipes and chimneys may be imaged in seismic reflection data and may indicate the presence of hydrate-
177 forming gas within the HSZ. The presence of hydrate increases seismic velocities and electrical
178 resistivities, while the presence of gas decreases seismic velocities but also increases electrical
179 resistivities. High seismic reflectivity (“bright spots”) can result from the presence of subsurface gas,
180 while seismic “blanking”, involving loss of coherent reflectivity, can result from the presence of gas or
181 of chaotic fluid escape structures. Conventional petroleum provinces can provide a source of
182 thermogenic gas entering the HSZ, while the various seabed features listed above provide possible
183 evidence for past or present gas escape through the seabed.

184

185 2.2 Hydrate exploration workflow

186 We developed a hydrate scientific exploration workflow consisting of four clearly defined steps:

187

1. Determining the likelihood of hydrate stability.

188 2. Imposing better constraints on the likelihood of hydrate presence considering relevant recent
189 geological, physical and chemical changes.

190 3. Hydrate petroleum system analysis.

191 4. Prospect identification and scientific drilling.

192 The first step is to determine the likelihood of hydrate thermodynamic stability under steady state
193 conditions, i.e., to calculate the HSZ. For this calculation, the bathymetry, seabed temperature, pore
194 water salinity, hydrate forming gases, and geothermal gradient or heat flow need to be known or
195 assumed. In general, sufficient bathymetric data exist or can be easily acquired, but seabed temperature
196 and/or geothermal gradient/heat flow data are generally sparse, and sometimes non-existent. Therefore
197 interpolation/extrapolation techniques need to be employed, with caution to avoid creation of artefacts.
198 In marine environments, the first estimate of the HSZ is commonly made by assuming a salinity of
199 3.5% and that the hydrate-forming gas is 100% methane.

200

201 The second step involves constraining the likelihood of hydrate presence by assessing existing
202 geological, geophysical and geochemical data. This step also considers the temporal variability of the
203 system and includes: (i) the identification of BSR(s) and their character (continuous or discontinuous)
204 in existing seismic data; (ii) assessment of the sediment thickness that may contain hydrate, based on
205 the identification of source beds and quantification of total organic carbon; (iii) re-assessment of the
206 hydrate-forming gas and its saturation based on possible thermogenic sources; (iv) re-calculation of the
207 HSZ using better constraints on the hydrate-forming gas and any time-dependent parameters affecting
208 the volume of the HSZ, including the influence of geologically recent oceanographic, seabed and
209 tectonic changes on seabed pressure and temperature, geothermal gradient and salinity.

210

211 The third step involves developing a hydrate system analysis, beginning with identifying what
212 additional data need to be acquired. This step might involve the following surveys: (i) a regional 2D
213 seismic survey to study the large scale structure of the geological system and identify BSRs (e.g., Lee
214 et al., 2005); (ii) an ocean bottom seismometer (OBS) survey and/or a 2D long streamer seismic survey
215 to derive information on seismic-wave velocity, porosity, and hydrate and gas saturation (e.g.,
216 Westbrook et al., 2008); (iii) a high resolution local 2D/3D seismic survey to clearly identify direct
217 indicators of hydrate and/or potential clues (e.g., Riedel et al., 2002); (iv) a controlled source
218 electromagnetic survey (CSEM) to impose better constraints in porosity contrasts and pore phase
219 saturations (e.g., Weitemeyer et al., 2006); (v) less well established exploration techniques such as heat
220 flow-based methods for additional information and/or for independent validation of the seismic and
221 electromagnetic observations. Such surveys might lead to a more formal analysis for gas hydrate
222 identification and saturation estimation (e.g., Dai et al., 2008). A joint interpretation approach can be
223 applied to the different geophysical datasets (e.g., Goswami et al., 2015), and focus the interpretation
224 on identifying the depositional environments within and immediately beneath the HSZ, gas sources,

225 and depocentres for sand, turbidite and mass transport deposits, and on assessing the morphology of the
226 sand deposits. At this stage, there are enough data to estimate the approximate volume of methane that
227 might be recoverable from hydrate using average hydrate saturations, and the dominant hydrate
228 distribution and morphology.

229

230 The fourth step, prospect identification, brings the detailed information needed to make an informed
231 decision about scientific drilling targets. This step includes a detailed analysis of seismic and CSEM
232 data to identify features such as sweet spots or structures with enhanced fluid flow, or elevated
233 resistivities or seismic velocities. Such analysis may be followed by rock physics and geotechnical
234 laboratory experiments to determine the elastic (e.g., Priest et al., 2005), electrical (e.g., Spangenberg
235 and Kulenkampff, 2006) and thermo-hydro-mechanical (e.g., Santamarina et al., 2015) properties of
236 hydrate-bearing samples. These properties are then used to calibrate rock physics and geotechnical
237 models (e.g., Marín-Moreno et al., 2017; Uchida et al., 2012) that provide a quantitative understanding
238 of the above properties, of the likely response of the target natural hydrate bearing deposits to natural
239 and/or anthropogenic perturbations, and of local relationships between relevant properties such as
240 porosity and permeability. Then potential drilling targets can be chosen and a geohazard assessment
241 performed for each target to help to decide which, if any, should be prioritized. Finally, scientific
242 drilling should take place to evaluate more fully the prospectivity of the area.

243

244 Below we cover in a series of regional sections the areas where there is evidence for the presence of
245 hydrate. Some large sections of the eastern Atlantic margin have been extensively sampled using both
246 seismic and acoustic techniques, as well as direct sampling. However, to date there are no published
247 reports of hydrate BSRs, gas seeps, chlorinity anomalies or other significant hydrate indicators within
248 or in close proximity to the HSZ. Examples include the northwest margin of the UK and the Bay of
249 Biscay; in both areas, gas seeps have been detected at shelf depths (e.g., Judd et al., 1997; Ruffine et
250 al., 2017) but not in regions of hydrate stability. In most of the areas described below, only the first step
251 and some aspects of the second step have been conducted (Table 1). To date, scientific drilling for
252 hydrate in Europe has been limited to the west Svalbard margin and the western Black Sea, though
253 hydrate has been encountered several times during drilling for other purposes.

254 Table 1: Summary of the most relevant hydrate-related information for all the regions described in the
 255 text. ODP = Ocean Drilling Program; MV = mud volcano; see text for definitions of indicators.

Region	Location	Data	Direct hydrate indicator	Indirect hydrate indicator	Occurrence and host sediment	Gas source and migration path	Hydrate extent and amount
Offshore Greenland	Northeast	ODP 909; 2D seismic; heat flow; seabed temperature	Possible BSR	Gassy sediment sampling; bright spots; chimneys	No hydrate recovered	No information available	Not estimated
	West	Gravity core; 2D & 3D seismic; heat flow; seabed temperature	BSRs	Seismic blanking; oil and gas shows; Ikaite crystals; fluid/gas escape structures; pockmarks	No hydrate recovered	Thermogenic gas; migration through faults and fractures	Not estimated
Offshore Svalbard	Vestnesa Ridge and slope	2D & 3D seismic; OBS; CSEM; cores; MeBo drilling; seafloor imaging; HSZ modelling	Hydrate sampled; gas seeps; BSR	Chimneys; pockmarks; seismic blanking	Topographically & structurally controlled; Small, thin chips, in veins or as chunks in the upper 2-4 m of fine-grained hemipelagic sediments	Dominant thermogenic; thermogenic input increases with depth; thermogenic gas migration through faults	700 km ³ extent of HSZ at ~800-2000 mbsl; saturation from Vp 6-18%; from CSEM 20-30% and 40-68% in chimneys
	Prinz Karl Forland	2D seismic; OBS; CSEM; cores; MeBo drilling; seafloor imaging; HSZ modeling	Hydrate sampled; gas seeps; patchy BSR	Chimneys; bright spots	Hydrate recovered from one pockmark	Microbial with significant thermogenic contribution	Not estimated
	Elsewhere West	2D & 3D seismic; cores; HSZ modelling	Gas seeps; BSRs	Bright spots; gas chimneys	No hydrate recovered	Abiotic gas inferred in the South Molloy Transform Fault & West Knipovich Ridge region	Not estimated
Onshore Svalbard		HSZ modelling; scientific and industry drilling; 2D seismic	None	Hydrate stability; hydrate found offshore; fluid escape structures; gas seeps	Fractured sandstones and shales; coal beds	Partly thermogenic; migration via fractures and seeps	Not estimated
Norwegian Margin	Barents Sea	2D seismic; cores; HSZ modelling	Hydrate sampled; gas seeps; BSRs	Bright spots; chimneys; pockmarks	Structurally controlled; BSRs in consolidated low-porosity sediments and glacial sediments	Mostly thermogenic gas; migration through faults and fractures	Volume 0.19 GSm ³ in Bjornoya Basin; 93-650 GSm ³ in SW Barents Sea or 470-3320 GSm ³ if higher hydrocarbons
	Mid-Norwegian Margin	Core sampling; 2D seismic; OBS; Multi-component seismic; CSEM; HSZ modelling	Hydrate sampled; BSRs	Fluid escape structures; pockmarks	Finely bedded contourite and hemipelagic deposits – mainly silty clays	Microbial with thermogenic component	4000 km ² BSR along N flank of Storegga Slide; saturation 2-10%; volume of 625 GSm ³

256

257 Table 1: Continuation

Region	Location	Data	Direct hydrate indicator	Indirect hydrate indicator	Occurrence and host sediment	Gas source and migration path	Hydrate extent and amount
Offshore Ireland	Rockall and Porcupine Basins	Scientific & industry drilling; 2D & 3D seismic; HSZ modelling	Possible BSRs	Hydrocarbon seeps; fluid escape structures; bright spots	No hydrate recovered	Thermogenic gas migration through faults above active petroleum systems	Not estimated
NW Iberian Margin		Cores; 2D seismic; HSZ modelling	None	Pockmarks; fluid/gas escape structures; seismic blanking; bright spots; chimneys	No hydrate recovered	Not known	Not estimated
Offshore South Iberia & NW Africa Margin	Gulf of Cadiz	Cores; 2D seismic	Hydrate sampled; chlorinity anomalies; BSRs	MV; gas chimneys; pockmarks; degassing structures; seismic blanking; backscatter anomalies	Hydrate found in MV; localised deposits and hosted in fine-grained sediments with low permeability	Thermogenic gas migration through focused fluid flow; abiogenic crustal-derived fluids	Saturation of 5-31% in cores
	Alborán Sea	Cores	Chlorinity anomalies	Gas release from cores	No hydrate recovered	Thermogenic gas from ~5 km depth	Not estimated
	Anaximander Seamount	Cores; HSZ modelling	Hydrate sampled; chlorinity anomalies; gas seeps	MV; pockmarks	Hydrate found in MV	Thermogenic	mm to cm scale disseminated H; saturation of 0.7-16.7%
Eastern Mediterranean	Olimpi Field	Cores	Hydrate sampled; chlorinity anomalies; gas seeps	MV; pockmarks	Hydrate found in MV	Mainly thermogenic	c. 5 GSm ³ in Milano dome
	Nile fan and Levant Basin	2D & 3D seismic; seafloor video	Possible BSR; gas seeps	Pockmarks, bright spots, seismic blanking	Sandy buried systems	Mostly microbial; thermogenic at MV	Estimated c. 100 Tcf in the Levant Basin
Sea of Marmara		Cores; 2D & 3D seismic	Hydrate sampled; gas seeps	MV; bright spots; gas chimneys; pockmarks	Thermogenic	Thermogenic G migration from deep Oligocene-Eocene reservoirs	Not estimated

258
259
260
261

262 Table 1: Continuation

Region	Location	Data	Direct hydrate indicator	Indirect hydrate indicator	Occurrence and host sediment	Gas source and migration path	Hydrate extent and amount
Western Black Sea	Bulgaria & Rumania	Cores; 2D & 3D seismic; OBS; CSEM; HSZ modelling	Hydrate sampled; gas seeps; BSRs	Seismic blanking; gas pipes and chimneys; high resistivity values	H formed in levees or base of channels	Microbial	Saturation from CSEM of 30% and from OBS of 10% or 30-40%.
	İğneada	2D seismic, cores	Hydrate sampled; BSRs	Seismic blanking; bright spots; gas chimneys; possible MV	Hydrate fragments in possible MV	Migration via faults and possible MV	Not estimated
	Zonguldak-Amasra	Cores; 2D seismic; HSZ modelling	BSRs	Seismic blanking; MV; gas chimneys	Not known	Thermogenic and microbial	Not estimated
Eastern Black Sea	Samsun	Cores; 2D seismic	None	Seismic blanking; gas chimneys; pockmarks	Not known	Possible hydrogen sulphide in the gas	Not estimated
	Hopa-Rize-Trabzon-Giresun	2D & 3D seismic	BSRs	Seismic blanking; MV; gas chimneys	Not known	Deep thermogenic gas migration through faults and microbial gas	Not estimated

263

264 **3. Offshore Greenland**

265 **3.1 Geological Setting**

266 The West Greenland margin formed during Cretaceous to Paleogene continental rifting that eventually
 267 resulted in seafloor spreading in the Baffin Bay and the Labrador Sea (e.g., Oakey and Chalmers, 2012).
 268 A change in spreading direction during the latest Paleocene to Eocene resulted in a general northward
 269 drift of Greenland into the Arctic Ocean, resulting in compression and inversion that becomes more
 270 pronounced the farther north along the Baffin Bay part of the margin. Significant strike-slope motion
 271 along many parts of the margin are also recorded at this time.

272

273 After the cessation of the Caledonian Orogeny during Late Silurian–Early Devonian, the northeast
 274 Greenland margin experienced repeated episodes of rifting with intervening quiescent periods, and
 275 occasionally minor compression and inversion. During the Cretaceous to Paleogene, rifting and breakup
 276 resulted in the onset of opening of the North Atlantic, and continued seafloor spreading formed large
 277 sedimentary basins (Hopper et al., 2014 and references therein). By early Neogene times, the seafloor
 278 spreading resulted in the opening of the Fram Strait and creation of the Atlantic-Arctic gateway (Jokat
 279 et al., 2008; Ritzmann and Jokat, 2003).

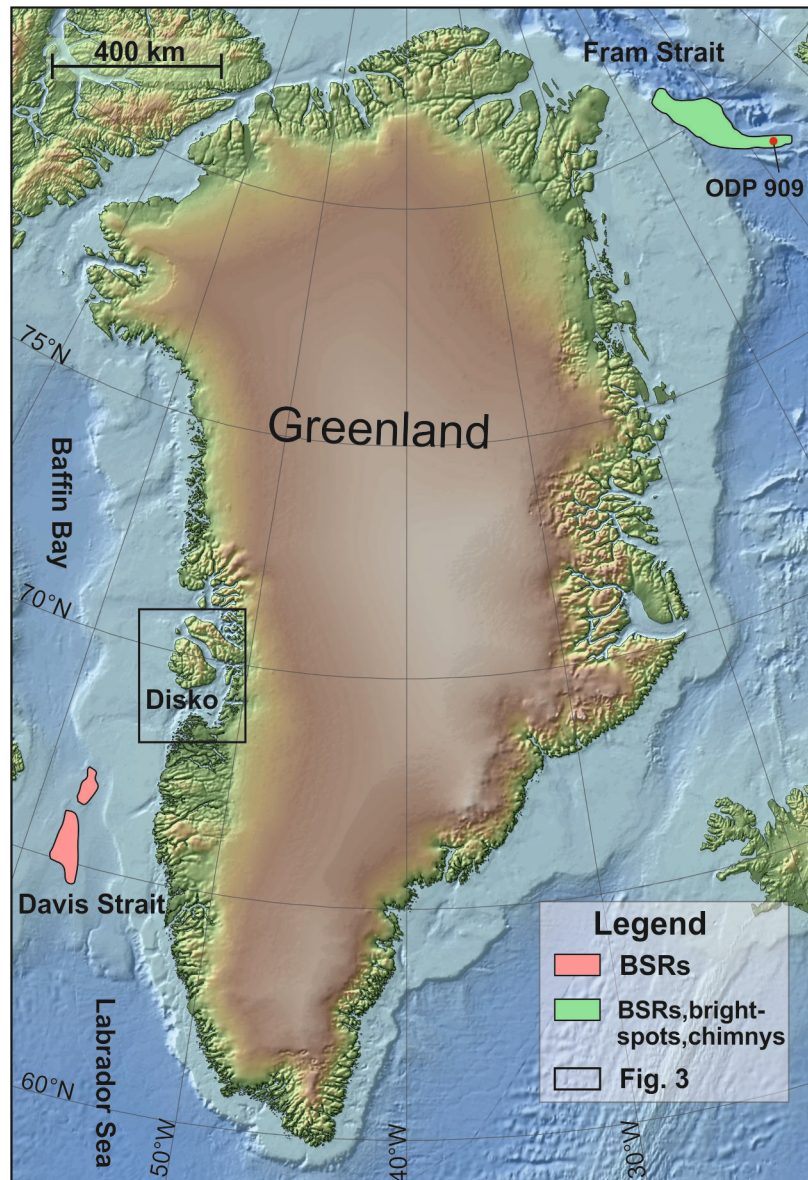
280

281 Along the southeast Greenland margin, no Paleozoic–Jurassic rocks are exposed onshore or otherwise
 282 known to exist. Small outcrops of Cretaceous sediments are known both onshore and offshore (e.g.,

283 Gerlings et al., 2017). Paleocene to Eocene breakup was accompanied by extremely voluminous
284 volcanism as seafloor spreading was established (e.g., Larsen and Saunders, 1998).

285

286 In late Neogene, all of Greenland's margins became glaciated, resulting in erosion of the inner and
287 middle shelf areas and deposition of kilometer thick glacial wedges on the outer shelf and slope
288 areas, while thick contourite deposition occurred in the basinal areas.



289

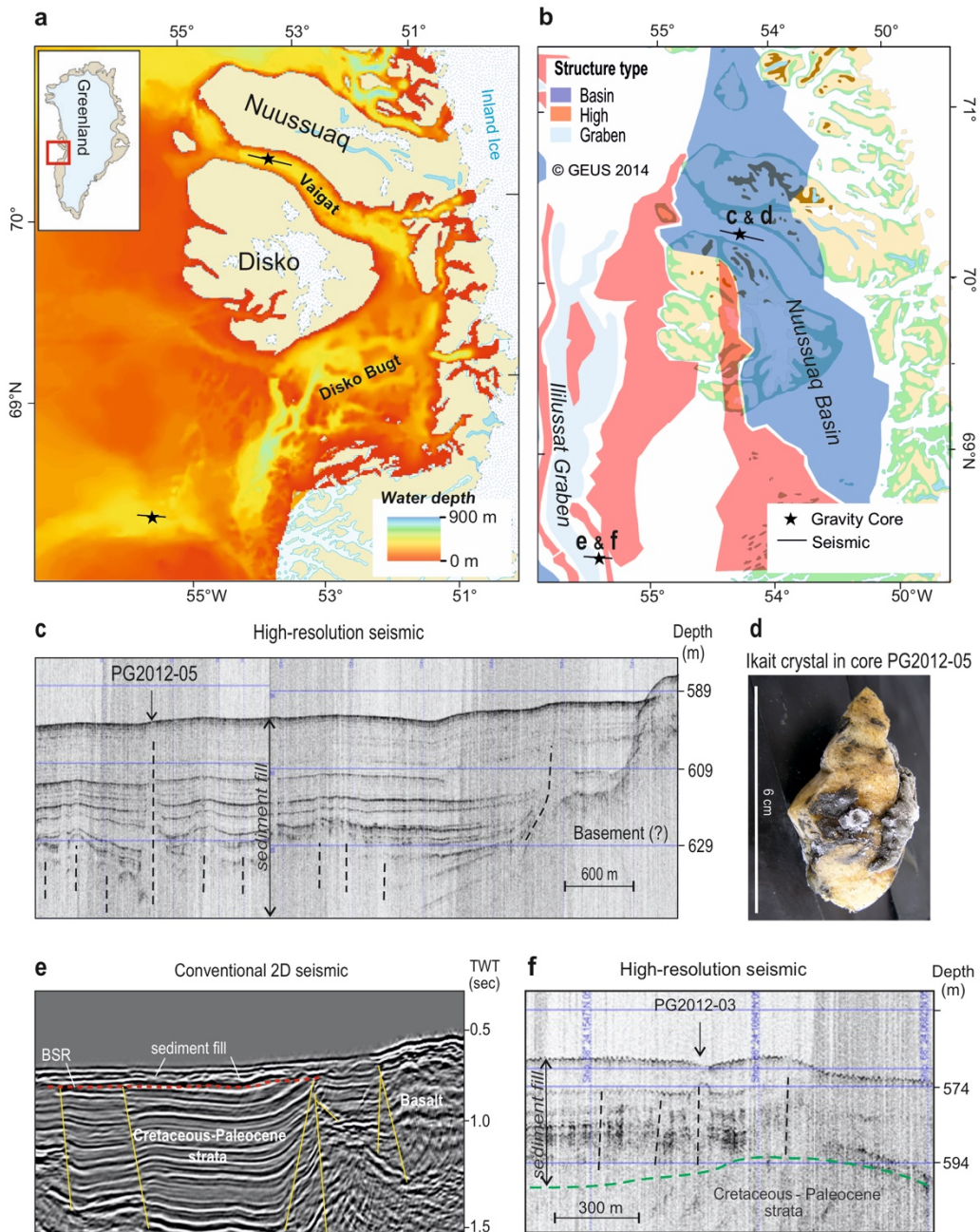
290 Figure 2: Bathymetric map of the Greenland margins and outline of larger offshore areas with seismic
291 indications of hydrate. Box marks the area shown in Fig. 3.

292

293 3.2 Hydrate occurrence

294 Greenland is surrounded by wide shelf areas with water depths of 200-500 m and 1000-4000 m deep
295 basinal areas (Fig. 2), all swept by cold bottom water currents. Therefore the Greenland continental
296 margins should have physical and oceanographic settings suitable for marine hydrate formation. In
297 addition, a study addressing as yet undiscovered hydrocarbon resources north of the Arctic Circle

298 suggests that the offshore Mesozoic sedimentary basins on the west and northeast Greenland margins
 299 could hold large quantities of oil and gas (Gautier et al., 2011). Due to late Cenozoic uplift and glacial
 300 erosion (Japsen et al., 2006), these basins are now exposed on the shelves at or near the seabed
 301 (Gregersen and Bidstrup, 2008; Hamann et al., 2005; Hopper et al., 2014), increasing the probability of
 302 seepages of gas and thus for formation of hydrate.



303
 304 Figure 3: Indications of hydrate occurrence in the Disko area offshore central west Greenland, where
 305 bottom water temperature is c. 3°C (after Nielsen et al., 2014) a) Bathymetric map with locations of
 306 seismic and cores shown in c)-f) ; b) Simplified map of Cretaceous–Paleogene major structural
 307 elements, outlining the hydrocarbon-bearing Nuussuaq Basin (Bojesen-Koefoed et al., 2007) and the
 308 likely hydrocarbon-bearing Ilulissat Graben (Gregersen and Bidstrup, 2008), with locations of seismic
 309 and cores; c) High-resolution seismic line along Vaigat showing younger sediments with chimneys
 310 (dashed black lines) indicating gas/fluid seepage from below, and location of gravity core PG2012-05
 311 taken on top of one of these features; d) 6-cm-long ikaite crystal collected from the core catcher of

312 gravity core PG2012-05, presumably originating from seepage of methane; e) 2D seismic record
313 showing a seabed depression with sub-cropping faulted Cretaceous–Paleocene strata (yellow lines)
314 and a BSR at about 75 ms sub-bottom depth (red dashed line); f) High-resolution seismic line inside
315 the seabed depression, showing Cretaceous–Paleocene strata overlain by younger sediments that are
316 disrupted by gas/fluid escape features (black dashed lines). Gas-bearing gravity core PG2012-03 was
317 located in a pockmark underlain by a large diapiric feature.
318

319 Nevertheless, little work has been done on the hydrate potential of offshore Greenland. At present, most
320 of the available data derive from conventional oil and gas exploration, including more than 100,000 km
321 of 2D seismic reflection data offshore west and northeast Greenland as well as several 3D surveys on
322 the western margin. Some information of heat flow and seabed temperature data offshore Greenland
323 exist, but these are sparse and mostly limited to the few exploration wells that have been drilled along
324 the western margin. Echo-sounder, high-resolution subbottom profiler and swath bathymetry data exist
325 for smaller areas along all the margins, but most are not in the public domain.
326

327 Offshore northeast Greenland no commercial wells have been drilled yet. However, in the southern
328 Fram Strait, Ocean Drilling Program (ODP) well 909 encountered gassy sediments (Knies and Mann,
329 2002), which can be traced up-slope the northeast Greenland margin, where bright spots, chimneys and
330 possible BSRs indicate that hydrate may be present (Fig. 2; Nielsen and Jokat, 2009). Offshore west
331 Greenland, several commercial wells have gas and oil shows, but there have been no significant
332 discoveries so far. Several oil seeps as well as hydrate and gas encountered by shallow onshore drilling
333 demonstrate that working petroleum systems exist in the Nuussuaq Basin (Fig. 3; Bojesen-Koefoed et
334 al., 2007; Christiansen et al., 1994; Pedersen et al., 2006). A pilot study of the marine part of the
335 Nuussuaq Basin found various indirect indicators for the presence of hydrate in shallow seismic and
336 gravity core data (Nielsen et al., 2014; Fig. 3), demonstrating that the offshore part of the Nuussuaq
337 Basin likely contains significant quantities of hydrate. Further offshore west Greenland, in the up to
338 700 m deep Davis Strait area (Fig. 2), BSRs with associated amplitude variations indicating hydrate
339 above free gas can be seen on several seismic profiles (Nielsen et al., 2000), further demonstrating a
340 possible marine hydrate occurrence in the region.
341

342 Direct sampling of hydrate offshore Greenland has not been reported to date and, despite the above-
343 mentioned indications of hydrate presence, no systematic study or compilation has yet been undertaken.
344 In addition, due to the very sparse information on heat flow and seabed temperature, there is currently
345 no published detailed study of the hydrate stability zone offshore Greenland.
346

347 **4. Offshore and onshore Svalbard**

348 4.1 Geological Setting

349 The west Svalbard margin shares a common geological history with the northeast Greenland margin
350 (section 3.1) until the opening of the Fram Strait. Subsequently, deep-water circulation between the

351 Arctic Ocean and the Norwegian-Greenland Sea led to deposition of thick contourite sequences that
352 extend from the Svalbard margin towards the mid-ocean ridges. Two sediment types dominate the west
353 Svalbard margin: glaciogenic debris flows in trough mouth fans beyond the shelf break; and turbiditic,
354 glaciomarine and hemipelagic sediments, which are to some extent reworked by contour currents
355 (Vorren and Laberg, 1997; Vorren et al., 1998). The eastern margins of the Fram Strait were dominated
356 by contourites during the late Miocene to Pleistocene (Mattingsdal et al., 2014) leading to the
357 development of large sediment drifts such as the Vestnesa Ridge (Fohrmann et al., 2001) on young and
358 relatively warm oceanic crust. The Vestnesa Ridge is located in the eastern Fram Strait at $\sim 79^\circ\text{N}$, north
359 of the Knipovich Ridge and Molloy transform fault (Fig. 4), representing one of the northernmost
360 occurrences of hydrate in the world.

361

362 In contrast, the Svalbard archipelago is the most uplifted part of the Barents Shelf and is dominated by
363 older strata providing a “window” into the tectono-stratigraphic evolution of the Barents Sea area.
364 Approximately 60% of the archipelago is covered by glaciers, with the remainder strongly affected by
365 continuous permafrost. Ice caps are found predominantly in northeastern Svalbard, with ice thicknesses
366 of up to 550 m observed for the Austfonna ice cap on Nordaustlandet (Furst et al., 2018). Permafrost
367 thickness varies from less than 100 m in coastal settings to over 500 m in the highlands (Humlum et al.,
368 2003). The nearly complete Devonian-Paleogene stratigraphic record is exceptionally well exposed due
369 to the lack of vegetation, giving insights into reservoir and source rock intervals targeted further south
370 (Henriksen et al., 2011b; Nøttvedt et al., 1993; Worsley, 2008).

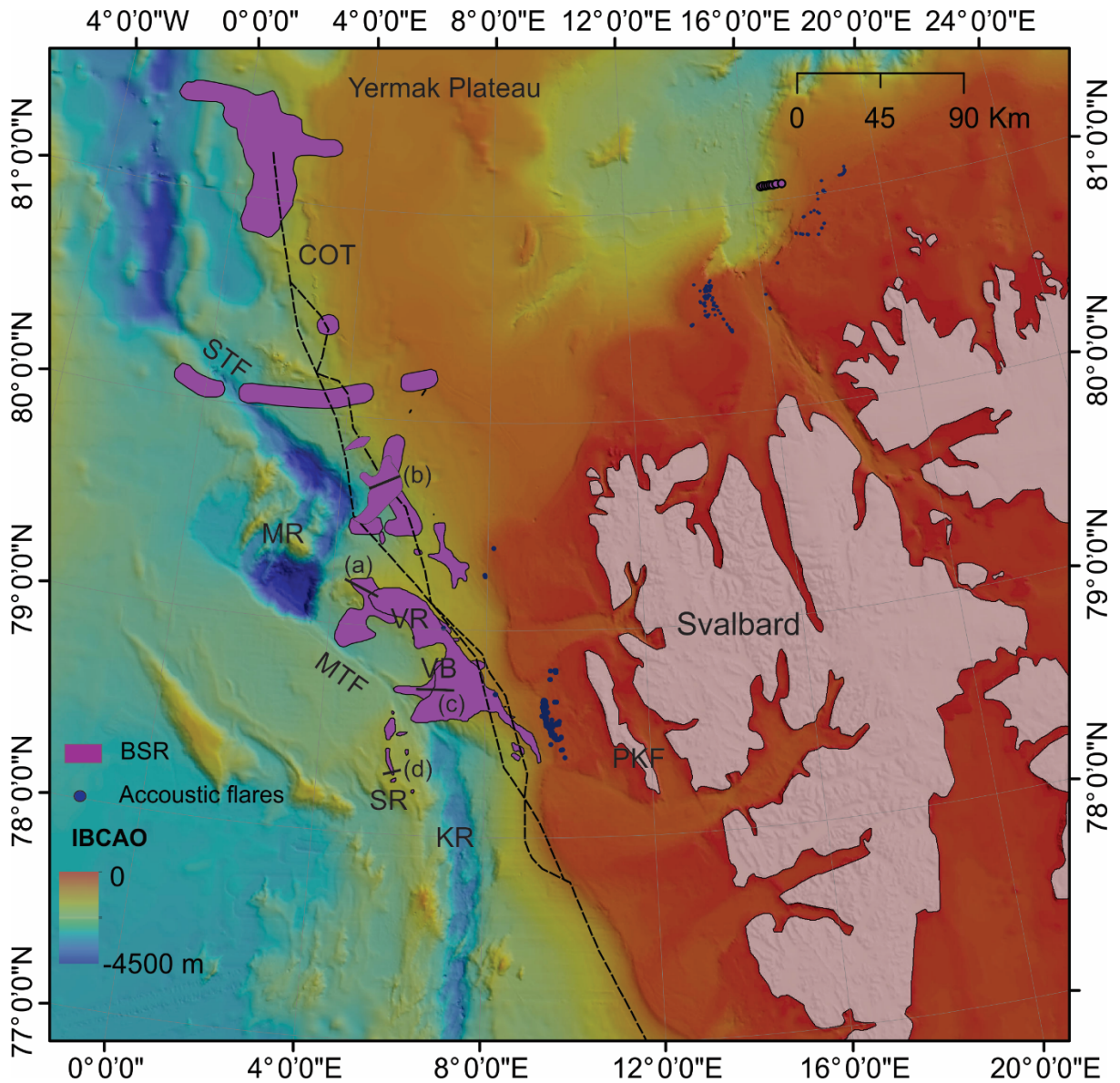
371

372 4.2 Hydrate occurrence

373 4.2.1 Offshore west Svalbard

374 The presence of a prominent hydrate BSR was revealed by several seismic reflection studies in the
375 Vestnesa basin (e.g., Dumke et al., 2016; Eiken and Hinz, 1993; Vanneste et al., 2005; Fig. 4). The BSR
376 can be traced from the continental slope at c. 800 m water depth to the Molloy Transform Fault and
377 beyond to > 2000 m water depth (Hustoft et al., 2010; Sarkar et al., 2012; Vanneste et al., 2005). It
378 appears as a nearly continuous reflection with amplitudes that vary laterally and generally decrease
379 towards the flanks of sedimentary ridges (Fig. 5). This variation indicates that hydrate and gas
380 accumulations are primarily topographically and structurally controlled (Bünz et al., 2012). The BSR
381 covers the whole of the Vestnesa Ridge (i.e., from c. 1100 m to 1700 m water depth), exhibiting a strong
382 impedance contrast between hydrate-bearing and gas-charged sediments (Bünz et al., 2012; Petersen et
383 al., 2010; Plaza-Faverola et al., 2017). An interconnected zone of free gas beneath the BSR is more
384 prominent along the eastern segment of the Vestnesa Ridge, where currently active gas seepage is
385 concentrated (Hustoft et al., 2009; Panieri et al., 2017; Smith et al., 2014). Faults are identified on
386 seismic profiles, extending from the seafloor to beneath the BSR. These faults control the ascent of
387 fluids and the distribution of gas seeps on the Vestnesa Ridge (Plaza-Faverola et al., 2015; Vanneste et

388 al., 2005). Basin modeling studies show that generation of thermogenic gas from relatively shallow and
 389 young source rocks sustains shallow gas and hydrate accumulations, at least within the eastern part of
 390 the Vestnesa basin (Dumke et al., 2016; Knies et al., 2014). In this setting, very close to the mid-ocean
 391 ridge, the hydrate system is strongly influenced by the young and hot oceanic crust. Geothermal
 392 gradients increase gradually from 70 to 115 °C/km towards the Molloy Transform Fault (Crane et al.,
 393 1991; Vanneste et al., 2005).
 394

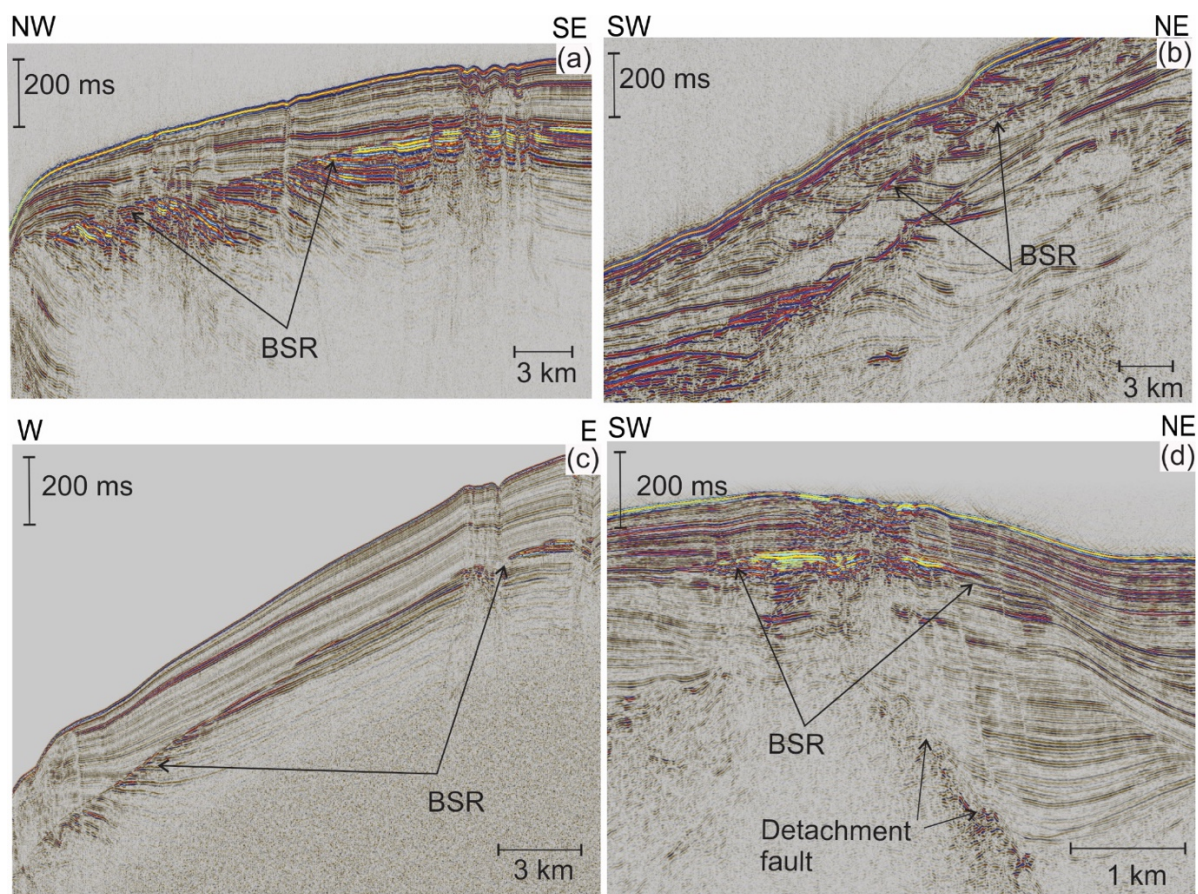


395
 396 Figure 4: BSR distribution projected over IBCAO bathymetry off Svalbard. The BSR outline
 397 corresponds to observations from Vanneste et al. (2005); Petersen et al. (2010); Hustoft et al. (2009);
 398 Sarkar et al. (2012); Bünz et al. (2012); Geissler et al. (2014); Johnson et al. (2015); (Dumke et al.,
 399 2016); Plaza-Faverola et al. (2017); and Waghorn et al. (2018). Gas flares compiled from multiple
 400 expeditions to the area by NOC, AWI, CAGE. PKF=Prins Karl Forland; COT=Continent-Ocean
 401 Transition (Engen et al., 2008); KR=Knipovich Ridge; MR=Molloy Ridge; VR=Vestnesa Ridge;
 402 VB=Vestnesa Basin; SR=Svyatogor Ridge; MTF=Molloy Transform Fault; STF=Spitsbergen
 403 Transform Fault. (a)-(d) mark seismic profiles shown in Fig. 5.
 404

405 South of the Molloy Transform Fault and to the west of the Knipovich ridge spreading axis, a well-
 406 developed hydrate system has been documented along the Svyatogor ridge, a contourite drift similar to
 407 the Vestnesa Ridge (Fig. 4, 5). Here the gas hydrate system is believed to be sustained by input of
 408 abiotic gas, a product of serpentinization at detachment faults (Johnson et al., 2015; Waghorn et al.,
 409 2018).

410

411 Elsewhere on the west Svalbard Margin, the BSR is weak and in some areas it is patchy (e.g., Geissler
 412 et al., 2014). Observations of shallow gas in accumulations that roughly follow the seafloor further
 413 upslope on the continental margin may be linked to hydrate dissociation (Riedel et al., 2018; Sarkar et
 414 al., 2012). To the west and east of the Yermak Plateau, relatively weak BSRs and some double BSRs
 415 have been documented (e.g., Geissler et al., 2014).



416

417 Figure 5: Examples of BSRs offshore west-Svalbard: (a) western segment of the Vestnesa Ridge (Plaza-
 418 Faverola et al., 2017); (b) western flank of Yermak Plateau (Geissler et al., 2014); (c) slope between
 419 Prins Karl Forland and the Molloy Transform Fault (Vanneste et al., 2005); (d) southern part of the
 420 Svyatogor Ridge (Johnson et al., 2015; Waghorn et al., 2018). The location of each example is indicated
 421 in Fig. 4. The BSR is continuous and strong along the Svyatogor Ridge, the Vestnesa Ridge and its
 422 southern flank. The BSR is weak and patchy towards the Yermak Plateau.
 423

424 Hydrate has been recovered from several of the pockmarks that lie above chimney structures on the
 425 eastern Vestnesa Ridge segment. Here, hydrate appears as small, thin chips, in veins or as chunks of
 426 several 10s of cm, embedded in the upper 2-4 m of muddy sediments (e.g., Panieri et al., 2017; Smith

427 et al., 2014). The gas compositions of these hydrate samples and of core head-space gas samples
428 provide strong evidence for a thermogenic input into the HSZ (Plaza-Faverola et al., 2017; Smith et al.,
429 2014). Massive hydrate has been collected in a zone of weak BSRs at a focused fluid flow structure on
430 the continental slope (e.g., Graves et al., 2017; Sarkar et al., 2012). Hydrate is suspected but so far not
431 found in regions where the HSZ pinches out near the shelf break off Prins Karl Forland, where pervasive
432 seepage exists (e.g., Berndt et al., 2014; Wallmann et al., 2018; Westbrook et al., 2009). A HSZ volume
433 of ca. 700 km³ was derived from mapped BSRs in the Vestnesa Basin (Plaza-Faverola et al., 2015).

434
435 Several studies provide constraints on hydrate saturations on the eastern Vestnesa Ridge based on P-
436 wave velocity variations from seismic data and resistivity from CSEM data. From P wave velocity
437 anomalies, Hustoft et al. (2009) estimated mean hydrate saturations of ~6% within a 30-100 m thick
438 zone above the BSR, reaching a maximum of 11%. Their velocity model was derived from multi-
439 channel seismic reflection data along an E-W profile that intersects the crest of the Vestnesa ridge at
440 the eastern end of an area of active seepage. They found the highest hydrate saturations at the crest of
441 the ridge and near fault zones. In a more recent study along the ridge crest nearby, Singhroha et al.
442 (2019) estimated hydrate saturations of 10-18% of the pore space within a 100 m thick zone above the
443 BSR, based on P wave velocities and full waveform inversion of wide-angle seismic data from OBSs.
444 By comparison, joint analysis of resistivity from CSEM data and OBS data along a transect in the same
445 area suggests mean hydrate saturations of 20-30% outside of chimney structures and 40-68% in the
446 lowermost c. 80 m of the HSZ within a highly brecciated gas chimney (Goswami et al., 2015). Despite
447 similar velocities to those of Hustoft et al. (2009) and Singhroha et al. (2019), these estimated saturations
448 are much higher because free gas is assumed to co-exist with hydrate in the HSZ, contributing positively
449 to the resistivity anomaly and negatively to the velocity anomaly. All three studies systematically found
450 the highest hydrate saturations associated with faults and fractures within the GHZ. The free gas
451 saturations estimated by these studies in zones outside gas chimneys consistently range between 1.5
452 and 4% of the pore space within a low-velocity zone below the BSR.

453 454 4.2.2 Onshore Svalbard

455 As part of early petroleum exploration of the Barents Sea, eighteen petroleum exploration wells were
456 drilled on Svalbard from 1961 to 1994 (Senger et al., 2017). While none of these wells resulted in
457 commercial discoveries, numerous boreholes encountered gas. In addition, research drilling in
458 Adventdalen and coal exploration in Petuniabukta discovered producible natural gas, some of which
459 is directly associated with permafrost (Senger et al., 2019). These discoveries, as well as the presence
460 of hydrate offshore (Section 4.2.1), prompted efforts to assess the feasibility of finding hydrate
461 onshore Svalbard (Betlem et al., 2019).

462

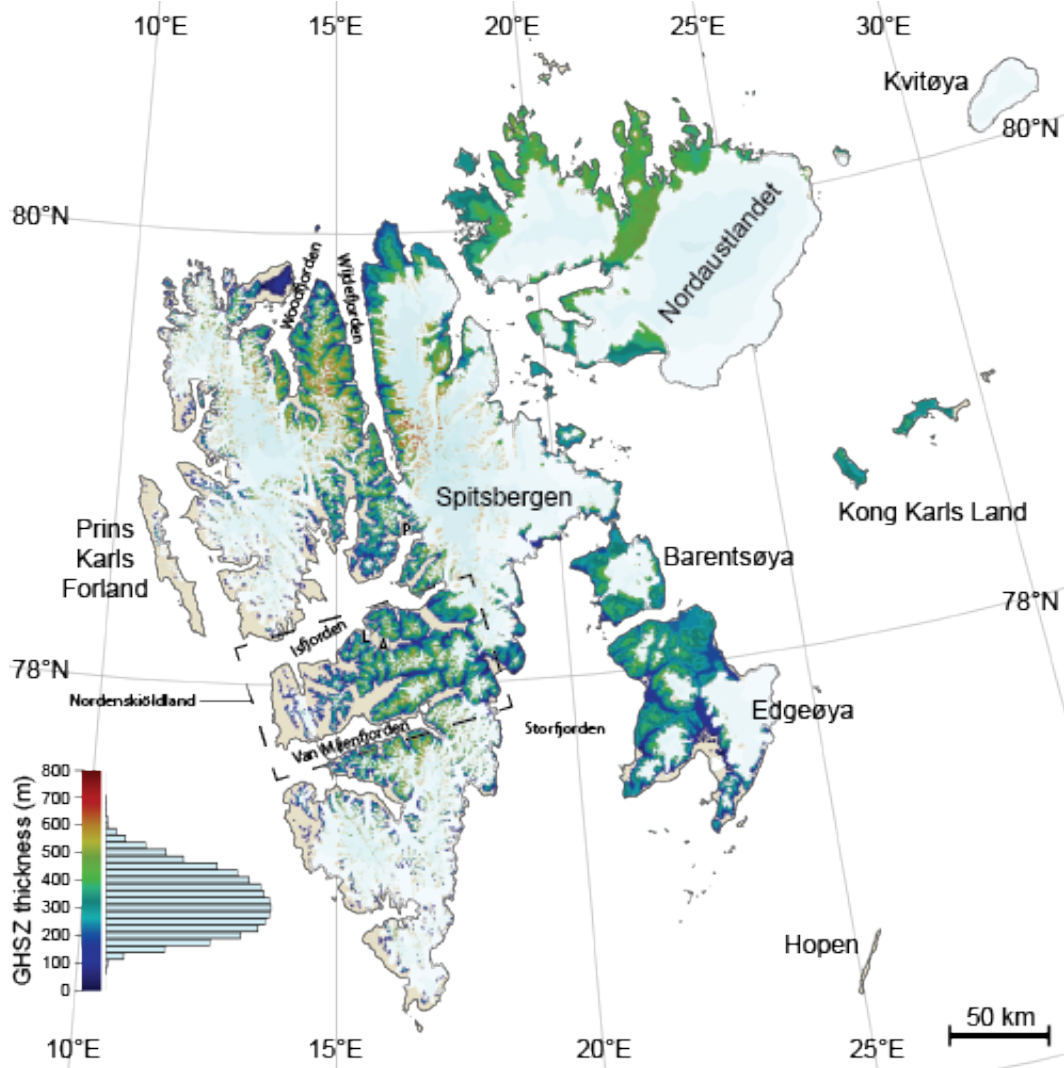
463 Recent modelling efforts constrain a potentially stable marine hydrate stability zone in the fjords around
464 Svalbard (Betlem, 2018; Roy et al., 2012), and a permafrost-associated hydrate stability zone onshore
465 central Spitsbergen (Betlem et al., 2019). The latter has been extended to all unglaciated areas of
466 Svalbard's main islands (Spitsbergen, Nordaustlandet, Prins Karls Forland, Barentsøya and Edgeøya;
467 Fig. 6). Thus far hydrate has not been directly sampled onshore Svalbard, largely due to a lack of
468 dedicated exploration efforts. Circumstantial evidence for probable hydrate presence is provided by
469 long-term gas bubbling in numerous coal exploration boreholes (Jochmann, M., pers. comm. 2017),
470 though these are unfortunately not well documented.

471
472 Thus the Svalbard archipelago possesses three important factors contributing to the presence of hydrate:
473 1) suitable thermobaric conditions, 2) an active petroleum system, and 3) a constant flux of thermogenic
474 and microbial gas. Suitable thermobaric conditions (i.e., shallow-to-deep permafrost) are brought about
475 by laterally changing mean annual air temperatures of between -3.5 °C and -8 °C (Betlem et al., 2019;
476 Przybylak et al., 2014). Where permafrost surpasses 100-125 m depth, subsurface thermal regimes are
477 cold enough to allow hydrate formation under hydrostatic pressure. Thickening of ice caps and glaciers
478 towards the north is likely to contribute further to local regions of hydrate stability as a result of loading
479 (i.e. pressure increase) and favourable thermal regimes at glacier bases. However, the extent of hydrate
480 stability remains difficult to assess due to uncertainties in properties such as sub-glacial thermal state,
481 densities, and local thicknesses, as well as the limited resolution and accuracy of relevant datasets.

482
483 Widespread organic-rich source rocks (e.g., Upper Jurassic to Lower Cretaceous Agardhfjellet
484 Formation and Middle-Triassic Botneheia Formation) and coal beds (e.g., Lower Carboniferous
485 Billefjorden Group and Paleogene Firkanten Formation) may act as unconventional reservoirs hosting
486 disseminated or fracture-filled hydrate. These Mesozoic organic rich source rocks have the same
487 origin as those contributing to hydrocarbon discoveries in the Barents Sea (Abay et al., 2014) and
488 have been linked to hydrocarbon finds onshore. Suitable reservoir rocks are found in both sandstone-
489 dominated sequences (e.g., the Paleogene Van Mijenfjorden Group, the Lower Cretaceous
490 Helvetiafjellet Formation and the Upper Triassic-Middle Jurassic Wilhelmøya Subgroup) and
491 carbonates (e.g., the Permian Tempelfjorden and Gipsdalen Groups). Limited reservoir quality, with
492 poor matrix porosity and permeability related to extensive diagenesis (e.g., Mork, 2013) is a major
493 challenge. However, pervasive natural fracturing contributes by enhancing fracture-related fluid flow
494 (Ogata et al., 2012).

495
496 Significant quantities of thermogenic gas (mixed with microbial gas in shallower intervals) were
497 encountered during research drilling for the Longyearbyen CO₂ Lab project in Adventdalen (Ohm et
498 al., 2019) and in petroleum and coal exploration wells (Senger et al., 2019). Furthermore, high
499 concentrations of microbial gas are observed in onshore pingo discharge waters (Hodson et al., 2019).

500 Gas flares, pockmarks and thermogenic methane are observed in several fjords of Svalbard (Liira et
 501 al., 2019; Roy et al., 2019). Thus there is evidence for active fluid seepage both onshore and offshore.
 502



503
 504 Figure 6: Thickness of the HSZ onshore Svalbard, for a plausible gas composition of 93% methane, 7%
 505 ethane and seawater salinity. Geothermal gradients are derived from boreholes and inferred from the
 506 depth of the base of permafrost thickness in central Spitsbergen (Betlem, 2018; Betlem et al., 2019).
 507 Lapse rate is set at $-6\text{ }^{\circ}\text{C}/\text{km}$, and surface air temperatures are incorporated from Przybylak et al. (2014).
 508 A: Adventdalen; L: Longyearbyen; P: Petuniabukta. The map uses topographic and coastline data from
 509 the Norwegian Polar Institute.

510
 511 Assuming that structure I hydrate dominates, a zone of hydrate stability likely occurs in the interior of
 512 Spitsbergen along a relatively unglaciated corridor stretching from Nordenskiöldland in the centre to
 513 Wijdefjorden in the north. Strandflats and valley systems limit hydrate stability on Svalbard’s western
 514 flanks due to elevated temperatures associated with the West Spitsbergen Current (Przybylak et al.,
 515 2014). Mean annual temperatures decrease to the east, so that similar settings on Edgeøya, Barentsøya
 516 and Nordaustlandet fall well within the hydrate stability field, even in coastal settings. Most of the

517 archipelago thus appears to be on the edge of hydrate stability, with vertical and lateral variations
518 tipping particular locations in and out of the hydrate stability field.

519

520 **5. Norwegian Margin**

521 5.1 Geological setting

522 The Barents Sea is a large epi-continental shelf sea bound by the North Atlantic to the west, the
523 Norwegian and Russian landmasses to the south, the Arctic Ocean to the north and Novaya Zemlya to
524 the east. Formed in association with the opening of Norwegian-Greenland Sea and Eurasia Basin during
525 the Cenozoic (Faleide et al., 1984), it is composed of a complex mosaic of basins, platforms, and
526 structural highs and is a major petroleum province (Doré, 1995; Nøttvedt et al., 1988). Tectonic uplift,
527 erosion and multiple glaciations affected the Barents Sea during the Cenozoic and resulted in the
528 removal of up to 2 km of sediments from the region (Henriksen et al., 2011a; Ktenas et al., 2017; Vorren
529 et al., 1991). These processes resulted in the spillage of hydrocarbons from reservoir rocks, and recent
530 exploration has shown predominantly gas reservoirs and underfilled reservoirs with low oil saturation
531 (Doré and Jensen, 1996; Henriksen et al., 2011a).

532

533 Along the mid-Norwegian margin, the Møre and the Vøring basins are the two most prominent. They
534 developed as a result of several rifting episodes until Late Paleocene/Early Eocene continental break-
535 up (Brekke, 2000; Lundin and Doré, 1997). Post break-up thermal subsidence during the Cretaceous
536 resulted in up to 10-km-thick sedimentary basin fill. The second youngest sedimentary succession is
537 the Miocene/lowermost Pliocene Kai Formation with predominantly fine-grained hemipelagic
538 sediments (Dalland, 1988; Rise et al., 2005). The overlying Naust formation encompasses sediments of
539 the Plio-Pleistocene glacial-interglacial cycles that significantly changed the sedimentation pattern,
540 yielding a thick wedge of clastic sediments on the shelf (Hjelstuen et al., 1999; Stuevold and Eldholm,
541 1996). Within this formation, contourites deposited along slope during deglaciation and interglacials
542 frequently interlayer the glacialic downslope-transported debris flows (Laberg et al., 2001). A mass-
543 wasting event, the Storegga Slide, removed large amounts of sediment within the Møre Basin and along
544 its northern border with the Vøring Plateau at about 8.2 ka (Bryn et al., 2005).

545

546 5.2 Hydrate occurrence

547 5.2.1 Barents Sea

548 Leaking reservoirs in the Barents Sea have given rise to widespread occurrence of fluid-flow features
549 such as shallow gas accumulations, gas seeps, gas chimneys, pockmarks of various sizes, pingos and
550 hydrate (Fig. 7; Andreassen et al., 2017; Chand et al., 2012; Laberg and Andreassen, 1996; Rise et al.,
551 2015; Serov et al., 2017; Vadakkepuliyaambatta et al., 2013; Vadakkepuliyaambatta et al., 2017). Fluid
552 migration in the area is structurally controlled, with major faults and fractures acting as pathways
553 (Vadakkepuliyaambatta et al., 2013).

554

555 The presence of hydrate has been inferred at multiple locations in the Barents Sea from BSRs in multi-
556 channel seismic data (Vadakkepuliambatta et al., 2017 and references therein). BSRs occur in close
557 association with vertical fluid-flow systems, shallow gas accumulations, faults, and fractures (Ostanin
558 et al., 2013; Vadakkepuliambatta et al., 2013; Vadakkepuliambatta et al., 2017;
559 Vadakkepuliambatta et al., 2015). They generally occur in consolidated sediments of Jurassic and
560 younger ages as well as in the glacial sediments of Pleistocene to Holocene age (e.g., Andreassen et al.,
561 1990; Vadakkepuliambatta et al., 2017). Although multiple active seeps have been detected in the
562 southwest Barents Sea (e.g., Andreassen et al., 2017; Chand et al., 2012), no hydrate sample has been
563 recovered yet. However, in the Storfjordrenna region of the northwest Barents Sea, Serov et al. (2017)
564 reported sampling of hydrate just below the seafloor. Hydrate was also recovered on the continental
565 slope of southwest Barents Sea at the Håkon Mosby mud volcano (Ginsburg et al., 1999).

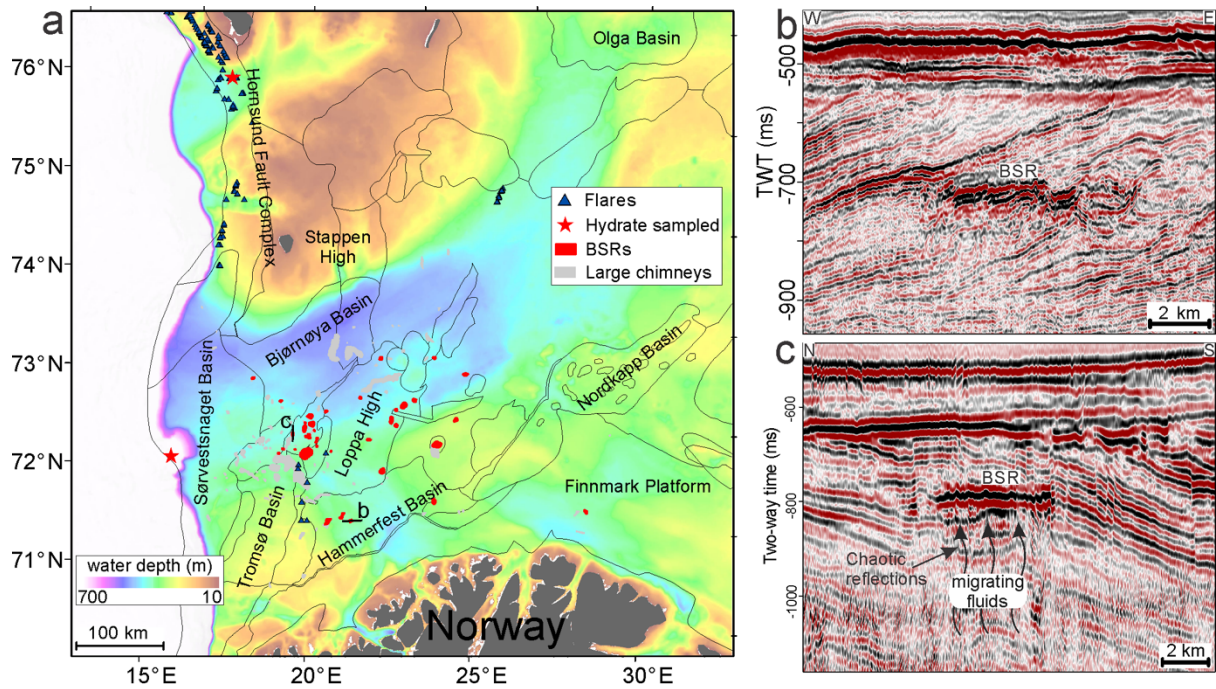
566

567 Results from thermal modelling suggest a prevalence of thermogenic methane and higher order
568 hydrocarbons forming hydrate in the region (Chand et al., 2008; Vadakkepuliambatta et al., 2017).
569 Methane hydrate is not stable in most parts of the Barents Sea, primarily due to the shallow water depth
570 (<350 m; Chand et al., 2008; Klitzke et al., 2016; Vadakkepuliambatta et al., 2017). Hydrate
571 occurrence is highly variable, controlled primarily by thermogenic gas discharge into the shallow
572 sediments (Vadakkepuliambatta et al., 2017). Variations in the geothermal gradient, salt tectonics, and
573 the inflow of warm Atlantic water also influence hydrate stability in the region (Chand et al., 2008;
574 Vadakkepuliambatta et al., 2017). Major factors controlling hydrate stability, such as the bottom water
575 temperature and geothermal gradient, vary greatly across the various basins and highs of southwest
576 Barents Sea. Bottom-water temperatures can vary between 1 and 6 °C across the region, where warm
577 Atlantic waters mix with cold Arctic waters (Vadakkepuliambatta et al., 2017). Seasonal variations in
578 bottom water temperature are up to 2 °C (Ferré et al., 2012). Geothermal gradients vary from 25 to 65
579 °C/km, mainly due to the presence of salt diapirs on the eastern part of this area (Bugge et al., 2002).
580 The southwest Barents Sea may be a focus of hydrate dissociation due to ocean warming in the near
581 future (Vadakkepuliambatta et al., 2017).

582

583 The volume of hydrate in the Barents Sea is still uncertain, primarily due to the uncertainties related to
584 gas composition, hydrate saturation and hydrate distribution within the host sediments. Based on multi-
585 channel seismic data and well logs, Laberg et al. (1998) estimated ~0.19 GSm³ (GSm³ = 10⁹ standard
586 cubic metres) of gas hydrate trapped within the Eocene succession of a small part of Bjørnøya Basin
587 where a BSR was observed. Vadakkepuliambatta et al. (2017) proposed a hydrate volume of ~93-650
588 GSm³ in the southwest Barents Sea from hydrate stability models that assumed that the hydrate-forming
589 gas was pure methane. Due to the presence of higher-order hydrocarbons, the hydrate volume could be
590 as high as ~470–3320 GSm³. The patchy occurrence of hydrate systems in the southwest Barents Sea

591 and their occurrence in consolidated, low-porosity sediments indicates low resource density for
 592 economic exploitation.



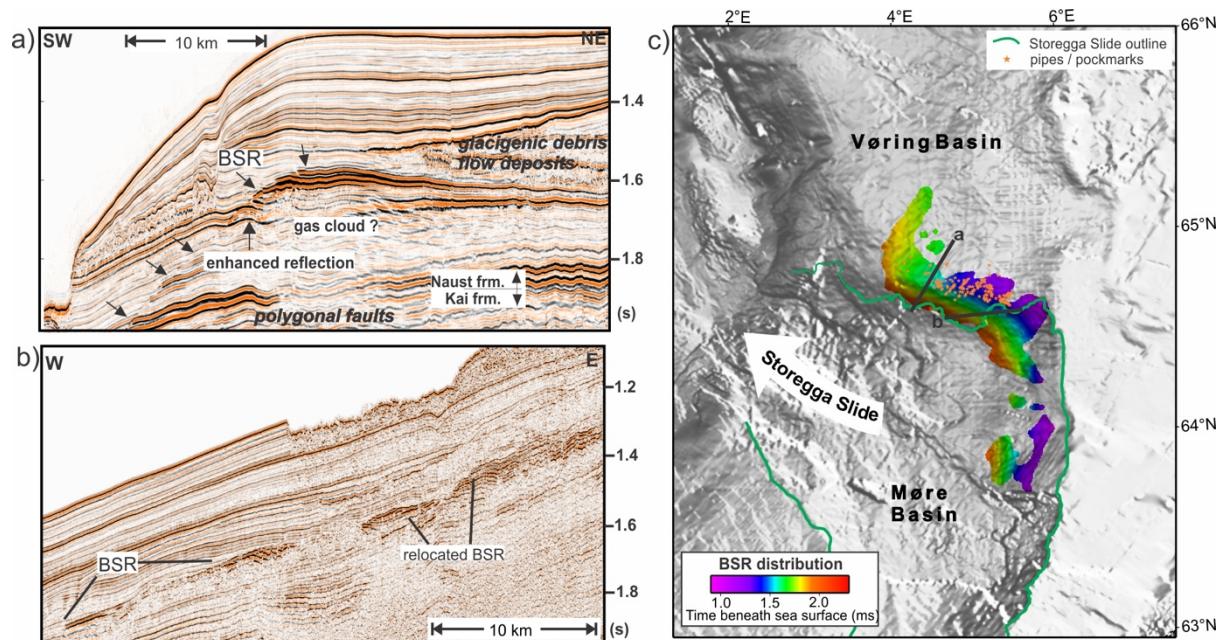
593
 594 Figure 7: a) Bathymetry of the western Barents Sea with locations of hydrate indicators (compiled from
 595 Andreassen et al., 2017; Chand et al., 2012; Mau et al., 2017; Serov et al., 2017; Vadakkepuliambatta
 596 et al., 2013; Vadakkepuliambatta et al., 2017). b) and c) Seismic examples of a BSR in the southwest
 597 Barents Sea clearly cross-cutting the tilted sedimentary strata and showing reversed polarity compared
 598 to the seafloor reflection (modified from Vadakkepuliambatta et al., 2017).
 599

600 5.2.2 Mid-Norwegian margin

601 Bugge et al. (1988) first recognised evidence for hydrate in the northern Storegga Slide area of the mid-
 602 Norwegian Margin in the form of a weak BSR. Later, Posewang and Mienert (1999) and Bouriak et al.
 603 (2000) confirmed the geophysical evidence that hydrate exists in this area. In high-resolution seismic
 604 data, the BSR is generally characterised as an abrupt upper boundary of increased reflection amplitude
 605 (Fig. 8a; Bouriak et al., 2000; Bünz et al., 2003). In areas of dipping seafloor the BSR is readily
 606 identified cross-cutting the almost horizontally layered strata.

607
 608 A double BSR observed in a small area along the northern flank of the Storegga Slide is attributed to a
 609 hydrate structure involving high-order hydrocarbons (Andreassen et al., 2000; Posewang and Mienert,
 610 1999). Analysis of multi-component seismic data does not show a BSR in shear-wave components,
 611 indicating that hydrate here does not increase the shear stiffness of the sediments (Andreassen et al.,
 612 2003; Bünz et al., 2005). The presence of a BSR inside the slide area indicates that the hydrate system
 613 is dynamically adjusting to post-slide pressure-temperature equilibrium conditions (Fig. 8b; Bouriak et
 614 al., 2000; Bünz et al., 2003).
 615

616 Bünz et al. (2003) mapped the extent of the BSR, which predominantly occurs over an area of about
 617 4000 km² on the mid-Norwegian margin along the northern flank of the Storegga Slide (Fig. 8c). The
 618 glacial evolution of this margin resulted in widespread deposition of glacial sediments that built out
 619 the continental shelf (e.g., Hjelstuen et al., 2005; Stuevold and Eldholm, 1996). These low-
 620 permeability sediments are not conducive to hydrate growth and limit the extent of hydrate to the
 621 northern flank of the Storegga Slide, where they occur in marine contourite deposits. The large-scale
 622 distribution of hydrate in this area can be classified as a stratigraphic accumulation. The hydrate
 623 occurrence coincides with a vertical fluid flow system as documented by features such as pockmarks
 624 on the seafloor and pipe and chimney structures in subsurface seismic data (Bouriaik et al., 2000; Bünz
 625 et al., 2003; Hustoft et al., 2010; Hustoft et al., 2007). A hydrate stability model was developed by
 626 Mienert et al. (2005), who speculated that ocean warming since the last deglaciation promoted the
 627 development of instabilities along the mid-Norwegian margin.
 628



629
 630 Figure 8: Examples of BSRs on the mid-Norwegian margin (modified from Bünz and Mienert, 2004):
 631 a) typical expression of a BSR identified as an abrupt upper boundary of increased reflection amplitude,
 632 occurring in glaciomarine contourite deposits along the northern flank of the Storegga Slide (vertical
 633 exaggeration ~35). b) The BSR also occurs inside the Storegga Slide area where it has readjusted to
 634 post-slide pressure-temperature equilibrium conditions (vertical exaggeration ~33). c) The BSR
 635 predominantly occurs along the northern Storegga Slide flank and patchily west of the Storegga Slide
 636 headwall over a total area of 4000 km².
 637

638 Velocity analyses of seismic data provided evidence for the existence of hydrate in sub-seafloor
 639 sediments (Bünz and Mienert, 2004; Bünz et al., 2005; Plaza-Faverola et al., 2010; Westbrook et al.,
 640 2008). Hydrate saturations have been estimated from OBS data and range from 2 to 15% of pore space.
 641 The first hydrate sample in this area was from a pockmark in the Nyegga area, located at the northeastern
 642 corner of the Storegga Slide (Ivanov et al., 2007). Isotopic analysis of the gas in hydrate from this

643 pockmark suggests a primarily microbial origin but with a significant thermogenic component (Vaular
644 et al., 2010). In the Nyegga area, many focused fluid flow structures pierce the HSZ (Hjelstuen et al.,
645 2010; Hustoft et al., 2010; Plaza-Faverola et al., 2011) and form such pockmarks at the seafloor
646 (Hovland et al., 2005; Mazzini et al., 2006). Analysis of velocities from wide-angle seismic data and
647 resistivities from CSEM data showed that these chimneys likely contain much larger amounts of gas
648 hydrate than the surrounding stratified sediments (Attias et al., 2016; Plaza-Faverola et al., 2010).

649

650 Senger et al. (2010) compiled a large database of geophysical and geotechnical borehole data for a
651 resource evaluation of the Norwegian Sea gas hydrate prospect. Their method was based on a stochastic
652 approach and closely followed that of conventional hydrocarbon prospect evaluation. The calculated
653 in-place volume has a large uncertainty, primarily due to the lateral variations in reservoir parameters.
654 Senger et al. (2010) estimated that the prospect (both hydrate and free-gas zones) contains 625 GSm³
655 of gas. The amount of gas is significant compared to conventional hydrocarbon reservoirs in the
656 Norwegian Sea (e.g. the Ormen Lange field with about 439 GSm³). However, the resource density is
657 rather low, so future economic exploitation is unlikely.

658

659 **6. Offshore Ireland**

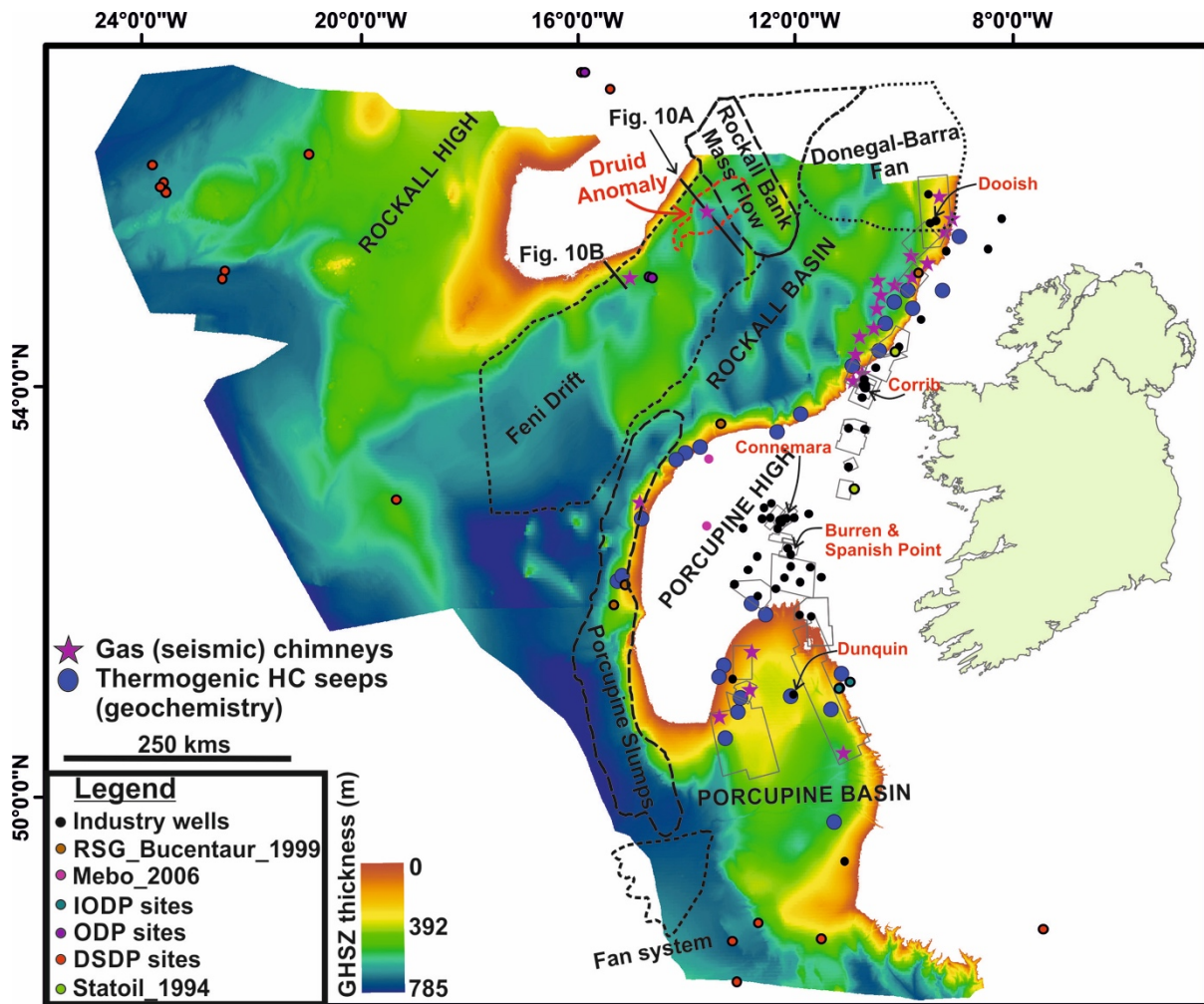
660 6.1 Geological Setting

661 The continental margin offshore Ireland bears the imprints and structures resulting from Variscan,
662 Caledonian and older orogenic events (Naylor and Shannon, 2011). The nature of the basement
663 successions, together with their inherent lineaments and structural fabrics, had a major influence on the
664 location and structural segmentation of the basins. Basins of various geometries, sizes and ages, filled
665 with thick Cenozoic successions, occur in the western Irish Atlantic shelf, in water depths of 400 m to
666 more than 4500 m. Four kilometres of Cenozoic strata occur in the Porcupine Basin and up to 2 km
667 have been identified on seismic profiles in the Rockall Basin (Shannon et al., 1993). Fluid flow within
668 the basins is likely to have been controlled by the overall basin geometry and by the distribution and
669 linkage of permeable strata with fault systems and unconformities. Active petroleum systems in the
670 Rockall and Porcupine basins have been documented by oil and gas exploration since the 1970s.

671

672 Potential source rocks include the Upper Carboniferous, Middle and Upper Jurassic successions, which
673 are generally mature throughout these basins. The Cretaceous and Cenozoic successions also have some
674 potential for oil and gas generation. The Kimmeridgian succession (Upper Jurassic) is a good proven
675 source rock that is well distributed in the Porcupine Basin. It has total organic carbon (TOC) values of
676 3 - 4%. The Lower Cretaceous succession has TOC values of 1.8 – 2.7% (Naylor and Shannon, 2011).
677 The Dooish gas condensate discovery on the eastern margin of the Rockall Basin demonstrates the
678 presence there of a thermogenic petroleum system. Middle Jurassic lacustrine mudstone is anticipated

679 as a potential source as in the Porcupine Basin. Other source rocks are the Lower Cretaceous with TOC
 680 values of 3-14%, and Albian lacustrine mudstones with TOC values of 2.04% (Hitchen, 2004).



681
 682 Figure 9: Calculated HSZ of Irish basins, for pure methane and 3.5% salinity and using seabed
 683 temperature from a compilation of oceanographic data and a geothermal gradient of 30-35°C/km (Roy
 684 et al., 2017). Also shown are locations of 3D seismic cubes, boreholes, gas chimneys, hydrocarbon
 685 (HC) seeps, and proven hydrocarbon systems (text in red).
 686

687 6.2 Hydrate Occurrence

688 High resolution bathymetric data (100 m resolution), seabed temperature from 4760 CTD casts, and
 689 geothermal data from four boreholes have been used to calculate the HSZ offshore western Ireland (Roy
 690 and Max, 2018; Fig. 9). An extensive set of geophysical and geological data was integrated for the
 691 assessment of lithology, migration pathways of natural gas-saturated water in the form of chimney
 692 structures (Van Rensbergen et al., 2005b), presence of source rocks or conventional reservoirs, as well
 693 as host rocks for hydrate within its stability zone. A brief summary of the datasets used is provided
 694 below, with locations shown in Fig. 9:

- 695 a) Industry scale exploration data: 31 2D multichannel seismic surveys, 11 3D seismic cubes, and
- 696 18 exploration wells drilled within the HSZ.

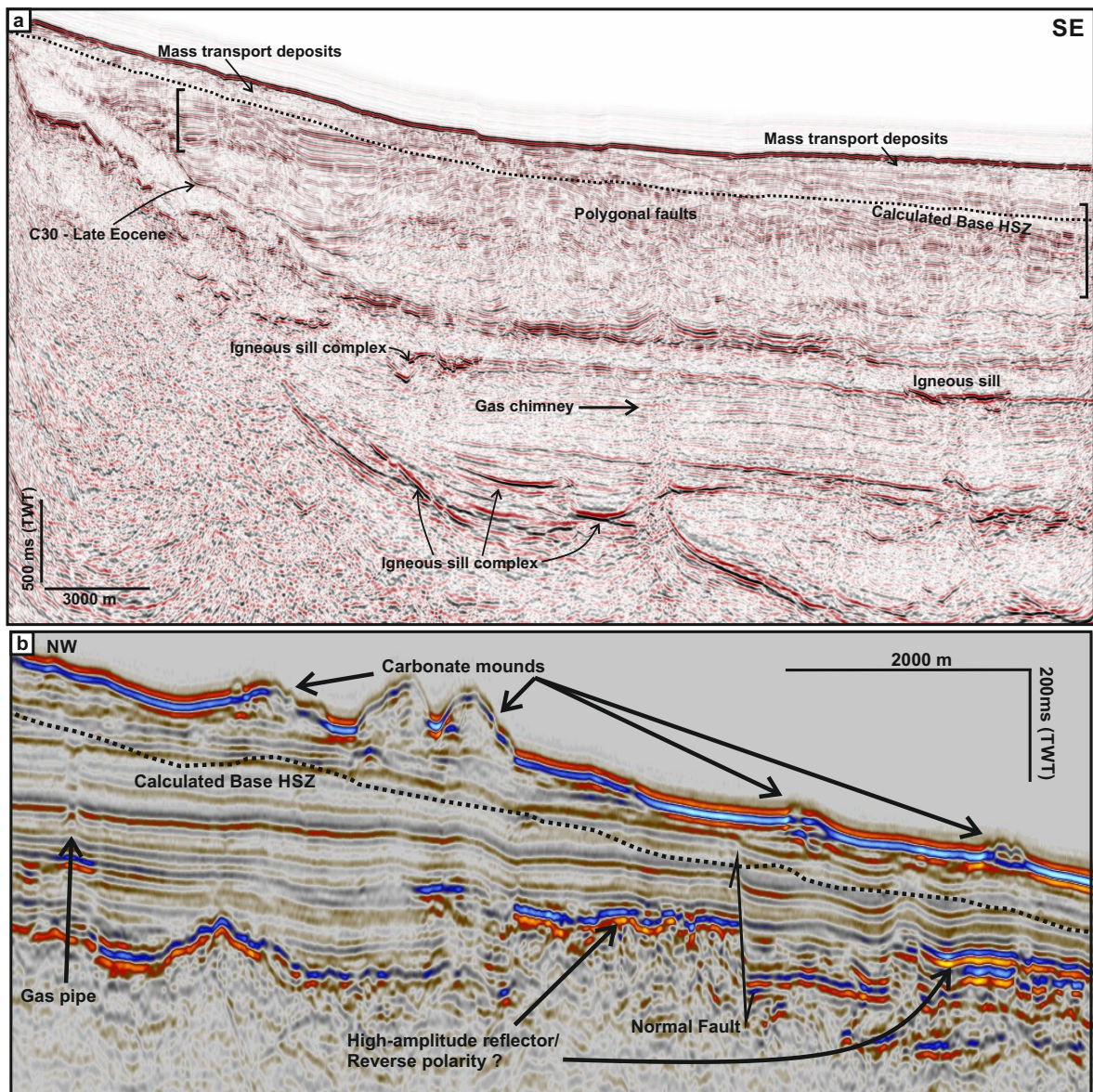
- 697 b) Scientific drilling campaigns: Integrated Ocean Drilling Programme (2 sites), Ocean Drilling
698 Programme (2 sites) and 12 Deep Sea Drilling Project (12 sites) within the HSZ.
699 c) Shallow drilling campaigns: Statoil 1994 (1 site), Rockall Study Group Bucentaur 1999 (3
700 sites), and Mebo 2006 (1 site).

701 The HSZ extends up to 645 m below the seafloor in the Rockall Basin, and 784 m in Porcupine Basin
702 (Fig. 9). Fluid escape features, gas chimneys, bright spots indicating shallow gas accumulations, and
703 faults that act as pathways for fluid migration, have been interpreted above potential source rocks and
704 active petroleum systems. Three types of depositional systems have been identified as potential hosts
705 for hydrate accumulations in Irish basins:

- 706 a) Mass transport deposits (MTDs): Slope failures are widespread along both the western and
707 eastern margins of the Rockall Basin. Sidescan sonar images show a broad interplay of along-
708 slope and downslope sediment transport, with sediment sourced from the northeastern margin
709 and redistributed by currents along the western margin (Unnithan et al., 2001). Along the
710 western margin, the Rockall Bank Mass Flow is a large, multi-phase submarine slope failure
711 comprising of several MTDs, with failure scarps extending over *c.* 6100 km². It lies upslope a
712 series of mass flow lobes covering *c.* 18,000 km² of the Rockall Basin seafloor (Elliott et al.,
713 2010). Low- to medium-porosity turbidites have been found in shallow gravity cores of the
714 lobes, which could be ideal hydrate reservoirs (Roy and Max, 2018).
- 715 b) Feni contourite drift: The Feni drift lies along the northwest flank of Rockall Basin, formed
716 under the influence of deep, geostrophic currents formed by intermittent overflows of Arctic
717 Intermediate Water from the Norwegian Sea. Sites 980 and 981 from ODP Leg 162 are located
718 on the Feni Drift sediments. It is predominantly composed of rapidly accumulated nanofossil
719 oozes with variable amounts of clay and silt. The lithology of Feni Drift is similar to that of
720 Blake Ridge sediments but bed differentiation may be better. Extensive fluid escape features
721 from deeper Lower Jurassic source rocks extend over an area \sim 2000 km², known as the Druid
722 Anomaly (Fig. 9). Gas chimneys terminate beneath polygonal faults observed partly within the
723 HSZ, which has an average thickness of 225 m (Roy and Max, 2017; Fig. 10).
- 724 c) Turbidite and contourite deposits: Isolated sand bodies, contourite furrows (erosional features),
725 and turbidite channel systems have been mapped from 3D seismic data within the HSZ in the
726 Porcupine Basin (Roy and Max, 2018). Associated gas chimneys and fault systems mark
727 upwelling fluid migration from deeper sources to these potential hydrate reservoirs.

728 BSRs have not been identified in the Irish basins. A reason for the absence of a BSR in the available
729 seismic data could be that these data were processed to better identify deeper structural and
730 stratigraphic geological traps. The processing sequence may have obscured shallower structures.
731 Various seismic amplitude anomalies (e.g., bright spots, seismic gas pipes and chimneys, reverse
732 polarity) have been observed in close proximity to the calculated base of the HSZ (Fig. 10b). Possible

733 BSRs have been documented within contourite deposits in the southern and central parts of Porcupine
 734 Basin, at water depths of 1500 - 2200 m (Roy and Max, 2018).



735 Figure 10: a) Seismic reflection profile showing gas chimney (part of the Druid anomaly) in the Rockall
 736 Basin, originating from potential source rock, with polygonal faults, sill complexes, mass transport
 737 deposits (Rockall Mass Flow), and C30 late Eocene unconformity (Roy et al., 2017). The extent of
 738 polygonal faults, which extend into the HSZ in the southeast, is shown by square brackets. These faults
 739 could act as potential fluid migration pathways for deeper fluids to reach the HSZ (interpolated from
 740 the grid of Fig. 9). b) Interpretation of suspected shallow gas accumulation (enhanced high-amplitude
 741 reflections) beneath the calculated base of HSZ, and fluid migration pathways such as gas pipes and
 742 normal faults in Rockall Basin. Locations are marked in Fig. 9.

744

745 **7. Northwest Iberian Margin**

746 7.1 Geological Setting

747 The northwest Iberia continental margin developed during the northward propagation of the North
748 Atlantic Ocean rift system (Boillot, 1995; Boillot et al., 1979; Pérez-Gussinyé and Reston, 2001).
749 Several extensional phases from the Triassic to the Early Cretaceous lead to a complex fault system
750 formed by north-south to northwest-southeast normal faults and northeast-southwest to east-west
751 transfer faults (Pinheiro et al., 1996; Wilson et al., 1989). North-south compression during the Alpine
752 orogeny resulted in the reactivation and partial inversion of previous rift structures and the generation
753 of new compressional structures (Murillas et al., 1990; Pinheiro et al., 1996; Vázquez et al., 2008).

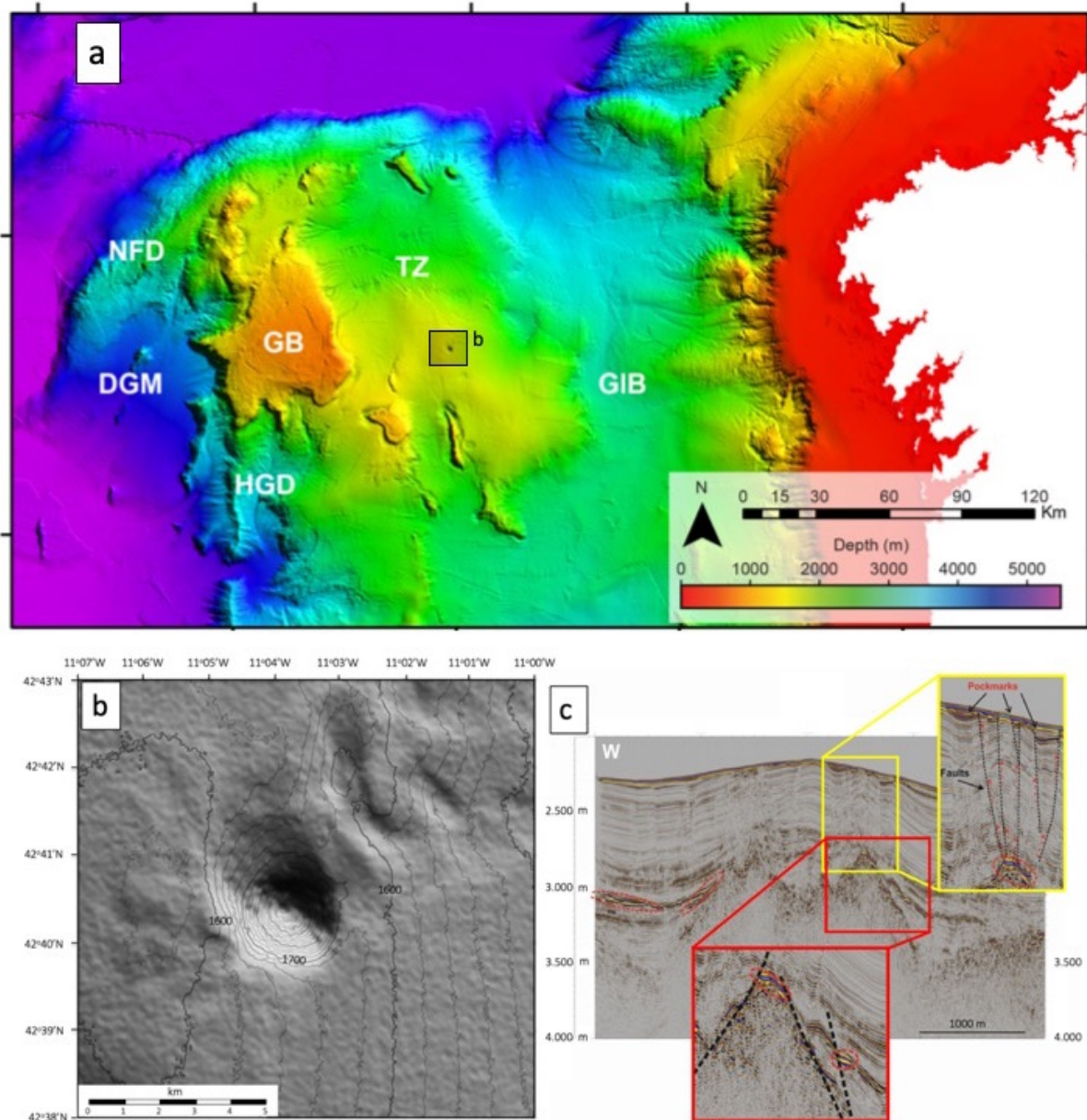
754

755 The present-day northwest Iberia continental margin is characterised by a roughly north-south, ~40 km
756 wide continental shelf and a relatively steep slope down to ~2000 m water depth. Beyond the continental
757 slope, the continental margin can be divided into three main geomorphological provinces (Fig. 11;
758 Reston, 2005): 1) the Galicia Interior Basin (GIB); 2) the Western Banks – an area of seamounts that
759 includes the Galicia Bank; and 3) the Deep Galicia Margin (DGM). The sedimentary cover ranges from
760 0 to 4 km, with maximum thickness in the Galicia Interior Basin depocenter (Pérez-Gussinyé et al.,
761 2003).

762

763 7.3 Hydrate Occurrence

764 The data available for determining the likelihood of methane hydrate stability and presence on the
765 northwest Iberia margin come from diverse sources of varying resolution. Bathymetry data with a
766 minimum 250 x 250 m resolution are publicly available on the EMODnet bathymetry data portal (
767 EMODnet Bathymetry Consortium, 2016). A higher resolution bathymetric grid (100 x100 m)
768 compiled by the Spanish Naval Hydrographic Institute has limited public availability (Druet et al., 2018;
769 Maestro et al., 2018; Somoza et al., 2014). Only two research cruises have been focused on shallow gas
770 occurrence there (Rey and Gran Burato Science Team, 2010, 2011). These cruises acquired high-
771 resolution multichannel and very-high-resolution single channel (3.5 kHz) seismic data and multibeam
772 data to characterise three giant pockmarks depressions in the Transitional Zone (Fig. 11) between the
773 highly thinned crust of the Galicia Interior Basin and the relatively unthinned crust of the Galicia Bank.



774

775 **Figure 11:** a) Bathymetry of the northwest Iberian Margin. GIB: Galicia Interior Basin, TZ:
 776 Transitional Zone, GB: Galicia Bank, NFD: Northwest Flank Domain, DGM: Deep Galicia Margin,
 777 HGD: Half-graben Domain. Note the three large circular structures in the Transitional Zone; b) Detail
 778 of the Gran Burato (GB) giant pockmark (after Druet, 2015) corresponding to grey square in a); c)
 779 Seismic line located south of the Gran Burato pockmark in b) showing how amplitude anomalies
 780 (circled in red) sourced fluid activity (after Ribeiro, 2011).

781

782 Evidence for shallow gas in the proximal northwest Iberia continental margin has been described since
 783 the early 2000s (Durán et al., 2007; Ferrín et al., 2003; García-García et al., 2003; García-Gil et al.,
 784 2015). However, the possibility of hydrate occurrence did not emerge until a decade later based on the
 785 presence of several seabed features related to fluid escape imaged in the Transitional Zone (Druet, 2015;
 786 Ercilla et al., 2011; López Pérez et al., 2019; Ribeiro, 2011). Some of the fluid escape structures have
 787 a seafloor expression (e.g., pockmarks), while others were detected by seismic amplitude anomalies.

788 Pockmarks were identified with a wide range of size and depths, on almost all the seismic profiles
789 acquired in the Transitional Zone (Rey and Gran Burato Science Team, 2010, 2011; Ribeiro, 2011).
790 The three biggest pockmarks, in water depths of 1600-1850 m, correspond to semicircular depressions
791 that have depths up to 375 m and diameters between 2 and 5 km. A detailed study of the Gran Burato
792 (Fig. 11b), the northernmost and largest pockmark in the Transitional Zone, showed evidence for fluid
793 (most likely gas) migration and accumulation in both deep and shallow stratigraphic units (Ribeiro,
794 2011). Additionally, two fields of medium-size pockmarks with a density of more than five pockmarks
795 per square kilometer were described (Rey and Gran Burato Science Team, 2011). Stratigraphic analysis
796 of seismic data suggests that some these pockmarks are related to middle Miocene to Quaternary
797 sedimentary units. Some of the pockmarks still appear to be active (Ribeiro, 2011). The most recent
798 and intense fluid escape takes place in the northernmost sector. An estimate of the HSZ based on the
799 regional geothermal gradient suggests widespread hydrate stability in the area (Rey and Gran Burato
800 Science Team, 2011).

801

802 Various seismic amplitude anomalies (e.g., areas of seismic blanking, bright spots, chimney structures)
803 have been identified close to the pockmark fields and are interpreted as evidence of gas presence within
804 the sediments (Ribeiro, 2011). Fig. 11c shows high-amplitude anomalies on a structural high that pinch
805 out against faults. Pockmarks observed immediately above may result from extensive structurally
806 controlled fluid seepage via faults and fractures (Ribeiro, 2011). A high-amplitude reflector that mimics
807 the seabed was observed in some seismic profiles at the estimated hydrate phase boundary depth, but
808 the polarity inversion typically associated with BSRs could not be identified, so its origin remains
809 uncertain (Rey and Gran Burato Science Team, 2011).

810

811 Analysis of sediment samples from piston cores collected close to the Gran Burato were inconclusive
812 (Rey and Gran Burato Science Team, 2011). Some signs of liquefaction were observed in one piston
813 core, but no associated thermal anomalies were registered, though long core travel times may have
814 attenuated such anomalies. Also, no evidence for chlorinity anomalies or significant sulphate depletion
815 was reported (Rey and Gran Burato Science Team, 2010, 2011). Benthic fauna associated with gas
816 seepage were reported, although the observed species are not exclusive to these environments.

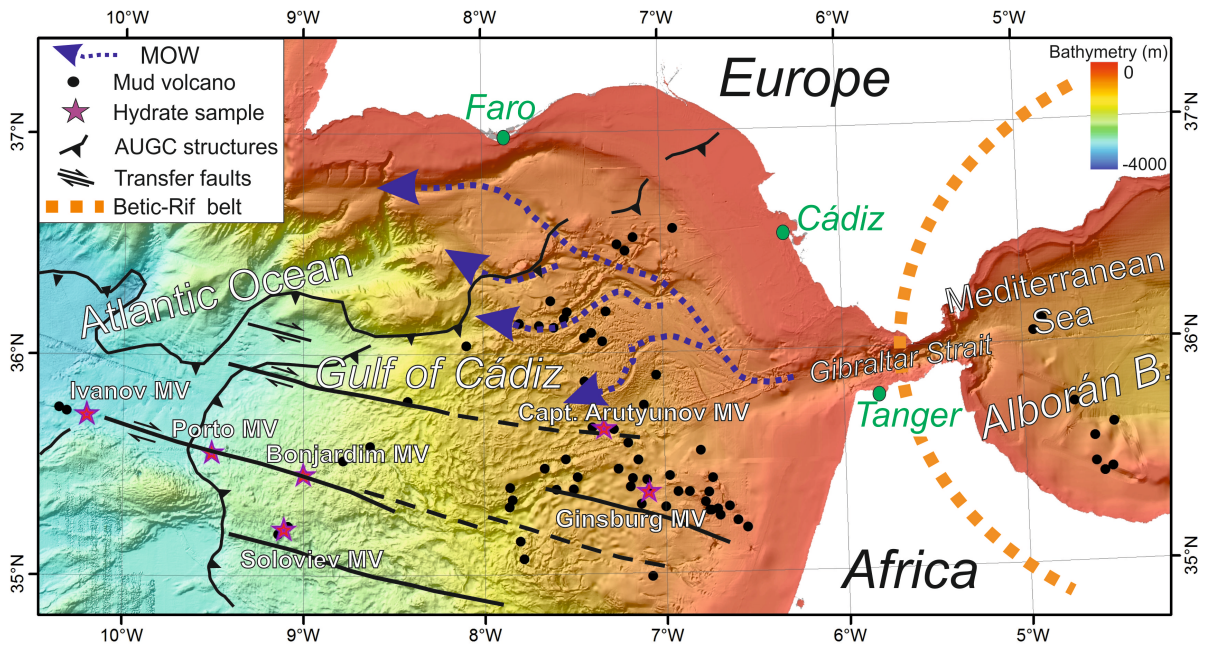
817

818 **8. South Iberia and Northwest African Margin**

819 8.1 Geological Setting

820 The South Iberia and Northwest Africa margins are located in the context of the Betic–Rif orogen either
821 side of the Gibraltar Strait: the Gulf of Cádiz (Eastern Atlantic) and Alborán Sea basin (Western
822 Mediterranean) (Fig. 12). The Atlantic margins of the Gulf of Cádiz were formed during Mesozoic
823 rifting close to the boundary between the Central and North Atlantic. From the late Oligocene to the
824 early Tortonian, these margins were deformed by north-south convergence between the African and

825 Eurasian plates due to the westward drift of the Alborán Domain and development of the Betic-Rif belt
 826 (Platt et al., 2003). Simultaneously the Alborán Basin was developed by extensional normal faulting
 827 and crustal thinning in the back-arc area of the Alborán Domain. Northwest-southeast convergence
 828 caused a post-Tortonian compressive regime that produced the progressive inversion of the basin, Betic-
 829 Rif range uplift, two sets of strike-slip faults, reverse faults and folds (Estrada et al., 2018; Martínez-
 830 García et al., 2017). There was subsequent mud diapirism and related mud volcanism and the formation
 831 of pockmark fields (Pérez-Belzuz et al., 1997; Somoza et al., 2012), which occur mainly in the western
 832 part of the Alborán Basin (Pérez-Belzuz et al., 1997).



833
 834 Figure 12. Bathymetry of the South Iberia and Northwest Africa margins. Arrows mark flow directions
 835 of Mediterranean outflow water. Stars mark mud volcanoes (MV) at which hydrate has been sampled.
 836 Black dots mark other mud volcanoes. The boundaries of the Allochthonous Unit of the Gulf of Cádiz
 837 (AUGC) are modified from Medialdea et al. (2009). Black lines mark southwest Iberia Margin (SWIM)
 838 faults (dashed where discontinuous).

839
 840 In the Gulf of Cádiz, the westward migration of the Alborán Domain forced the emplacement of a large
 841 tectono-sedimentary allochthonous unit in the continental margin and oceanic realm of the Gulf of
 842 Cádiz, generally known as the allochthonous unit of the Gulf of Cádiz (AUGC) (Medialdea et al., 2009).
 843 The AUGC is responsible for diapirism of huge volumes of mud and salt of Triassic units and also for
 844 under-compacted early to middle Miocene plastic marls and shales (Fernandez-Puga et al., 2007;
 845 Maldonado et al., 1999; Medialdea et al., 2009). Numerous seabed fluid escape structures result from
 846 this diapirism, including mud volcanoes, of which some bear hydrate (León et al., 2012; Mazurenko et
 847 al., 2002; Pinheiro et al., 2003; Somoza et al., 2003; Van Rensbergen et al., 2005a), hydrocarbon-
 848 derived authigenic carbonate (HDAC)-bearing chimneys (Diaz-del-Rio et al., 2003; Magalhaes et al.,
 849 2012; Palomino et al., 2016) and pockmarks (Baraza and Ercilla, 1996; León et al., 2014; León et al.,
 850 2010; León et al., 2006). The distribution of these fluid migration and escape structures is also related

851 to the arcuate wedge and the west-northwest to east-southeast SWIM transcurrent fault system (Fig.
852 12; Hensen et al., 2015). The deeper mud volcanoes (2500-4500 m water depth), located in the
853 Southwest Iberia Margin segment of the Gulf of Cádiz area, are closely linked to the presence of the
854 active strike-slip SWIM faults, which provide pathways for deep-seated fluids sourced from oceanic
855 crust older than 140 Ma (Hensen et al., 2015). A local and discontinuous BSR has been observed only
856 in the upper slope (between 200 and 400 m water depth) on the Iberian margin of the Gulf (Casas et al.,
857 2003) and within a mud volcano in the Moroccan slope (Depreiter et al., 2005). Hydrate and
858 hydrocarbon gases sampled from mud volcano sediments include both microbial and thermogenic
859 components (Mazurenko et al., 2002; Stadnitskaia et al., 2006).

860

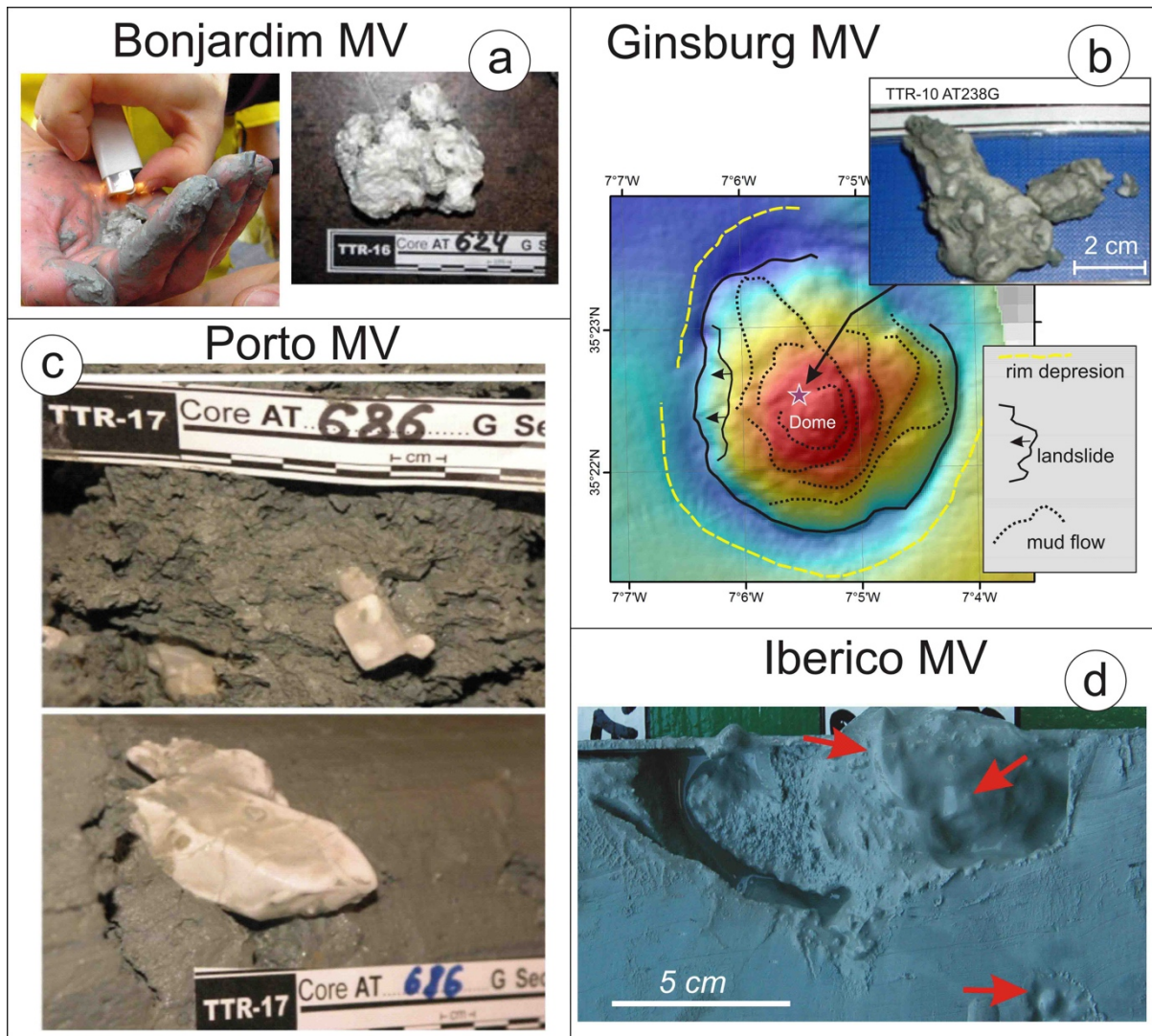
861 8.2 Hydrate Occurrence

862 Direct evidence for hydrate in the Gulf of Cádiz has been detected only in association with the mud
863 volcanoes. The first sample was recovered in 1999 at the Ginsburg mud volcano (Gardner, 2001;
864 Mazurenko et al., 2002). Subsequent work confirmed the presence of hydrate in six other mud volcanoes
865 at 930-4500 m water depth (Hensen et al., 2015; Mazurenko et al., 2002; Pinheiro et al., 2003; Fig. 12).
866 Hydrate appears in various morpho-stratigraphical types, including a tabular shape of irregular
867 thickness (up to 1-2 mm), forming layers within the sediment; or isometric sub-rounded aggregates or
868 individual clast-like occurrences, from millimetre size to several centimetres. The biggest samples (>
869 5cm) have been recovered in the Porto and Michael Ivanov mud volcanoes (Hensen et al., 2015). They
870 comprise disseminated clasts inside a homogeneous mud breccia of grey or dark grey color, saturated
871 in gas and with a porous structure resulting of degasification. In some of the mud volcanoes (e.g.
872 Ginsburg and Captain Arutyunov), based on chlorinity anomalies in sediment cores, hydrate content
873 can reach 3-16% of the sediment volume and 5-31% of the pore space volume (Mazurenko et al., 2002).
874 Hydrocarbon gases from gravity cores collected from Ginsburg mud volcano indicate allochthonous
875 natural gases of thermogenic origin, with 81% methane and 19% higher hydrocarbons (Mazurenko et
876 al., 2002; Stadnitskaia et al., 2006). The ratio iso-C₄/n-C₄ points to focused fluid flow as the principal
877 mechanism of gas migration (Stadnitskaia et al., 2006). Differences in the composition of hydrocarbon
878 gases between the deep Portuguese margin and the Atlantic Morocco middle continental slope suggest
879 two groups with distinctive fluid venting environments and geochemical behavior/properties of
880 migrating fluids, resulting from a complex of secondary migrated, microbially altered and mixed
881 hydrocarbons (Stadnitskaia et al., 2006).

882

883 Indirect evidence for hydrate has been found in other mud volcanoes and mud mounds in the Gulf of
884 Cádiz. The most common indirect evidence is liquefied and degassing structures in the mud breccia
885 sediments (Fig. 13). These structures have been detected in most mud volcanoes below 1000 m water
886 depth and in some carbonate mounds such as Cornide. In the Alborán Sea, degassing structures have
887 been detected only in one gravity core from the Carmen mud volcano. Coherent reversed-polarity

888 reflections beneath the slopes of mud volcanoes, interpreted as BSRs have been detected in the Atlantic
 889 Moroccan margin below Mercator mud volcano (Depreiter et al., 2005). Similar reflections that are
 890 quasi-parallel to the seafloor and interpreted as BSRs have been detected in seismic profiles from the
 891 Portuguese continental upper slope seaward the city of Faro. Finally, the presence of chloride ion
 892 concentrations below 450 mM, indicating the presence of dissociated hydrate (Hesse and Harrison,
 893 1981), has been detected in the hydrate-bearing mud volcanoes, as well as in the Yuma, Carlos Ribeiro
 894 and Olenin mud volcanoes, where hydrate was not recovered (Mazurenko et al., 2002).



895
 896 Figure 13. Direct and indirect hydrate evidence of the South Iberia and Northwest Africa margins. a)
 897 Hydrate sample from the Bonjardim mud volcano (AT624 from Akhmetzhanov et al., 2008); b)
 898 Bathymetry and geological interpretation of the Ginsburg mud volcano (modified from Toyos et al.,
 899 2016) with the location of the first hydrate sample recovered in the Gulf of Cádiz (AT238G from
 900 Kenyon et al., 2001); c) Hydrate crystals from a gravity core at Porto mud volcano (Ivanov et al., 2010);
 901 d) Liquefied structures (red arrows) inferred to represent hydrate dissociation in a gravity core from
 902 Ibérico mud volcano (Leon, 2007).
 903

904 Thus, hydrate in the Gulf of Cádiz seems to be present in localised deposits and hosted in fine-grained
 905 sediments with low permeability, although the thickness and extent of hydrate present are poorly

906 known. This type of occurrence cannot be considered to be of significant resource potential. No hydrate
907 has been detected in any other geological features, such as pockmarks in the Gulf of Cádiz, nor in the
908 Estremadura Spur of the west Iberia margin (Duarte et al., 2017). Hydrate indications are also absent in
909 the sandy or muddy contourite deposits of the continental slope of the Gulf of Cádiz. The lack of hydrate
910 evidence in pockmarks could also be related to the insufficient data collected on these sites. HDACs
911 recovered in pockmarks show an isotopic composition (depletion in $\delta^{13}\text{C}$ and enrichment in $\delta^{18}\text{O}$)
912 compatible with possible past massive hydrate dissociation episodes (Diaz-del-Rio et al., 2003).

913

914 Moreover, the BSRs that were identified occur only locally, without regional continuity, and in close
915 association with fluid escape areas (Casas et al., 2003; Depreiter et al., 2005). In multichannel seismic
916 profiles, areas of blanking and amplitude anomalies below pockmark fields, collapse structures and
917 mud volcanoes reflect the presence of fluids (very possibly hydrocarbon fluids) in the sediment column
918 (Medialdea et al., 2009). Suitable reservoirs for hydrate, comprising thick sandy contourite deposits
919 generated by the Mediterranean outflow water (MOW), exist in the Gulf of Cádiz at 400-1200 m water
920 depth. However, this water mass warms the seafloor and results in variation of the hydrate stability field
921 through time. Global sea-level changes and subsequent episodic warming by the MOW undercurrents
922 are the most plausible scenarios for massive hydrate dissociation in the Gulf of Cádiz during the
923 Quaternary (León et al., 2010). Thus, hydrate could extend beyond the seabed fluid escape structures
924 where it has been observed, and ultimately the amount of hydrate present is unknown.

925

926 Although hydrate has not been sampled in the mud volcanoes of the Alborán Sea, their presence has
927 been proposed due to indirect evidence from some mud volcano structures (e.g., Blinova et al., 2011).
928 Here, hydrate occurrence was inferred from the large gas release during core sampling. Pore water
929 geochemistry provided further evidence, with a 160 to 600 mMol chlorinity anomaly. The gas was
930 inferred to be thermogenic and from a deep (around 5 km) source (Blinova et al., 2011).

931

932 **9. Eastern Mediterranean**

933 9.1 Geological Setting

934 The Eastern Mediterranean Sea (Fig. 14) is a diverse composite of tectonic elements, which evolved
935 through the Mesozoic formation and fragmentation of the northern passive margin of Gondwanaland
936 and subsequent collision with Eurasia to form a subduction and accretionary complex (e.g., Garfunkel,
937 2004). An increasing supply of clastic sediments since the Oligocene formed the extensive present-day
938 Nile fan, extending into the Herodotus and Levant basins and reaching thicknesses of >8 km
939 (Macgregor, 2012). Restricted connectivity with the Atlantic Ocean during the Messinian salinity crisis
940 resulted in the deposition of evaporites across the Mediterranean basin and accumulation of ~2 km of
941 salt within the Levant and Herodotus basins (CIESM, 2008).

942

943 The Eastern Mediterranean Sea is expected to host a significant amount of hydrate (e.g., Merey and
944 Longinos, 2018) because large areas of the seabed are located within the HSZ (Fig. 1). The geological
945 variability of this region offers a variety of potential hydrate depositional environments. The deep-water
946 temperature ranges between 13 and 14 °C (e.g., Zavatarelli and Mellor, 1995), so that hydrate is only
947 stable at water depths of >1000 m (Praeg et al., 2011). The geothermal gradient varies significantly
948 between 20-30 °C/km in the Nile fan and associated deep basins to the south and ~60 °C/km in the
949 Aegean (e.g., Makris and Stobbe, 1984), resulting in a variable sub-seafloor depth of the base HSZ
950 across the area. The Eastern Mediterranean is extremely oligotrophic (Krom et al., 2004). The major
951 potential sources for hydrocarbon formation are Tethyan deposits, late Messinian shallow water
952 deposits and Miocene to recent sapropels and other organic-rich intervals (e.g., Merey and Longinos,
953 2018).

954

955 9.2 Hydrate Occurrence

956 Multiple observations indicate the availability of gas, required for the formation of hydrate, across the
957 seafloor. In particular, numerous mud volcanoes are present, primarily along the accretionary complex
958 and to a lesser degree in the Nile fan (e.g., Mascle et al., 2014; Zitter et al., 2005). Mud volcanoes in
959 the Olimpi Field and at Anaximander Seamount exhibit gas seeps and broad degassing areas, with
960 associated chemosynthetic fauna and authigenic carbonates (Aloisi et al., 2000; Zitter et al., 2005). In
961 both locations, pockmarks have been identified and some of these are filled with brines characterized
962 by high gas content (Dimitrov and Woodside, 2003). The gas seeps have clear thermogenic signatures,
963 indicating deep-rooted fluid expulsion sources (e.g., Pape et al., 2010). Away from mud volcanoes, an
964 abundance of gas, predominantly microbial methane (e.g., Römer et al., 2014; Rubin-Blum et al., 2014),
965 is indicated by a multitude of deep sea seafloor gas seepage features that have been identified over the
966 last two decades across the Nile fan (Dupre et al., 2010; Loncke et al., 2004), Levant basin (Tayber et
967 al., 2019) and Eratosthenes Seamount (Mitchell et al., 2013). These features include gas bubbling,
968 pockmarks, and authigenic carbonates at the seafloor, and a variety of seismic reflection anomalies
969 beneath the seabed, including bright spots and seismic blanking. The scope of known seepage is
970 continuously expanding as new data become available, providing further evidence for the potential for
971 hydrate formation.

972

973 To date, hydrate has been sampled only in several mud volcanoes of the accretionary complex, starting
974 in the Anaximander Seamount region (Fig. 14). These include the Kula mud volcano (Woodside et al.,
975 1997), the nearby Amsterdam, Kazan, Athina, and Thassaloniki mud volcanoes (Lykousis et al., 2009;
976 Pape et al., 2010; Perissoratis et al., 2011), and those in the Olimpi field offshore Crete, including the
977 Napoli, Milano, Maidstone and Moscow mud volcanoes (Fig. 14; e.g., Aloisi et al., 2000). Most hydrate
978 samples are within predominantly relatively fine muddy sediments. In most cases the presence and

979 dissolution of hydrate was indicated by the soupy texture of the sampled sediments (e.g., Lykousis et
980 al., 2009) or their signatures in pore water chlorinity and chemistry (e.g., de Lange and Brumsack,
981 1998a; Pape et al., 2010).

982

983 Analysis of sediments collected at the Mediterranean Ridge (ODP Leg 160, Site 971) suggests locally
984 massive hydrate occurrence at depths of 1 to over 40 m below seafloor across the summit of Milano
985 mud volcano (de Lange and Brumsack, 1998a). Based on a porosity of 60% to 40% (ODP Leg 160,
986 hole 970A), the total amount of methane stored in this mud volcano as hydrate and free gas equal is
987 estimated to be $5 \times 10^9 \text{ m}^3$ (De Lange and Brumsack, 1998b). In contrast, hydrate samples retrieved at
988 Kazan mud volcano had a mm-scale rice-like appearance. Those from the summit of Amsterdam mud
989 volcano occurred as several-cm scale flaky lumps resembling compacted snow, estimated to occupy a
990 volume fraction of 16.7% within the sediment interval between the sulphate base and the maximum
991 sampling depth of 2.5 m (Pape et al., 2010). This estimate is based on the analysis of four pressurized
992 near-surface sediment cores (following e.g., Heeschen et al., 2007). In addition, pore-water analysis
993 was used to assess the upper limit of hydrate stability. Both of the above hydrate morphologies were
994 found on the Thessaloniki mud volcano, but the estimated volume fraction in a single 70-cm autoclave
995 core was only 0.7% (Perissoratis et al., 2011). Lykousis et al. (2009) and Perissoratis et al. (2011) note
996 that on Thassaloniki mud volcano, located at about 1260 m water depth, methane hydrate is present
997 mostly just below the calculated upper limit of the HSZ. Thus, hydrate may dissociate due to small
998 increases in temperature or decreases in pressure or salinity, which might occur due to climate change
999 or local sediment transport.

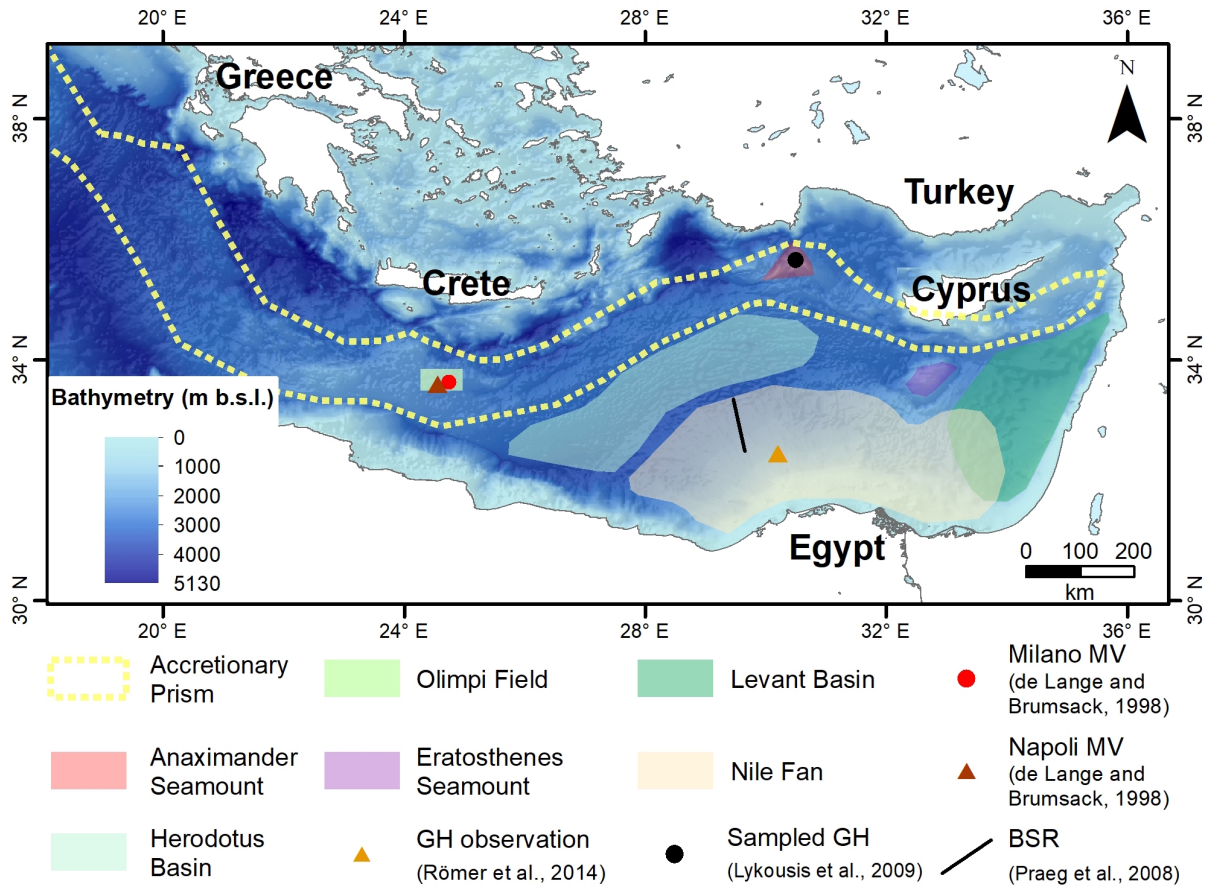
1000

1001 In spite of the broad coverage of the Eastern Mediterranean by 2D and 3D commercial and academic
1002 seismic data, only a single observation of a BSR has been reported (Fig. 14; Praeg et al., 2008; Praeg
1003 et al., 2011). The suggested BSR appears as a discontinuous negative polarity reflection, 220-330 ms
1004 below the seafloor at water depths of 2000–2500 m on the distal part of the western deep sea Nile fan.
1005 If a mean seismic velocity of 1.6-1.8 km/s is assumed above the reflection, its depth agrees well with
1006 the modelled base of the HSZ (Praeg et al., 2017). Direct indications of hydrate stability, and of the
1007 presence of gas within the HSZ, in the Nile deep sea fan were provided by Römer et al. (2014). They
1008 observed formation of hydrate within a funnel during the collection of gas emitted from the seafloor. In
1009 addition, hydrate coating formed on ascending bubbles and dissolved below the modeled top of the
1010 HSZ. This latter result was supported by echo-sounder imaging. Geochemical analyses of vented gas
1011 suggest that it predominantly originates from microbial methanogenesis, with traces of thermogenic
1012 input (Römer et al., 2014).

1013

1014 Based on a statistical analysis of a large 3D dataset covering a significant portion of the Levant basin,
1015 Tayber et al. (2019) suggest that observed scattered high-amplitude reflectivity there marks a pseudo

1016 BSR, representing the presence of hydrate and associated underlying gas within localised sandy buried
 1017 channel systems. Tayber et al. (2019) estimated the hydrate volume associated with these presumed
 1018 accumulations at ~100 Tcf (~3000 GSm³) and its carbon content at ~1.5 Gt.

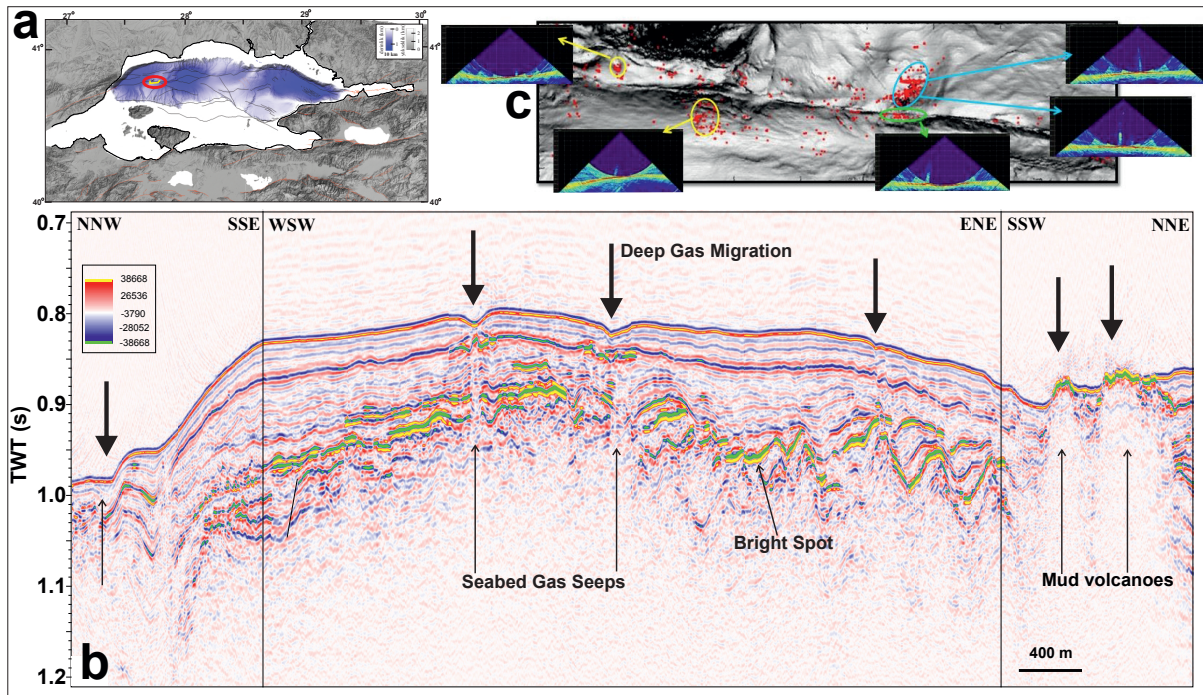


1019 Figure 14: Bathymetry of the Eastern Mediterranean Sea (from <https://www.gmrt.org/GMRTMapTool>)
 1020 with a range of seafloor features (e.g., Mascle et al., 2014). Filled circles mark sites where hydrate has
 1021 been sampled and coloured triangles mark other hydrate indicators, as detailed in the text. Black line
 1022 marks the seismic profile along which Praeg et al. (2008) reported a BSR.
 1023
 1024

1025 10. Sea of Marmara

1026 10.1 Geological Setting

1027 The Sea of Marmara is a pull-apart basin linking the onshore North Anatolian Fault with more
 1028 distributed extensional deformation in the Aegean. The current basin geometry appears to have formed
 1029 since 5 Ma by the rotation of several lithospheric blocks (Armijo et al., 1999). The basin reaches a depth
 1030 of over 1300 m and is subdivided into three sub-basins, from west to east named the Tekirdağ, Central
 1031 and Çınarcık basins, separated by basement highs named the Western and Central High, respectively
 1032 (e.g., Le Pichon et al., 2001). It has been extensively studied over the past two decades because of the
 1033 hazardous active fault system that crosses its centre.



1034
 1035 Figure 15: a) Faults, bathymetry and topography of the Sea of Marmara. Bathymetry is from Rangin et
 1036 al. (2001) and faults from Sorlien et al. (2012). Red circle shows the study area and yellow line inside
 1037 shows the location of the seismic profile in b). b) Seismic reflection profile showing evidence of shallow
 1038 gas (Saritaş et al., 2018). Thick black arrows show gas seeps to seabed. The amount of gas seeps is the
 1039 highest at mud volcano area. Hydrate of thermogenic origin is sampled in the mud volcanoes on the
 1040 western high. High amplitude and reverse polarity bright spots are formed due to gas accumulations. c)
 1041 Seabed morphology of the central Sea of Marmara calculated from 3D seismic data with red dots
 1042 showing gas flares (Saritas, 2013). Yellow circles mark gas seeps from pockmarks, blue circle marks
 1043 seeps from mud volcanoes and green circle marks seeps from the North Anatolian Fault.
 1044

1045 10.2 Hydrate occurrence

1046 Only small areas of the Sea of Marmara are deep enough to fall within the methane HSZ (Fig. 1).
 1047 However, hydrate has been sampled directly (Bourry et al., 2009) on the Western High, where
 1048 indications of sub-seabed fluid escape have been widely observed in seismic profiles around the North
 1049 Anatolian Fault system (e.g., Saritaş et al., 2018; Thomas et al., 2012; Fig. 15). Oil seeps have also been
 1050 observed (Crémière et al., 2012). Unequivocal BSRs have not been observed, but high-amplitude
 1051 reflections with reversed polarity that roughly mimic the seabed were clearly imaged in 2D and 3D
 1052 high-resolution multichannel seismic reflection data (e.g., Thomas et al., 2012). The reflections do not
 1053 cross-cut sedimentary strata, which also roughly parallel the seabed, so they may or may not mark the
 1054 base of the HSZ. They are similar to reflections seen in the Sorokin Trough in the Black Sea (Krastel
 1055 et al., 2003). Mud volcanoes, zones of seismic blanking and chimneys reaching the seabed were also
 1056 clearly imaged, suggesting the presence of abundant free gas in the shallow sedimentary column.

1057
 1058 Gas sampled from hydrate and bubble plumes was predominantly methane, but ethane, propane and i-
 1059 butane were also present, indicating a thermogenic source (Bourry et al., 2009). This thermogenic gas
 1060 may have migrated into shallow sediments via the North Anatolian Fault system from Oligocene to

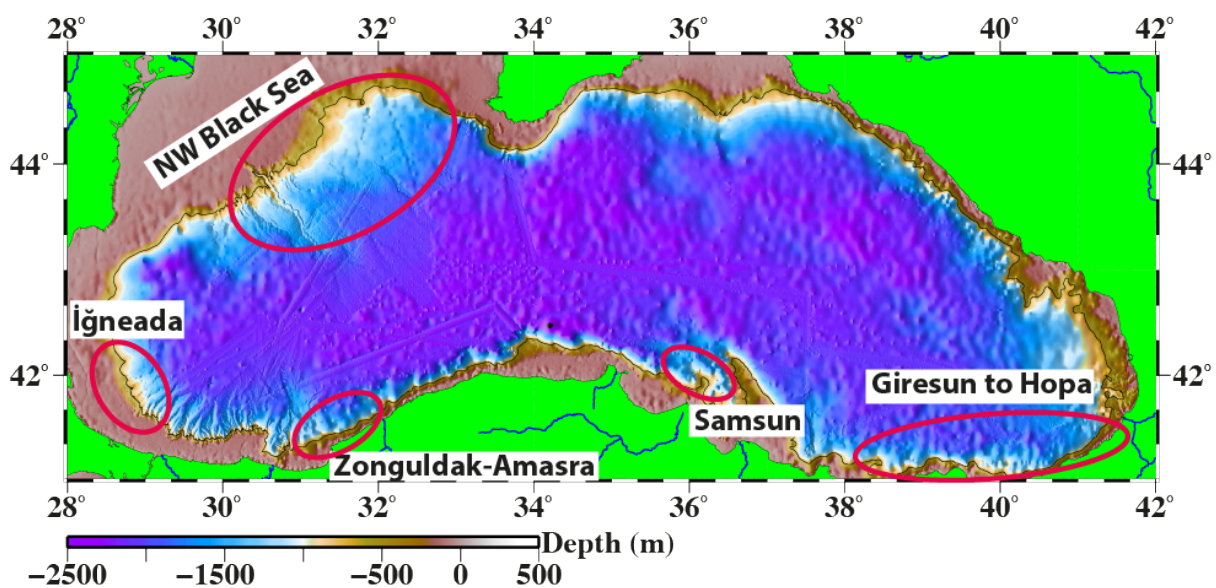
1061 Eocene reservoirs like those in the Thrace basin. Based on the gas compositions observed, both structure
1062 I and structure II hydrate may be present.

1063

1064 11. Black Sea

1065 11.1 Geological Setting

1066 The Black Sea (Fig. 16) is a semi-isolated extensional basin with a maximum water depth of 2212 m.
1067 Its deep waters (87% of the total volume) form the largest anoxic, hydrogen sulphide and methane
1068 reservoirs in the world. The amount of dissolved methane contained in the basin (96 Tg) is 2.4-6 times
1069 greater than the global annual geological methane contribution to the atmosphere (Reeburgh et al.
1070 1991). 91% of its seafloor is within the range of hydrate stability (Vassilev and Dimitrov, 2002), making
1071 the Black Sea an interesting target for a European hydrate field study.



1072

1073 Figure 16: Bathymetry of the Black Sea (Smith and Sandwell, 1997) with study areas described in the
1074 text.

1075

1076 The Black Sea basin is generally thought to have formed in a back-arc environment because of its
1077 spatial association with subduction of both the Paleo- and Neo-Tethys oceans (Letouzey et al., 1977).
1078 The timing and style of this opening history remain controversial, partly because the thick sediment
1079 cover means that the oldest sedimentary fill has not been drilled (e.g., Nikishin et al., 2015;
1080 Zonenshain and Le Pichon, 1986). The Black Sea is subdivided into eastern and western basins
1081 separated by the Mid Black Sea High, a SW-NE system of buried basement ridges (e.g, Nikishin et
1082 al., 2015). Sediments in the Western basin may reach a thickness of up to 19 km (Nikishin et al.,
1083 2003). They include 4-5 km of folded organic-rich Maikopian deposits (Oligocene to lower Miocene)
1084 and 2-3 km of Cenozoic deposits (e.g., Finetti et al., 1988; Nikishin et al., 2015), which become
1085 thinner or disappear on the basin margin. Sediments in the eastern basin are thinner – perhaps only 8-
1086 9 km (Shillington et al., 2008).

1087

1088 11.2 Hydrate occurrence in the western Black Sea

1089 11.2.1 Offshore Romania and Bulgaria

1090 The northwestern Black Sea forms the transition zone between the Moesian Platform in the west,
1091 Scythian Platform in the north and the Western Black Sea Basin in the southeast. Structural styles of
1092 the Moesian and Scythian Platforms, which correspond to the Bulgarian and Romanian-Ukrainian
1093 EEZs, are significantly different. The former is quite structured and features normal faults with tilted
1094 blocks, while the latter is a mosaic of structural styles, with mainly Miocene gravity-driven thrusting,
1095 folding, toe-thrust and growth and tectonic deformation (Bega and Ionescu, 2009).

1096

1097 The northwest margin of the Black Sea (Fig. 17) is made up of the two largest and thickest organic-rich
1098 fan complexes in the Black Sea, the Danube and Dniepr fans, built up by the rivers Danube, Dniepr,
1099 Dniestr and Bug. Sediment deposition and the evolution of these fan systems has been controlled by
1100 climate and sea-level change (e.g., Ryan et al., 1997). The Danube and Dniepr fans developed from a
1101 significant stack of paleo-channels and levee deposits (Popescu et al., 2001; Winguth et al., 2000).
1102 Periodic seabed anoxia made conditions favourable for gas generation, as documented by the presence
1103 of more than 3000 gas plumes in the water column (Egorov et al., 2011), arranged in a circum-Black-
1104 Sea belt of gas flares. The majority of flares occur in water depths shallower than 665 m, which marks
1105 the present-day upper limit of the gas hydrate stability zone in the Black Sea. Exceptions are the
1106 underwater mud volcanoes, generally located in deeper waters, which can expel significant amounts of
1107 fluids, including methane. However, only 1.9% of the total methane escape from the seafloor reaches
1108 the atmosphere (Egorov et al., 2011).

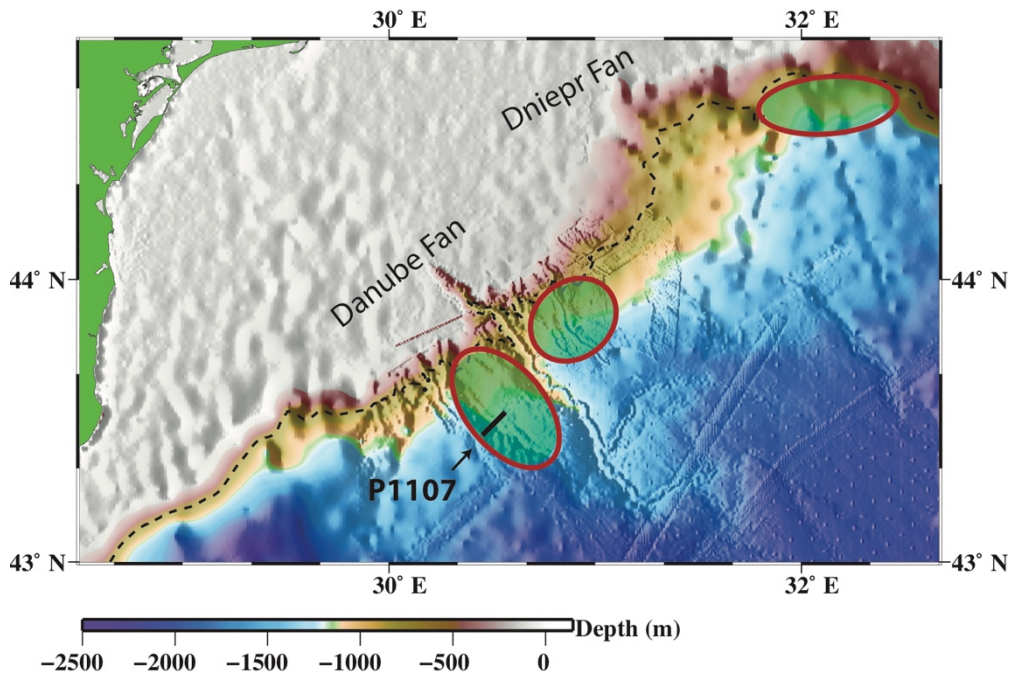
1109

1110 Hydrate was first discovered in the area in a core sample by Yefremova and Zhizchenko (1974), with
1111 the first hydrate sample in the Romanian sector recovered in 2017 (Riboulot et al., 2018). The existence
1112 of hydrate at depth was inferred from BSRs. However their distribution is not continuous and is limited
1113 to a few areas (e.g., Popescu et al., 2007; Zander et al., 2017). Hydrate there is of microbial origin, with
1114 methane $\delta^{13}\text{C}$ values of -84% to -70% and concentrations of 99.1–99.9% (Haeckel et al., 2017).
1115 Organic-rich Maykopian sedimentary deposits are not in a productive state yet and do not provide an
1116 observable thermogenic methane component.

1117

1118 The HSZ in the northwestern Black Sea is coincident with the Danube and Dniepr fans. Hydrate
1119 formation in the levees or channel base of these fans is inferred from the presence of BSRs, for example
1120 in the Danube fan, where multiple BSRs have been observed beneath ancient levee systems (e.g.,
1121 Popescu et al., 2007; Zander et al., 2017; Fig. 18). Zander et al. (2017) inferred that these multiple BSRs
1122 do not reflect gas composition changes or overpressured compartments, but rather past pressure and
1123 temperature conditions. Results from thermal models suggest that temperature changes related to

1124 rapid sediment deposition, rather than bottom-water temperature or sea level variations, have a primary
 1125 influence over the pressure and temperature conditions resulting in the formation of multiple BSRs
 1126 (Zander et al. 2017).

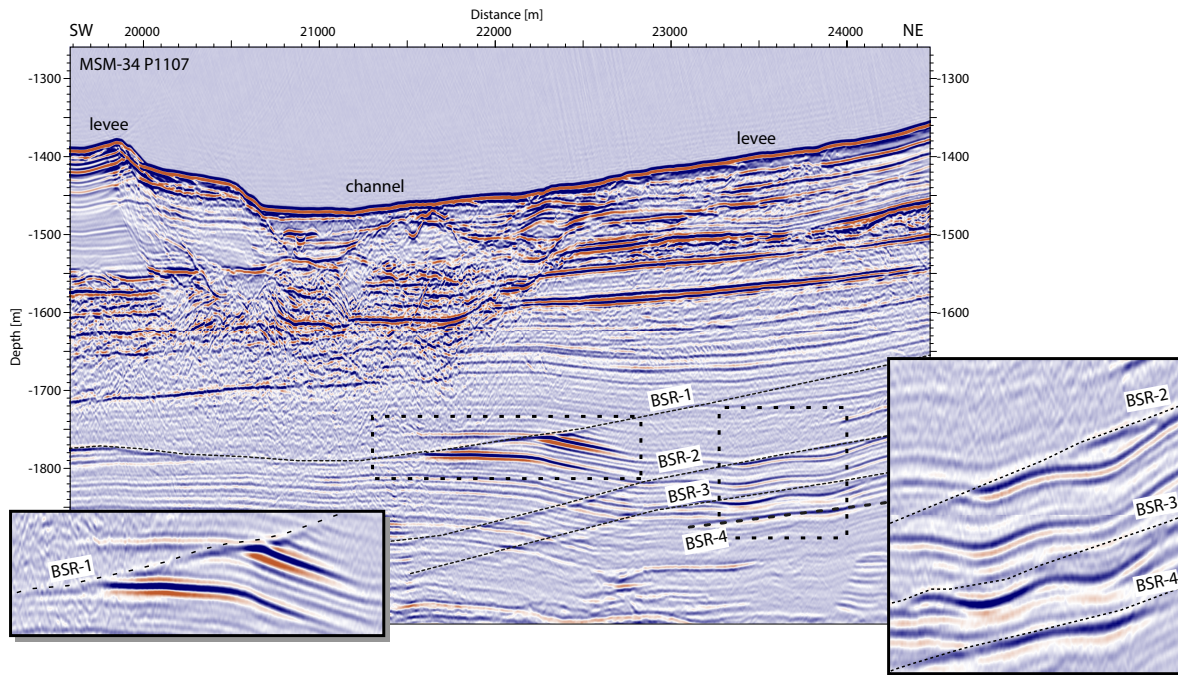


1127
 1128 Figure 17: Bathymetric map of the northwest Black Sea. Background shaded bathymetry from Smith
 1129 and Sandwell (1997) is overlain with shipboard bathymetry compiled by MARUM and GEOMAR.
 1130 Areas with reported gas hydrate indications are marked with shade ellipses. Dashed contour marks the
 1131 upper depth limit of the HSZ at 650 m water depth. Hydrate distribution is derived from Zillmer et al.
 1132 (2005), Popescu et al. (2006), Zander et al. (2017) and Hillman et al. (2018a).
 1133

1134 CSEM data collected across and within the channel levee system shown in Fig. 18 revealed highly
 1135 anomalous resistivity values at various depths within the HSZ, which are partly attributed to lower pore
 1136 water salinities (around 4 ppm; Bohrmann et al., 2018), but also suggest a high hydrate saturation of
 1137 possibly up to 20-30% within the channel filling sediments and below the western levee.
 1138

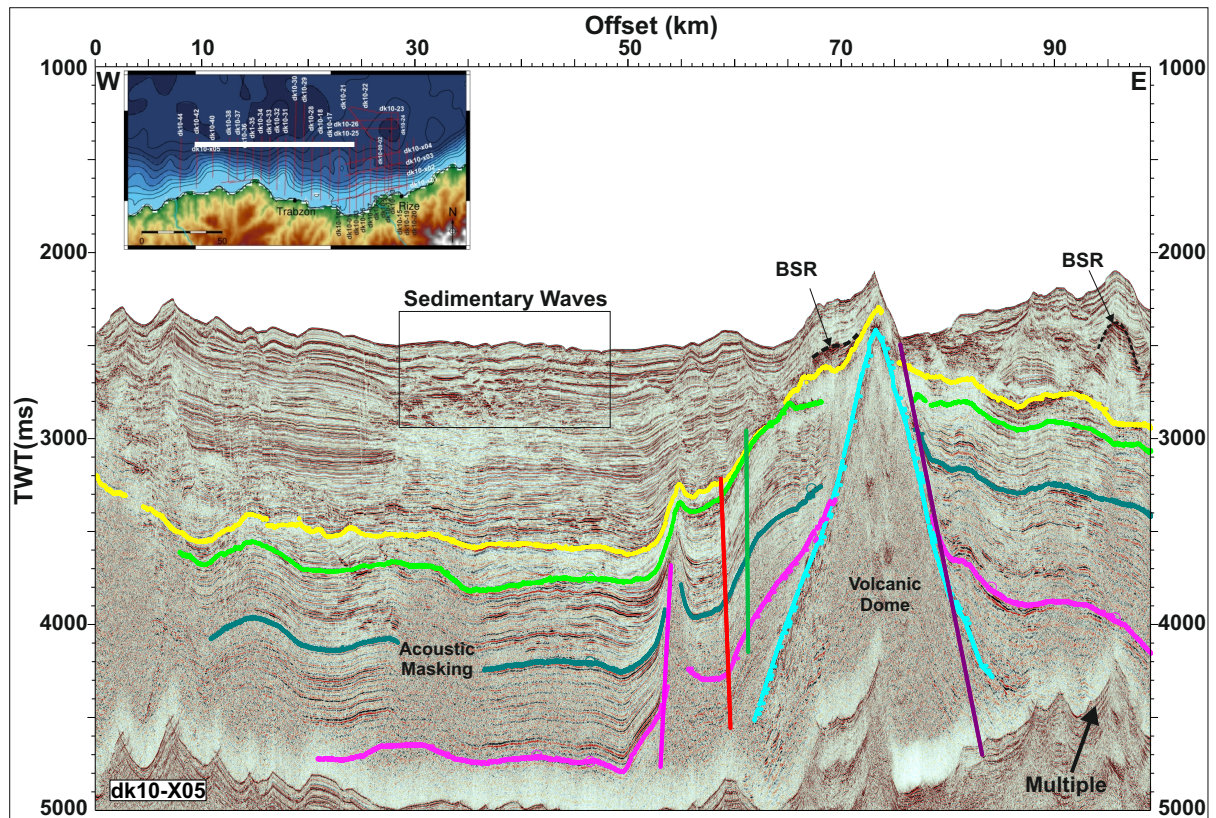
1139 The availability of structural and stratigraphic constraints from deep-penetrating seismic data has
 1140 enabled the development of a basin scale numerical model to investigate the production and migration
 1141 of gas and resulting hydrate distribution (Hillman et al., 2018a). Sediment structure, slope failures and
 1142 distribution of BSRs are imaged on shallow seismic data (Hillman et al., 2018b; Popescu et al., 2007;
 1143 Zander et al., 2017). These data have enabled the development of a stratigraphy for the slope deposits
 1144 and mass transport events inferred from that of Winguth et al. (2000), although in the absence of
 1145 sufficient sediment samples there remains some uncertainty in the dating of these deposits. Dating has
 1146 come from the ASSEMBLAGE project (Lericolais et al., 2013) and DSDP Leg 42 (Stoffers et al., 1978).
 1147 Mapping of active gas seeps using water column imaging, and gas-related structures in seismic profiles,
 1148 have been used to describe the plumbing system in the canyon and levee systems (Hillman et al., 2018b).
 1149 Many of the active gas seeps correlate with sub-seafloor gas migration structures such as chimneys or

1150 pipes. There is an apparent correlation between gas vents and submarine landslide features, but there
 1151 are insufficient data to determine whether gas migration has played a causative role in triggering such
 1152 slope failure events (Hillman et al., 2018b). Changes in climate, resulting in changes in the HSZ, and
 1153 the identification of paleo seafloors, have together been used to explain the origin of the multiple BSRs
 1154 (Zander et al., 2017). Modelling of the HSZ using inputs from 2D and 3D seismic data has indicated
 1155 that the hydrate system may be in a transient state, with factors such as topographic focusing of heat
 1156 flow playing a significant role in controlling the location and distribution of hydrate (Hillman et al.,
 1157 2018a).



1158
 1159 Figure 18: Multichannel seismic data example of today's BSR (BSR 1) and multiple BSR occurrences
 1160 (BSR 2 to 4) in the Danube fan. While BSR 1 extends over the entire channel levee system the multiple
 1161 BSRs disappear towards the channel structure (SUGAR channel). Insets zoom into the BSR events and
 1162 highlight the increased reflection amplitudes where inversion point and termination indicate the BSR
 1163 position. Data acquired during cruise MSM34 (Bialas et al., 2014).
 1164

1165 Seismic velocities from analysis of OBS data were used to provide the first estimates of possible gas
 1166 and hydrate concentrations in the Bulgarian sector of the northwestern Black Sea. The resulting
 1167 velocity-depth sections represent average velocities for sediment packages of about 100 m thickness.
 1168 Estimates of average hydrate saturations in the pore space based on these seismic velocity distributions
 1169 are up to 10% or 30-40%, depending on the hydrate morphology assumed. CSEM data were acquired
 1170 to further investigate gas and hydrate distribution in the sediments. Hydrate saturation estimates derived
 1171 from CSEM datasets depend on the porosity and pore water salinity, and the appropriate choice of
 1172 Archie parameters. These studies suggest saturations in the range of 20-30% in parts of the HSZ. It is
 1173 likely that the highest hydrate saturations are be located within coarser grained, sand-rich sediments in
 1174 the channel systems and intermittently distributed through the levees (Zander et al., 2017).



1175

1176 **Figure 19:** Seismic line parallel to coastline offshore Trabzon area, showing fault related volcanic
 1177 dome structure at the eastern side of the section and a BSR at around 300 ms below the seafloor
 1178 (Gunduz, 2015). The Trabzon fault is a strike-slip fault. Acoustic blanking below the BSR may
 1179 indicate free gas. Acoustic blanking is also present in deeper parts of the section.

1180

1181 11.2.2 Offshore İğneada

1182 Regional seismic data acquired across the continental shelf and slope offshore İğneada (Fig. 16) show
 1183 folded sediments with gas accumulations beneath structural highs, evidenced by seismic blanking
 1184 zones, fluid escape structures and a reef structure (Özel, 2012). Fault systems penetrate the shallow
 1185 sediments beneath these ridges and cross the gas-charged lithologies, suggesting the presence of
 1186 hydrocarbon migration pathways. One profile displays BSRs across the continental slope. However, the
 1187 distribution of hydrate at this site is not well understood due to large inline and cross-line intervals.
 1188 Other profiles show high-amplitude, reversed-polarity reflections that mimic the seabed but do not
 1189 cross-cut stratigraphy, at a depth that is significantly different from that of the unequivocal BSRs. The
 1190 origin of these features remains uncertain. Hydrate was recovered at an acoustically transparent feature
 1191 observed in sub-bottom profiler data that protrudes from beneath the hemipelagic cover, interpreted as
 1192 a mud volcano (Fokin et al., 2005). Numerous carbonate-cemented layers and a mousse-like breccia
 1193 below were also observed.

1194

1195

1196 11.2.3 Offshore Zonguldak-Amasra

1197 The Zonguldak-Amasra area is one of the best-studied in terms of shallow gas and hydrate. Geological
1198 and geophysical investigations, including conventional and high-resolution seismic data, chirp sub-
1199 bottom profiler data, multibeam bathymetry and direct sampling, have shown the presence of gas and
1200 indications of gas hydrate (Küçük et al., 2015). Dissolved gas in the shallow sediments contains
1201 hydrocarbons ranging from methane to hexane, suggesting a thermogenic gas source in addition to
1202 microbial gas in the shallow sediments. Seismic evidence for the presence of seven different mud
1203 volcanoes and a large number of buried and active gas chimneys was found in this region. Widespread
1204 seismic blanking zones were observed also beneath the HSZ, with up to 25 km lateral extent. Chirp
1205 sub-bottom profiler data show many chimney structures in the first 40-50 m below the seabed and sparse
1206 gas anomalies were observed on seismic data in various locations. Both continuous and discontinuous
1207 BSRs have been widely observed at this site. Multiple BSRs were also imaged, with up to five
1208 successive BSRs. These additional BSRs may have a similar origin to those imaged in the Danube fan
1209 (section 11.2.1) or may be attributed to a variety of different gas compositions with different stability
1210 limits. In addition to structure I and structure II hydrate, structure H hydrate might be present at this
1211 site, indicated by the presence of i-Pentane gas in a gas composition similar to that observed in the Gulf
1212 of Mexico (Sassen and MacDonald, 1994).

1213

1214 11.3 Hydrate occurrence in the eastern Black Sea

1215 11.3.1 Offshore Samsun

1216 High-resolution seismic data and sediment cores are available from this region (e.g., Dondurur and
1217 Çifçi, 2009). Indications of shallow gas, such as buried and active pockmarks and seismic blanking
1218 zones, were imaged in seismic data. Here, hydrate may be present at relatively shallow water depth
1219 (250-700 m). Bright reflections on the upper slope have been interpreted as hydrate-bearing
1220 sedimentary units. The presence of hydrate at such shallow water depths could be explained by the
1221 presence of hydrogen sulphide in the gas, which shifts the phase boundary to higher temperatures and
1222 lower pressures (Dondurur and Çifçi, 2009).

1223

1224 11.3.2 Offshore Hopa-Rize-Trabzon-Giresun

1225 Three-dimensional seismic data offshore Hopa show the presence of a widespread BSR that is most
1226 prominent beneath structural highs (Minshull and Keddie, 2010). A dense grid of seismic data offshore
1227 Rize and Trabzon showed widespread indications of shallow gas and gas hydrate (Fig. 19). Chimneys,
1228 seismic blanking zones, gas charged sediments, mud diapirs and mud volcanoes are all present. These
1229 were observed around crustal-scale faults that suggest migration from depth. Both continuous and
1230 discontinuous BSRs have been clearly imaged. No hydrate indicators have been identified in regional
1231 seismic data offshore Giresun.

1232

1233 **12. Discussion**

1234 Although methane hydrate is stable in large areas of European margins, numerical models of microbial
1235 gas generation suggest that significant microbial hydrate accumulations are unlikely to be widespread
1236 (e.g., Archer et al., 2009; Wallmann et al., 2012). This result is a consequence of low predicted organic
1237 carbon accumulation rates in the parts of European margins that are deep enough for hydrate stability.
1238 This prediction is supported by observations of particulate organic carbon concentrations in surface
1239 sediments (Wallmann et al., 2012). Consistent with these modelling considerations, most of the hydrate
1240 occurrences described above are associated with conventional hydrocarbon provinces, and where there
1241 are data available on hydrate-forming gas compositions or isotopic ratios, these data commonly suggest
1242 the presence of gas that is at least partly of thermogenic origin. Direct sampling of hydrate is mostly at
1243 fluid escape features such as pockmarks or mud volcanoes, so we cannot rule out the possibility that
1244 the sample locations are unrepresentative.

1245

1246 Offshore Greenland, the search for hydrate is still at an early stage, although the physical and
1247 oceanographic settings of these margins are perfect for hydrate formation. Investigations suggest a high
1248 potential for oil and gas within out- or shallow sub-cropping sedimentary basins in the west and
1249 northeast Greenland margins. The onshore observations of oil seeps in central west Greenland confirm
1250 the existence of an active hydrocarbon system here and the discovery of onshore hydrate indicates that
1251 gas is migrating from the system and likely forms hydrate. Such gas migration is also suggested by
1252 indirect evidence from seismic and shallow cores offshore. Further offshore on the west Greenland
1253 margin, observed BSRs and seismic blanking may also provide evidence of hydrate occurrence. Thus
1254 it is likely that hydrate is present on the central west Greenland margin and, based on the onshore oil
1255 discoveries, the hydrate could contain a high portion of thermogenic gas. Hydrate has not yet been
1256 reported on the east Greenland margin, which is likely due to the lack of research and wells on this
1257 margin. However, a gas-show in ODP well 909, together with the presence of BSRs and other seismic
1258 indicators, may provide evidence for an active hydrocarbon system forming hydrate in the northeast
1259 Greenland margin.

1260

1261 Offshore Svalbard, the hydrate system has characteristics that may be unique among hydrate systems
1262 worldwide. It stretches from the continental slope onto the mid-ocean ridge, thereby experiencing
1263 significant changes in thermodynamic conditions, and it may be the only hydrate system in the world
1264 that forms from hydrocarbon gas of three different sources, namely microbial, thermogenic and abiotic
1265 gas. However, the relative contribution of each of these sources is still unknown and may show
1266 significant local variations. The structural-stratigraphic development of this area has led to the
1267 formation of distinct sedimentary depocentres and fluid migration pathways, thereby controlling the
1268 distribution of hydrate. At present, the total distribution extends over approximately 4000 km² with the

1269 main accumulation in the Vestnesa Ridge and many smaller patches of hydrate in close vicinity. Yet
1270 large parts of this area remain unmapped and potentially hold much more hydrate if the hypothesized
1271 abiogenic origin of gas in hydrate is confirmed as a potential hydrate play. Nonetheless, current estimates
1272 of hydrate saturations so far are sufficiently low that the economic value of hydrate offshore Svalbard
1273 is questionable.

1274

1275 Onshore Svalbard, on average, the modelled HSZ thickness reaches 300 m, with the thickest zones
1276 extending from about 75 m to up to 725 m below the surface, which are the minimum and maximum
1277 depths at which hydrate is expected to form, based on regionally constrained thermobaric conditions.
1278 Variable pore water salinities, anomalous regional pressure regimes, uncertainties in regional
1279 geothermal gradients and changing temperature conditions put a limit on the model's accuracy further
1280 away from Nordenskiöldland, where regional datasets and constraints afford good control. In addition,
1281 the model takes no account of factors likely to control hydrate presence, such as fluid migration
1282 pathways and local biogeochemistry. The ongoing study of the onshore HSZ in central Spitsbergen and
1283 archipelago-wide is pivotal to the mapping of the potential occurrence of onshore hydrate
1284 accumulations and complements the significant findings made offshore.

1285

1286 The Barents Sea exhibits widespread evidence for thermogenic hydrate occurrence and is a unique
1287 region where hydrate is hosted in consolidated sedimentary formations and likely co-exists with
1288 conventional petroleum reservoirs. Seismic data analysis by Laberg et al. (1998) and patchy BSR
1289 distribution indicate relatively low resource potential, but the free gas trapped beneath the BSR could
1290 still be of commercial interest. Despite increased petroleum exploration activities in recent years,
1291 none of the BSRs identified in the southwest Barents Sea have yet been drilled or sampled. The
1292 presence of hydrate stability conditions within the major shallow reservoirs in the region, however,
1293 has attracted increased attention towards hydrate from commercial exploration companies (Norwegian
1294 Petroleum Directorate, 2018).

1295

1296 On the mid-Norwegian Margin, the BSR only occurs within finely bedded contouritic and
1297 hemipelagic deposits (mainly silty clays) of the Quaternary Naust formation, which seem to be the
1298 favourable host sediments for hydrate. The extent of hydrate is geologically controlled by hydrate
1299 stability conditions that exclude hydrate on the continental shelf, and the availability of the suitable
1300 host rock elsewhere. Bünz et al. (2003) suggest that hydrate on the mid-Norwegian margin develops
1301 from fluids that originate far beneath the HSZ. Deep-seated Cenozoic dome structures with inferred
1302 hydrocarbon reservoirs might be one source of gas, though gas compositions from limited sampling
1303 suggest a primarily microbial origin. Using the approach of Max and Johnson (2016), hydrate on the
1304 mid-Norwegian margin can be classified as a low grade deposit with little economic value.

1305

1306 Offshore Ireland, the Druid Anomaly over the Feni Drift in the Rockall Basin, and contourite deposits
1307 in the Porcupine Basin, have been identified as potential targets for further hydrate exploration.
1308 Furthermore, exploration in deep water for conventional hydrocarbons in the South Porcupine Basin
1309 requires better definition of the HSZ to mitigate against the risk of hydrate dissociation while drilling
1310 and consequent uncontrolled gas release. More seismic interpretation, followed by seabed sampling
1311 and shallow drilling, are required to identify hydrate. As more conventional oil and gas wells are
1312 drilled offshore Ireland, new geothermal gradient data will be acquired that will contribute to a better
1313 definition of the HSZ.

1314

1315 On the northwest continental margin of Iberia, the occurrence of hydrate is uncertain. Although some
1316 data suggest that the sedimentary and geomorphological evolution of the area is controlled by fluid
1317 dynamics associated with gas seepage, and occasional weak indicators of gas have been described (e.g.,
1318 possible BSR, seismic bright spots and liquefaction of a sediment core), none are conclusive.

1319

1320 On the South Iberia and Northwest Africa margins, direct evidence for hydrate has been found only in
1321 the mud volcanoes of the Gulf of Cádiz. Indirect evidence has been detected on both sides of the Straits
1322 of Gibraltar, mostly associated with mud volcanoes and mud diapirs, but also in the form of localised
1323 BSRs, degassing and liquefied sediments in cores, and by the presence of chlorinity anomalies. The
1324 preferred migration pathways for fluids into the basin are the main tectonic structures such as diapirs,
1325 folds and faults. The composition of the pore fluids and hydrate sampled in the Gulf of Cádiz indicate
1326 generally a mixture of microbial and thermogenic sources. However, in some mud volcanoes associated
1327 with the deep SWIM strike-slip faults, an abiotic source is also possible, connected to hydrothermal
1328 fluids in the oceanic domain. Thus the Gulf of Cádiz has a variety of sources of gas and geological
1329 settings for hydrate formation. In the case of the Alborán Sea, gas is present in diapiric formations
1330 originating in the basal allochthonous unit and is likely to be thermogenic.

1331

1332 In the Eastern Mediterranean, hydrate sampling is also limited to mud volcanoes. There is little
1333 published work on seismic indicators of hydrate presence, although extensive exploration datasets
1334 provide opportunities for further analysis. The high sensitivity of the ocean here to climate and
1335 oceanographic changes may provide a natural laboratory to investigate the influence of these changes
1336 on hydrate stability, as well as the potential impacts.

1337

1338 In the Sea of Marmara, there is abundant evidence for the presence of gas within the HSZ and hydrate
1339 has been directly sampled in the top of a mud volcano, but unequivocal BSRs have not been observed,
1340 so the amount of the hydrate present is difficult to assess.

1341

1342 In the Black Sea offshore Romania and Bulgaria, diverging results on possible hydrate saturations
1343 demonstrate the need to ground-truth models by collecting samples from deep drilling with logging and
1344 core sampling. Physical sediment parameters, heat-flow measurements, geochemical data and sediment
1345 dating are required to calibrate the remote sensing techniques and to enable the extension of available
1346 models along the margin. Changes in climate such as the last glacial maxima (LGM) caused a bottom
1347 water temperature decrease from 9° C to about 4-6° C, a sea-level decrease of about 120 m and the
1348 development of limnic conditions as the Bosphorus interface to the Mediterranean was closed. These
1349 changes caused a decrease in the maximum thickness of the hydrate stability field by about 33%, from
1350 550 m to 370 m (Zander et al. 2017). This change may have released 1.1-4.6 Gt of methane carbon as
1351 the hydrate dissociated (Poort et al. 2005). Ongoing salinity increases in the Black Sea sediments will
1352 shift the top of the HSZ in the future, causing further hydrate dissociation (Riboulot et al., 2018).
1353 Furthermore, a mis-match between modeled HSZ limits and observed BSR depths suggests that the
1354 hydrate system of the Black Sea is currently not in equilibrium but is approaching steady state (Hillman
1355 et al., 2018a).

1356
1357 On the southern continental slope and rise of Black Sea, BSR occurrences are mapped in water depths of
1358 750-2000 meters from high resolution multichannel seismic reflection data. Also, chirp data suggest the
1359 presence of gas accumulations at shallow sediment depths (30-40 m). Slope failures are widespread along
1360 both the western and eastern steep canyon systems. The presence of hydrate is not restricted to these areas
1361 but is probably much more extensive. Hydrate samples have been reported widely across the Turkish
1362 Black Sea margin in BSR and mud volcano areas. Free gas is inferred to occur beneath the BSR, as
1363 indicated by seismic bright spots and areas of seismic blanking. The presence of gas seeps to the seabed
1364 through the hydrate stability zone, via mud volcanoes and fault zones, provides evidence for free gas
1365 below the hydrate zone. Mapping of active gas seeps using water column imaging and sampling of free
1366 gas in water samples and sediments will give information about the origin of the gas, which could be
1367 microbial or thermogenic or both, as in the Amasra area.

1368
1369 Thus we can categorise areas covered by our study into three types:

- 1370 1. Areas of widespread BSRs: the Davis Strait, Fram Strait, the mid-Norwegian margin, and the
1371 southern margin of Black Sea.
- 1372 2. Areas where there is no BSR, or the BSR is localised rather than widespread, but hydrate has
1373 been directly sampled: the Barents Sea, the Gulf of Cadiz, the Eastern Mediterranean, the Sea of
1374 Marmara, and the Black Sea offshore Bulgaria and Romania.
- 1375 3. Areas with neither a clearly identified BSR nor direct sampling of hydrate, but where other more
1376 indirect hydrate indicators are present: the Disko area offshore west Greenland, the northeast
1377 Greenland margin, onshore Svalbard, offshore Ireland, and offshore northwest Iberia.

1378 Where hydrate has been sampled, it usually contains higher hydrocarbons, indicating a thermogenic
1379 component; an exception is the Black Sea offshore Romania and Bulgaria, where only trace amounts of
1380 higher hydrocarbons are present.

1381

1382 **13. Conclusions**

1383 From our review of hydrate occurrence around Europe, we conclude:

1384 1. There is direct or indirect evidence for the presence of hydrate in several European locations
1385 including the western and eastern margins of Greenland, onshore and offshore Svalbard, the
1386 Barents Sea, the mid-Norwegian margin, the Atlantic margin of Ireland, the eastern
1387 Mediterranean Sea, the Sea of Marmara, and the western and southern margins of the Black
1388 Sea.

1389 2. Hydrate is observed to be particularly widespread offshore Svalbard and Norway and in the
1390 Black Sea.

1391 3. Areas with strong evidence for the presence of hydrate commonly coincide with conventional
1392 thermogenic hydrocarbon provinces.

1393 4. Although hydrate systems are well explored in a few small areas, for most European margins,
1394 significant further research is needed to determine the regional abundance of hydrate beneath
1395 the seabed.

1396 **Acknowledgements**

1397 This work was supported by the European Commission via ESSEM COST action ES1405, entitled
1398 Marine gas hydrate – an indigenous source of natural gas for Europe (MIGRATE). We thank Jack
1399 Schuenmeyer for advice and Ingo Pecher and two anonymous reviewers for constructive comments.
1400 TAM was supported by a Wolfson Research Merit Award. ALC was supported by the ‘Programa de
1401 axudas á etapa posdoutoral da Xunta de Galicia’. LMP thanks CESAM (UID/AMB/50017/2019) and
1402 FCT/MCTES for financial support. DR thanks the Ministerio de Ciencia Innovación y Tecnología of
1403 Spain and Consellería de Industria of the Xunta de Galicia for funding data acquisition offshore
1404 Galicia and A. E. López Pérez for his help with the Galician Marine bathymetry. AV was supported
1405 by the Bulgarian National Science Fund (Project KP-06-OPR04/7 GEOHydrate). Metadata associated
1406 with this review are available at <https://www.migrate-cost.eu/wg1-reports>.

1407 **References**

1408

1409 Abay, T.B., Karlsen, D.A. and Pedersen, J.H. (2014) Source Rocks at Svalbard: An Overview of
1410 Jurassic and Triassic Formations and Comparison with Offshore Barents Sea Time Equivalent Source
1411 Rock Formations, AAPG International Conference & Exhibition, Istanbul, Turkey.

1412 Akhmetzhanov, A.M., Kenyon, N.H., Ivanov, M.K., Westbrook, G.K. and Mazzini, A. (2008) Deep-
1413 water depositional systems and cold seeps of the Western Mediterranean, Gulf of Cadiz and
1414 Norwegian continental margins. Preliminary results of investigations during the TTR-16 cruise of RV
1415 Professor Logachev May-July, 2006, Intergovernmental Oceanographic Commission (IOC) Technical
1416 Series. UNESCO, Paris, France, p. 91.

1417 Aloisi, G., Pierre, C., Rouchy, J.M., Foucher, J.P., Woodside, J. and Party, M.S. (2000) Methane-
1418 related authigenic carbonates of eastern Mediterranean Sea mud volcanoes and their possible relation
1419 to gas hydrate destabilisation. *Earth and Planetary Science Letters* 184, 321-338.

1420 Andreassen, K., Berteussen, K.A., Sognnes, H., Henneberg, K., Langhammer, J. and Mienert, J.
1421 (2003) Multicomponent ocean bottom cable data in gas hydrate investigation offshore of Norway.
1422 *Journal of Geophysical Research: Solid Earth* 108, 2399, doi:2310.1029/2002JB002245.

1423 Andreassen, K., Hogstad, K. and Berteussen, K.A. (1990) Gas hydrate in the southern Barents Sea,
1424 indicated by a shallow seismic anomaly. *First Break* 8, 235-245.

1425 Andreassen, K., Hubbard, A., Winsborrow, M., Patton, H., Vadakkepuliambatta, S., Plaza-Faverola,
1426 A., Gudlaugsson, E., Serov, P., Deryabin, A., Mattingsdal, R., Mienert, J. and Bünz, S. (2017)
1427 Massive blow-out craters formed by hydrate-controlled methane expulsion from the Arctic seafloor.
1428 *Science* 356, 948-953.

1429 Andreassen, K., Mienert, J., Bryn, P. and Singh, S.C. (2000) A Double Gas-Hydrate Related Bottom
1430 Simulating Reflector at the Norwegian Continental Margin. *Annals of the New York Academy of*
1431 *Sciences* 912, 126-135.

1432 Archer, D., Buffett, B. and Brovkin, V. (2009) Ocean methane hydrates as a slow tipping point in the
1433 global carbon cycle. *Proceedings of the National Academy of Sciences* 106, 20596-20601.

1434 Armijo, R., Meyer, B., Hubert, A. and Barka, A. (1999) Westward propagation of the North Anatolian
1435 fault into the northern Aegean: Timing and kinematics. *Geology* 27, 267-270.

1436 Attias, E., Weitemeyer, K., Minshull, T.A., Best, A.I., Sinha, M., Jegen-Kulcsar, M., Hölz, S. and
1437 Berndt, C. (2016) Controlled-source electromagnetic and seismic delineation of sub-seafloor fluid
1438 flow structures in a gas hydrate province, offshore Norway. *Geophysical Journal International* 206,
1439 1093-1110.

1440 Baraza, J. and Ercilla, G. (1996) Gas-charged sediments and large pockmark-like features on the Gulf
1441 of Cadiz slope (SW Spain). *Marine and Petroleum Geology* 13, 253-261.

1442 Bega, Z. and Ionescu, G. (2009) Neogene structural styles of the NW Black Sea region, offshore
1443 Romania. *The Leading Edge* 9, 1082-1089.

1444 Berndt, C., Bunz, S., Clayton, T., Mienert, J. and Saunders, M. (2004) Seismic character of bottom
1445 simulating reflectors: examples from the mid-Norwegian margin. *Marine and Petroleum Geology* 21,
1446 723-733.

1447 Berndt, C., Feseker, T., Treude, T., Krastel, S., Liebetrau, V., Niemann, H., Bertics, V.J., Dumke, I.,
1448 Dunnbier, K., Ferre, B., Graves, C., Gross, F., Hissmann, K., Huhnerbach, V., Krause, S., Lieser, K.,

- 1449 Schauer, J. and Steinle, L. (2014) Temporal Constraints on Hydrate-Controlled Methane Seepage off
1450 Svalbard. *Science* 343, 284-287.
- 1451 Betlem, P. (2018) 3D Thermo-baric Modelling of Central Spitsbergen: Implications for Gas Hydrate
1452 Occurrence. MSc thesis, University of Iceland, Reykjavik.
- 1453 Betlem, P., Senger, K. and Hodson, A. (2019) 3D thermobaric modelling of the gas hydrate stability
1454 zone onshore central Spitsbergen, Arctic Norway. *Marine and Petroleum Geology* 100, 246-262.
- 1455 Bialas, J., Klaucke, I. and Haeckel, M. (2014) FS Maria S. Merian Fahrtbericht/Cruise Report
1456 MSM34/1 and 2, SUGAR site. GEOMAR, Kiel, Germany.
- 1457 Blinova, V.N., Comas, M.C., Ivanov, M.K., Poludetkina, E.N. and Matveeva, T.V. (2011) Active
1458 mud volcanism in the West Alboran Basin: Geochemical evidence of hydrocarbon seepage. *Marine
1459 and Petroleum Geology* 28, 1483-1504.
- 1460 Bohrmann, G., Ahrlich, F., Bachmann, K., Bergenthal, M., Beims, M., Betzler, C., Brünjes, J.,
1461 Deusner, C., Domeyer, B., Düßmann, R., Ewert, J., Gaide, S., Frank, C., Freudenthal, T., Fröhlich, S.,
1462 Greindl, T., Haeckel, M., Heitmann-Bacza, C., Ion, G., Kaszemeik, K., Keil, H., Kinski, O., Klein, T.,
1463 Kossel, E., Linowski, E., Malnati, J., Mau, S., Meyer, B., Pape, T., Popa, A., Renken, J., Reuter, J.,
1464 Reuter, M., Riedel, M., Riemer, P., Rohleder, C., Rosiak, U., Rotaru, S.-G., Rothenwänder, T.,
1465 Stachowski, A., Schmidt, W., Seiter, C., Utecht, C., Vasilev, A., Wallmann, K., Wegwerth, A.,
1466 Wintersteller, P. and Wunsch, D. (2018) R/V Meteor Cruise Report M142: Drilling gas hydrates in
1467 the Danube deep-sea fan, Black Sea, Varna–Varna–Varna, 04 November–22 November–09
1468 December 2017. MARUM – Center for Marine Environmental Sciences, Bremen, Germany, p. 121.
- 1469 Boillot, G. (1995) A lithospheric syn-rift shear zone at the ocean-continent transition: preliminary
1470 results of the GALINAUTE II cruise (Nautile dives on the Galicia Bank, Spain). *Comptes Rendus -
1471 Academie des Sciences, Serie II: Sciences de la Terre et des Planetes* 321, 1171-1178.
- 1472 Boillot, G., Dupeuble, P.A. and Malod, J. (1979) Subduction and tectonics on the continental margin
1473 off northern Spain. *Marine Geology* 32, 53-70.
- 1474 Bojesen-Koefoed, J.A., Bidstrup, T., Christiansen, F.G., Dalhoff, F., Gregersen, U., Nytoft, H.P.,
1475 Nohr-Hansen, H., Pedersen, A.K. and Sonderholm, M. (2007) Petroleum seepages at Asuk, Disko,
1476 West Greenland: Implications for regional petroleum exploration. *Journal of Petroleum Geology* 30,
1477 219-236.
- 1478 Boswell, R. and Collett, T.S. (2011) Current perspectives on gas hydrate resources. *Energy &
1479 Environmental Science* 4, 1206-1215.
- 1480 Boswell, R., Shipp, C., Reichel, T., Shelander, D., Saeki, T., Frye, M., Shedd, W., Collett, T.S. and
1481 McConnell, D.R. (2016) Prospecting for marine gas hydrate resources. *Interpretation* 4, SA13-SA24.
- 1482 Bouriak, S., Vanneste, M. and Saoutkine, A. (2000) Inferred gas hydrates and clay diapirs near the
1483 Storegga Slide on the southern edge of the Vøring Plateau, offshore Norway. *Marine Geology* 163,
1484 125-148.
- 1485 Bourry, C., Chazallon, B., Charlou, J.L., Pierre Donval, J., Ruffine, L., Henry, P., Geli, L., Çagatay,
1486 M.N., Inan, S. and Moreau, M. (2009) Free gas and gas hydrates from the Sea of Marmara, Turkey.
1487 Chemical and structural characterization. *Chemical Geology* 264, 197-206.
- 1488 Brekke, H. (2000) The tectonic evolution of the Norwegian Sea Continental Margin with emphasis on
1489 the Vøring and Møre Basins. Geological Society, London, Special Publications 167, 327-378.

- 1490 Bryn, P., Berg, K., Forsberg, C.F., Solheim, A. and Kvalstad, T.J. (2005) Explaining the Storegga
1491 Slide. *Marine and Petroleum Geology* 22, 11-19.
- 1492 Bugge, T., Belderson, R.H. and Kenyon, N.H. (1988) The Storegga slide. *Philosophical Transactions*
1493 *of the Royal Society of London* A325, 357-388.
- 1494 Bugge, T., Elvebakk, G., Fanavoll, S., Mangerud, G., Smelror, M., Weiss, H.M., Gjelberg, J.,
1495 Kristensen, S.E. and Nilsen, K. (2002) Shallow stratigraphic drilling applied in hydrocarbon
1496 exploration of the Nordkapp Basin, Barents Sea. *Marine and Petroleum Geology* 19, 13-37.
- 1497 Bünz, S. and Mienert, J. (2004) Acoustic imaging of gas hydrate and free gas at the Storegga Slide.
1498 *Journal of Geophysical Research* 109, B04102, doi:04110.01029/02003JB002863.
- 1499 Bünz, S., Mienert, J. and Berndt, C. (2003) Geological controls on the Storegga gas-hydrate system of
1500 the mid-Norwegian continental margin. *Earth and Planetary Science Letters* 209, 291-307.
- 1501 Bünz, S., Mienert, J., Vanneste, M. and Andreassen, K. (2005) Gas hydrates at the Storegga Slide:
1502 Constraints from an analysis of multicomponent, wide-angle seismic data. *Geophysics* 70, B19-B34.
- 1503 Bünz, S., Polyanov, S., Vadakkepuliambatta, S., Consolaro, C. and Mienert, J. (2012) Active gas
1504 venting through hydrate-bearing sediments on the Vestnesa Ridge, offshore W-Svalbard. *Marine*
1505 *Geology* 332-334, 189-197.
- 1506 Casas, D., Ercilla, G. and Baraza, J. (2003) Acoustic evidences of gas in the continental slope
1507 sediments of the Gulf of Cadiz (E Atlantic). *Geo-Mar Lett* 23, 300-310.
- 1508 Chand, S., Mienert, J., Andreassen, K., Knies, J., Plassen, L. and Fotland, B. (2008) Gas hydrate
1509 stability zone modelling in areas of salt tectonics and pockmarks of the Barents Sea suggests an active
1510 hydrocarbon venting system. *Marine and Petroleum Geology* 25, 625-636.
- 1511 Chand, S., Thorsnes, T., Rise, L., Brunstad, H., Stoddart, D., Bøe, R., Lågstad, P. and Svolsbru, T.
1512 (2012) Multiple episodes of fluid flow in the SW Barents Sea (Loppa High) evidenced by gas flares,
1513 pockmarks and gas hydrate accumulation. *Earth and Planetary Science Letters* 331–332, 305-314.
- 1514 Christiansen, F.G., Dam, G., Nørh-Hansen, H. and Sønderholm, M. (1994) Shallow core drilling
1515 summary sheets: Cretaceous sediments of Nuussuaq and Svartenhuk Halvø (GGU 400701-400712),
1516 GGU Open File Series.
- 1517 CIESM (2008) Impacts of acidification on biological, chemical and physical systems in the
1518 Mediterranean and Black Seas, in: Briand, F. (Ed.), *CIESM Workshop Monographs*, Monaco, p. 124.
- 1519 Collett, T.S., Johnson, A., Knapp, C. and Boswell, R. (2009) Natural gas hydrates: a review, in:
1520 Collett, T., Johnson, A., Knapp, C., Boswell, R. (Eds.), *Natural Gas Hydrates: Energy Resource*
1521 *Potential and Associated Geologic Hazards*. American Association of Petroleum Geologists Memoir
1522 89.
- 1523 Crane, K., Sundvor, E., Buck, R. and Martinez, F. (1991) Rifting in the northern Norwegian-
1524 Greenland Sea - Thermal tests of asymmetric spreading. *Journal of Geophysical Research* 96, 14529-
1525 14550.
- 1526 Crémière, A., Pierre, C., Blanc-Valleron, M.M., Zitter, T., Çağ atay, M.N. and Henry, P. (2012)
1527 Methane-derived authigenic carbonates along the North Anatolian fault system in the Sea of Marmara
1528 (Turkey). *Deep-Sea Research Part I: Oceanographic Research Papers* 66, 114-130.

- 1529 Dai, J., Snyder, F., Gillespie, D., Koesoemadinata, A. and Dutta, N. (2008) Exploration for gas
1530 hydrates in the deepwater, northern Gulf of Mexico: Part I. A seismic approach based on geologic
1531 model, inversion, and rock physics principles. *Marine and Petroleum Geology* 25, 830-844.
- 1532 Dalland, A., Worsley, D., Ofstad, K. (1988) A lithostratigraphical scheme for the Mesozoic and
1533 Cenozoic succession offshore mid- and northern Norway. *Norwegian Petroleum Directorate Bulletin*
1534 4.
- 1535 de Lange, G. and Brumsack, H.-J. (1998a) Pore-water indications for the occurrence of gas hydrates
1536 in eastern Mediterranean mud dome structures. *Proceedings of the Ocean Drilling Program, Scientific*
1537 *Results* 160, 569-574.
- 1538 De Lange, G.J. and Brumsack, H.J. (1998b) The occurrence of gas hydrates in Eastern Mediterranean
1539 mud dome structures as indicated by pore-water composition. *Geological Society Special Publication*
1540 137, 167-175.
- 1541 Depreiter, D., Poort, J., Van Rensbergen, P. and Henriët, J.P. (2005) Geophysical evidence of gas
1542 hydrates in shallow submarine mud volcanoes on the Moroccan margin. *Journal of Geophysical*
1543 *Research: Solid Earth* 110, doi:10.1029/2005JB003622.
- 1544 Diaz-del-Rio, V., Somoza, L., Martinez-Frias, J., Mata, M.P., Delgado, A., Hernandez-Molina, F.J.,
1545 Lunar, R., Martin-Rubi, J.A., Maestro, A., Fernandez-Puga, M.C., León, R., Llave, E., Medialdea, T.
1546 and Vázquez, J.T. (2003) Vast fields of hydrocarbon-derived carbonate chimneys related to the
1547 accretionary wedge/olistostrome of the Gulf of Cadiz. *Marine Geology* 195, 177-200.
- 1548 Dimitrov, L. and Woodside, J. (2003) Deep sea pockmark environments in the eastern Mediterranean.
1549 *Marine Geology* 195, 263-276.
- 1550 Dondurur, D. and Çifçi, G. (2009) Anomalous strong reflections on high resolution seismic data from
1551 the Turkish shelf of the Eastern Black Sea: Possible indicators of shallow hydrogen sulphide-rich gas
1552 hydrate layers. *Turkish Journal of Earth Sciences* 18, 299-313.
- 1553 Doré, A.G. (1995) Barents Sea geology, petroleum resources and commercial potential. *Arctic* 48,
1554 207-221.
- 1555 Doré, A.G. and Jensen, L.N. (1996) The impact of late Cenozoic uplift and erosion on hydrocarbon
1556 exploration: offshore Norway and some other uplifted basins. *Global and Planetary Change* 12, 415-
1557 436.
- 1558 Druet, M. (2015) Geodinámica del Margen Continental de Galicia: Estructura Profunda y
1559 Morfotectónica. PhD thesis, Madrid Complutense University.
- 1560 Druet, M., Muñoz-Martín, A., Granja-Bruña, J.L., Carbó-Gorosabel, A., Acosta, J., Llanes, P. and
1561 Ercilla, G. (2018) Crustal Structure and Continent-Ocean Boundary Along the Galicia Continental
1562 Margin (NW Iberia): Insights From Combined Gravity and Seismic Interpretation. *Tectonics* 37,
1563 1576-1604.
- 1564 Duarte, D., Magalhaes, V.H., Terrinha, P., Ribeiro, C., Madureira, P., Pinheiro, L.M., Benazzouz, O.,
1565 Kim, J.H. and Duarte, H. (2017) Identification and characterization of fluid escape structures
1566 (pockmarks) in the Estremadura Spur, West Iberian Margin. *Marine and Petroleum Geology* 82, 414-
1567 423.
- 1568 Dumke, I., Burwicz, E.B., Berndt, C., Klaeschen, D., Feseker, T., Geissler, W.H. and Sarkar, S.
1569 (2016) Gas hydrate distribution and hydrocarbon maturation north of the Knipovich Ridge, western
1570 Svalbard margin. *Journal of Geophysical Research: Solid Earth* 121, 1405-1424.

- 1571 Dupre, S., Woodside, J., Klaucke, I., Mascle, J. and Foucher, J.P. (2010) Widespread active seepage
1572 activity on the Nile Deep Sea Fan (offshore Egypt) revealed by high-definition geophysical imagery.
1573 *Marine Geology* 275, 1-19.
- 1574 Durán, R., García-Gil, S., Diez, R. and Vilas, F. (2007) Stratigraphic framework of gas accumulations
1575 in the Ría de Pontevedra (NW Spain). *Geo-Mar Lett* 27, 77-88.
- 1576 Egorov, V., Artemov, Y.G., Gulin, S.B. and Polikarpov, G.G. (2011) Methane seeps in the Black Sea:
1577 discovery, quantification and environmental assessment. *J. Black Sea Mediterranean Environment* 17,
1578 171-185.
- 1579 Eiken, O. and Hinz, K. (1993) Contourites in the Fram Strait. *Sedimentary Geology* 82, 15-32.
- 1580 Elliott, G.M., Shannon, P.M., Houghton, P.D.W. and Ovrebo, L.K. (2010) The Rockall Bank Mass
1581 Flow: Collapse of a moated contourite drift onlapping the eastern flank of Rockall Bank, west of
1582 Ireland. *Marine and Petroleum Geology* 27, 92-107.
- 1583 EMODnet Bathymetry Consortium (2016) EMODnet Digital Bathymetry (DTM),
1584 <http://doi.org/10.12770/c7b53704-999d-4721-b1a3-04ec60c87238>.
- 1585 Engen, Ø., Faleide, J.I. and Dyreng, T.K. (2008) Opening of the Fram Strait gateway: A review of
1586 plate tectonic constraints. *Tectonophysics* 450, 51-69.
- 1587 Ercilla, G., Casas, D., Vázquez, J.T., Iglesias, J., Somoza, L., Juan, C., Medialdea, T., León, R.,
1588 Estrada, F., García-Gil, S., Farran, M., Bohoyo, F., García, M. and Maestro, A. (2011) Imaging the
1589 recent sediment dynamics of the Galicia Bank region (Atlantic, NW Iberian Peninsula). *Mar Geophys*
1590 *Res* 32, 99-126.
- 1591 Estrada, F., Galindo-Zaldivar, J., Vázquez, J.T., Ercilla, G., D'Acremont, E., Alonso, B. and Gorini,
1592 C. (2018) Tectonic indentation in the central Alboran Sea (westernmost Mediterranean). *Terra Nova*
1593 30, 24-33.
- 1594 Faleide, J.I., Gudlaugsson, S.T. and Jacquart, G. (1984) Evolution of the western Barents Sea. *Marine*
1595 *and Petroleum Geology* 1, 123-150.
- 1596 Fernandez-Puga, M.C., Vázquez, J.T., Somoza, L., del Rio, V.D., Medialdea, T., Mata, M.P. and
1597 Leon, R. (2007) Gas-related morphologies and diapirism in the Gulf of Cadiz. *Geo-Mar Lett* 27, 213-
1598 221.
- 1599 Ferré, B., Mienert, J. and Feseker, T. (2012) Ocean temperature variability for the past 60 years on the
1600 Norwegian-Svalbard margin influences gas hydrate stability on human time scales. *Journal of*
1601 *Geophysical Research* 117, C10017, doi:10.1029/2012JC008300.
- 1602 Ferrín, A., Durán, R., Diez, R., García-Gil, S. and Vilas, F. (2003) Shallow gas features in the
1603 Galician Rías Baixas (NW Spain). *Geo-Mar Lett* 23, 207-214.
- 1604 Finetti, I., Bricchi, G., Del Ben, A., Pipan, M. and Xuan, Z. (1988) Geophysical Study of the Black
1605 Sea. *Bollettino Di Geofisica Teorica ed Applicata* 30, 197-324.
- 1606 Fohrmann, H., Backhaus, J.O., Blaume, F., Haupt, B.J., Kämpf, J., Michels, K., Mienert, J.,
1607 Posewang, J., Ritzrau, W., Rumohr, J., Weber, M. and Woodgate, R. (2001) Modern Ocean Current-
1608 Controlled Sediment Transport in the Greenland-Iceland-Norwegian (GIN) Seas, in: Schäfer, P.,
1609 Ritzrau, W., Schlüter, M., Thiede, J. (Eds.), *The Northern North Atlantic: A Changing Environment*.
1610 Springer Berlin Heidelberg, Berlin, Heidelberg, pp. 135-154.

- 1611 Fokin, I., Klaucke, I. and Akhmethanov, A. (2005) Side Scan Sonar data, Trakya Area, 2005, Deep
 1612 Water cold seeps, sedimentary environments and ecosystems of the Black and Tyrrhenian Seas and
 1613 the Gulf of Cadiz, Intergovernmental Oceanographic Commission (IOC) Technical Series. UNESCO,
 1614 Paris, France.
- 1615 Furst, J.J., Navarro, F., Gillet-Chaulet, F., Huss, M., Moholdt, G., Fettweis, X., Lang, C., Seehaus, T.,
 1616 Ai, S.T., Benham, T.J., Benn, D.I., Bjornsson, H., Dowdeswell, J.A., Grabiec, M., Kohler, J.,
 1617 Lavrentiev, I., Lindback, K., Melvold, K., Pettersson, R., Rippin, D., Saintenoy, A., Sanchez, G.,
 1618 Schuler, T.V., Sevestre, H., Vasilenko, E. and Braun, M.H. (2018) The Ice-Free Topography of
 1619 Svalbard. *Geophysical Research Letters* 45, 11760-11769.
- 1620 Gabitto, J.B., M. (2010) Gas hydrates research programs: an international review. Office of Scientific
 1621 and Technical Information, US Department of Energy, <https://www.osti.gov/servlets/purl/978338/>.
- 1622 García-García, A., García-Gil, S. and Vilas, F. (2003) Monitoring the Spanish gas fields in the Ría de
 1623 Vigo (1991-2001). *Geo-Mar Lett* 23, 200-206.
- 1624 García-Gil, S., Cartelle, V., De Blas, E., De Carlos, A., Díez, R., Durán, R., Ferrín, A., García-
 1625 Moreiras, I., García-García, A., Iglesias, J., Martínez-Carreño, N., Muñoz Sobrino, C. and Ramírez-
 1626 Pérez, A.M. (2015) Shallow gas in the Iberian continental margin. *Boletín Geológico y Minero* 126,
 1627 575-608.
- 1628 Gardner, J.M. (2001) Mud volcanoes revealed and sampled on the Western Moroccan continental
 1629 margin. *Geophysical Research Letters* 28, 339-342.
- 1630 Garfunkel, Z. (2004) Origin of the Eastern Mediterranean basin: a reevaluation. *Tectonophysics* 391,
 1631 11-34.
- 1632 Gautier, D.L., Bird, K.J., Charpentier, R.R., Grantz, A., Houseknecht, D.W., Klett, T.R., Moore, T.E.,
 1633 Pitman, J.K., Schenk, C.J., Schuenemeyer, J.H., Sørensen, K., Tennyson, M.E., Valin, Z.C. and
 1634 Wandrey, C.J. (2011) Chapter 9: Oil and gas resource potential north of the Arctic Circle, *Geological*
 1635 *Society Memoir* 35. Geological Society, London, pp. 151-161.
- 1636 Geissler, W.H., Pulm, P.V., Jokat, W. and Gebhardt, A.C. (2014) Indications for the Occurrence of
 1637 Gas Hydrates in the Fram Strait from Heat Flow and Multichannel Seismic Reflection Data. *Journal*
 1638 *of Geological Research* 2014, doi:10.1155/2014/582424.
- 1639 Gerlings, J., Hopper, J.R., Fyhn, M.B.W. and Frandsen, N. (2017) Mesozoic and older rift basins on
 1640 the SE Greenland Shelf offshore Ammassalik, in: Peron Pinvidic, G., Hopper, J.R., Funck, T., Stoker,
 1641 M.S., Gaina, C., Doornenbal, J.C., Arting, U.E. (Eds.), *NE Atlantic Region: A Reappraisal of Crustal*
 1642 *Structure, Tectonostratigraphy and Magmatic Evolution*. Geological Soc Publishing House, Bath, pp.
 1643 375-392.
- 1644 Ginsburg, G.D., Milkov, A.V., Soloviev, V.A., Egorov, A.V., Cherkashev, G.A., Vogt, P.R., Crane,
 1645 K., Lorenson, T.D. and Khutorskoy, M.D. (1999) Gas hydrate accumulation at the Håkon Mosby Mud
 1646 Volcano. *Geo-Mar Lett* 19, 57-67.
- 1647 Goswami, B.K., Weitemeyer, K.A., Minshull, T.A., Sinha, M.C., Westbrook, G.K., Chabert, A.,
 1648 Henstock, T.J. and Ker, S. (2015) A joint electromagnetic and seismic study of an active pockmark
 1649 within the hydrate stability field at the Vestnesa Ridge, West Svalbard margin. *Journal of Geophysical*
 1650 *Research: Solid Earth* 120, 6797-6822.
- 1651 Graves, C.A., James, R.H., Sapart, C.J., Stott, A.W., Wright, I.C., Berndt, C., Westbrook, G.K. and
 1652 Connelly, D.P. (2017) Methane in shallow subsurface sediments at the landward limit of the gas
 1653 hydrate stability zone offshore western Svalbard. *Geochimica Et Cosmochimica Acta* 198, 419-438.

- 1654 Gregersen, U. and Bidstrup, T. (2008) Structures and hydrocarbon prospectivity in the northern Davis
1655 Strait area, offshore West Greenland. *Petroleum Geoscience* 14, 151-166.
- 1656 Gunduz, S. (2015) Investigation of active tectonism structure of the Eastern Black Sea with using
1657 multichannel seismic data, Masters Thesis, Institute of Marine Sciences and Technology. Dokuz Eylul
1658 University.
- 1659 Haeckel, M., Zander, T., Burwicz, E., Bialas, J., Berndt, C., Dannowski, A., Hensen, C., Hölz, S.,
1660 Jegen, M., Klaucke, I., Rottke, W. and Schwalenberg, K. (2017) The gas hydrate system of the
1661 Danube deep-sea fan in the Black Sea, 9th International Conference on Gas Hydrates, Denver,
1662 Colorado, USA.
- 1663 Hamann, N.E., Whittaker, R.C. and Stemmerik, L. (2005) Geological development of the Northeast
1664 Greenland shelf. *Petroleum Geology Conference Proceedings* 6, 887-902.
- 1665 Heeschen, K.U., Hohnberg, H.J., Haeckel, M., Abegg, F., Drews, M. and Bohrmann, G. (2007) In situ
1666 hydrocarbon concentrations from pressurized cores in surface sediments, Northern Gulf of Mexico.
1667 *Marine Chemistry* 107, 498-515.
- 1668 Henriksen, E., Bjørnseth, H.M., Hals, T.K., Heide, T., Kiryukhina, T., Kløvjan, O.S., Larssen, G.B.,
1669 Ryseth, A.E., Rønning, K., Sollid, K. and Stoupakova, A. (2011a) Uplift and erosion of the greater
1670 Barents Sea: impact on prospectivity and petroleum systems. *Geological Society, London, Memoir*
1671 35, 271-281.
- 1672 Henriksen, E., Ryseth, A.E., Larssen, G.B., Heide, T., Rønning, K., Sollid, K. and Stoupakova, A.V.
1673 (2011b) Tectonostratigraphy of the greater Barents Sea: Implications for petroleum systems.
1674 *Geological Society, London, Memoir* 35, 163-195.
- 1675 Hensen, C., Scholz, F., Nuzzo, M., Valadares, V., Gracia, E., Terrinha, P., Liebetrau, V., Kaul, N.,
1676 Silva, S., Martinez-Lorient, S., Bartolome, R., Pinero, E., Magalhaes, V.H., Schmidt, M., Weise,
1677 S.M., Cunha, M., Hilario, A., Perea, H., Rovelli, L. and Lackschewitz, K. (2015) Strike-slip faults
1678 mediate the rise of crustal-derived fluids and mud volcanism in the deep sea. *Geology* 43, 339-342.
- 1679 Hesse, R. and Harrison, W.E. (1981) Gas hydrates (clathrates) causing pore-water freshening and
1680 oxygen isotope fractionation in deep-water sedimentary sections of terrigenous continental margins.
1681 *Earth and Planetary Science Letters* 55, 453-462.
- 1682 Hillman, J.I.T., Burwicz, E., Zander, T., Bialas, J., Klaucke, I., Feldman, H., Drexler, T. and
1683 Awwiller, D. (2018a) Investigating a gas hydrate system in apparent disequilibrium in the Danube
1684 Fan, Black Sea. *Earth and Planetary Science Letters* 502, 1-11.
- 1685 Hillman, J.I.T., Klaucke, I., Bialas, J., Feldman, H., Drexler, T., Awwiller, D., Atgin, O., Cifci, G. and
1686 Badhani, S. (2018b) Gas migration pathways and slope failures in the Danube Fan, Black Sea. *Marine
1687 and Petroleum Geology*, 1-16.
- 1688 Hitchen, K. (2004) The geology of the UK Hatton-Rockall margin. *Marine and Petroleum Geology*
1689 21, 993-1012.
- 1690 Hjelstuen, B.O., Eldholm, O. and Skogseid, J. (1999) Cenozoic evolution of the northern Vøring
1691 margin. *GSA Bulletin* 111, 1792-1807.
- 1692 Hjelstuen, B.O., Haflidason, H., Sejrup, H.P. and Nygård, A. (2010) Sedimentary and structural
1693 control on pockmark development—evidence from the Nyegga pockmark field, NW European
1694 margin. *Geo-Mar Lett* 30, 221-230.

- 1695 Hjelstuen, B.O., Petter Sejrup, H., Haflidason, H., Nygård, A., Ceramicola, S. and Bryn, P. (2005)
 1696 Late Cenozoic glacial history and evolution of the Storegga Slide area and adjacent slide flank
 1697 regions, Norwegian continental margin. *Marine and Petroleum Geology* 22, 57-69.
- 1698 Hodson, A.J., Nowak, A., Redeker, K.R., Holmlund, E.S., Christiansen, H.H. and Turchyn, A.V.
 1699 (2019) Seasonal Dynamics of Methane and Carbon Dioxide Evasion From an Open System Pingo:
 1700 Lagoon Pingo, Svalbard. *Frontiers in Earth Science* 7, doi:10.3389/feart.2019.00030.
- 1701 Honoré, A. (2014) The outlook for natural gas demand in Europe, Oxtord, UK, p. 174pp.
- 1702 Hopper, J.R., Funck, T., Stoker, M., Ártung, U., Peron-Pindivic, G., Gaina, C. and Doornenbal, H.
 1703 (2014) Tectonostratigraphic Atlas of the North- East Atlantic Region, Geological Survey of Denmark
 1704 and Greeland (GEUS), Copenhagen.
- 1705 Hovland, M., Svensen, H., Forsberg, C.F., Johansen, H., Fichler, C., Fosså, J.H., Jonsson, R. and
 1706 Rueslåtten, H. (2005) Complex pockmarks with carbonate-ridges off mid-Norway: Products of
 1707 sediment degassing. *Marine Geology* 218, 191-206.
- 1708 Humlum, O., Instanes, A. and Sollid, J.L. (2003) Permafrost in Svalbard: a review of research history,
 1709 climatic background and engineering challenges. *Polar Res* 22, 191-215.
- 1710 Hustoft, S., Bünz, S. and Mienert, J. (2010) Three-dimensional seismic analysis of the morphology
 1711 and spatial distribution of chimneys beneath the Nyegga pockmark field, offshore mid-Norway. *Basin*
 1712 *Research* 22, 465-480.
- 1713 Hustoft, S., Bünz, S., Mienert, J. and Chand, S. (2009) Gas hydrate reservoir and active methane-
 1714 venting province in sediments on <20 Ma young oceanic crust in the Fram Strait, offshore NW-
 1715 Svalbard. *Earth and Planetary Science Letters* 284, 12-24.
- 1716 Hustoft, S., Mienert, J., Bünz, S. and Nouzé, H. (2007) High-resolution 3D-seismic data indicate
 1717 focussed fluid migration pathways above polygonal fault systems of the mid-Norwegian margin.
 1718 *Marine Geology* 245, 89-106.
- 1719 Ivanov, M., Blinova, V., Kozlova, E., Westbrook, Graham K., Mazzini, A., Minshull, T. and Nouzé,
 1720 H. (2007) First sampling of gas hydrate from the Vøring Plateau. *Eos, Transactions American*
 1721 *Geophysical Union* 88, 209-212.
- 1722 Ivanov, M.K., Kenyon, N.H., Laberg, J.S. and Blinova, V.N. (2010) Cold seeps, coral mounds and
 1723 deep-water depositional systems of the Alborán Sea, Gulf of Cadiz and Norwegian Continental
 1724 Margin. Preliminary results of investigations during the TTR-17 cruise of RV Professor Logachev,
 1725 June–July, 2008, in: UNESCO (Ed.), Intergovernmental Oceanographic Commission (IOC) Technical
 1726 Series. UNESCO, Paris, France, p. 144.
- 1727 Japsen, P., Bonow, J.M., Green, P.F., Chalmers, J.A. and Lidmar-Bergström, K. (2006) Elevated,
 1728 passive continental margins: Long-term highs or Neogene uplifts? New evidence from West
 1729 Greenland. *Earth and Planetary Science Letters* 248, 330-339.
- 1730 Johnson, J.E., Mienert, J., Plaza-Faverola, A., Vadakkepuliambatta, S., Knies, J., Bünz, S.,
 1731 Andreassen, K. and Ferré, B. (2015) Abiotic methane from ultraslow-spreading ridges can charge
 1732 Arctic gas hydrates. *Geology* 43, 371-374.
- 1733 Jokat, W., Geissler, W. and Voss, M. (2008) Basement structure of the north-western Yermak Plateau.
 1734 *Geophysical Research Letters* 35, L05309, doi:05310.01029/02007GL032892.

- 1735 Judd, A., Davies, G., Wilson, J., Holmes, R., Baron, G. and Bryden, I. (1997) Contributions to
1736 atmospheric methane by natural seepages on the UK continental shelf (vol 137, pg 165, 1997). *Marine*
1737 *Geology* 140, 427-455.
- 1738 Kenyon, N.H., Ivanov, M.K., Akhmetzhanov, A.M. and Akhmanov, G.G. (2001) Interdisciplinary
1739 approaches to geoscience on the north east Atlantic margin and Mid-Atlantic Ridge. Preliminary
1740 results of investigations during the TTR-10 cruise of RV Professor Logachev. July-August, 2000, in:
1741 UNESCO (Ed.), Intergovernmental Oceanographic Commission (IOC) technical series. UNESCO,
1742 Paris, France, p. 104.
- 1743 Klitzke, P., Luzi-Helbing, M., Schicks, J.M., Cacace, M., Jacquey, A.B., Sippel, J., Scheck-
1744 Wenderoth, M. and Faleide, J.I. (2016) Gas Hydrate Stability Zone of the Barents Sea and Kara Sea
1745 Region. *Energy Procedia* 97, 302-309.
- 1746 Knies, J. and Mann, U. (2002) Depositional environment and source rock potential of Miocene strata
1747 from the central Fram Strait: introduction of a new computing tool for simulating organic facies
1748 variations. *Marine and Petroleum Geology* 19, 811-828.
- 1749 Knies, J., Mattingsdal, R., Fabian, K., Grøsfjeld, K., Baranwal, S., Husum, K., De Schepper, S., Vogt,
1750 C., Andersen, N., Matthiessen, J., Andreassen, K., Jokat, W., Nam, S.-I. and Gaina, C. (2014) Effect
1751 of early Pliocene uplift on late Pliocene cooling in the Arctic–Atlantic gateway. *Earth and Planetary*
1752 *Science Letters* 387, 132-144.
- 1753 Krastel, S., Spiess, V., Ivanov, M., Weinrebe, W., Bohrmann, G., Shashkin, P. and Heidersdorf, F.
1754 (2003) Acoustic investigations of mud volcanoes in the Sorokin Trough, Black Sea. *Geo-Mar Lett* 23,
1755 230-238.
- 1756 Krom, M.D., Herut, B. and Mantoura, R.F.C. (2004) Nutrient budget for the Eastern Mediterranean:
1757 Implications for phosphorus limitation. *Limnology and Oceanography* 49, 1582-1592.
- 1758 Ktenas, D., Henriksen, E., Meisingset, I., Nielsen, J.K. and Andreassen, K. (2017) Quantification of
1759 the magnitude of net erosion in the southwest Barents Sea using sonic velocities and compaction
1760 trends in shales and sandstones. *Marine and Petroleum Geology* 88, 826-844.
- 1761 Küçük, H.M., Dondurur, D., Özel, O., Atgun, O., Sınayuç, Ç., Merey, Ş. and Çifçi, G. (2015)
1762 Acoustic Investigations of Gas and Gas Hydrate Formations, Offshore Southwestern Black Sea,
1763 American Geophysical Union Fall Meeting, San Francisco, USA.
- 1764 Laberg, J.S. and Andreassen, K. (1996) Gas hydrate and free gas indications within the Cenozoic
1765 succession of the Bjørnøya Basin, western Barents Sea. *Marine and Petroleum Geology* 13, 921-940.
- 1766 Laberg, J.S., Andreassen, K. and Knutsen, S.M. (1998) Inferred gas hydrate on the Barents Sea shelf
1767 — a model for its formation and a volume estimate. *Geo-Mar Lett* 18, 26-33.
- 1768 Laberg, J.S., Dahlgren, T., Vorren, T.O., Haflidason, H. and Bryn, P. (2001) Seismic analyses of
1769 Cenozoic contourite drift development in the Northern Norwegian Sea. *Mar Geophys Res* 22, 401-
1770 416.
- 1771 Larsen, H.C. and Saunders, A.D. (1998) Tectonism and volcanism at the Southeast Greenland rifted
1772 margin; a record of plume impact and later continental rupture. *Proceedings of the Ocean Drilling*
1773 *Program, Scientific Results* 152, 1-503.
- 1774 Le Pichon, X., Sengor, A.M.C., Demirbag, E., Rangin, C., Imren, C., Armijo, R., Gorur, N., Cagatay,
1775 N., de Lepinay, B.M., Meyer, B., Saatçilar, R. and Tok, B. (2001) The active Main Marmara Fault.
1776 *Earth and Planetary Science Letters* 192, 595-616.

- 1777 Lee, J.H., Baek, Y.S., Ryu, B.J., Riedel, M. and Hyndman, R.D. (2005) A seismic survey to detect
1778 natural gas hydrate in the East Sea of Korea. *Mar Geophys Res* 26, 51-59.
- 1779 Leon, R. (2007) Modelo SIG del campo de estabilidad de los hidratos de gas: aplicación a las
1780 estructuras geológicas ligadas a las emisiones submarinas de fluidos hidrocarburos en el Golfo de
1781 Cádiz. Instituto Geológico y Minero de España, Madrid, Spain.
- 1782 León, R., Somoza, L., Medialdea, T., Gonzalez, F.J., Gimenez-Moreno, C.J. and Perez-Lopez, R.
1783 (2014) Pockmarks on either side of the Strait of Gibraltar: formation from overpressured shallow
1784 contourite gas reservoirs and internal wave action during the last glacial sea-level lowstand? *Geo-Mar*
1785 *Lett* 34, 131-151.
- 1786 León, R., Somoza, L., Medialdea, T., Hernandez-Molina, F.J., Vázquez, J.T., Diaz-del-Rio, V. and
1787 Gonzalez, F.J. (2010) Pockmarks, collapses and blind valleys in the Gulf of Cadiz. *Geo-Mar Lett* 30,
1788 231-247.
- 1789 León, R., Somoza, L., Medialdea, T., Maestro, A., Diaz-del-Rio, V. and Fernandez-Puga, M.D.
1790 (2006) Classification of sea-floor features associated with methane seeps along the Gulf of Cadiz
1791 continental margin. *Deep-Sea Research Part II - Topical Studies in Oceanography* 53, 1464-1481.
- 1792 León, R., Somoza, L., Medialdea, T., Vázquez, J.T., Gonzalez, F.J., Lopez-Gonzalez, N., Casas, D.,
1793 Mata, M.D., Fernandez-Puga, M.D., Gimenez-Moreno, C.J. and Diaz-del-Rio, V. (2012) New
1794 discoveries of mud volcanoes on the Moroccan Atlantic continental margin (Gulf of Cadiz): morpho-
1795 structural characterization. *Geo-Mar Lett* 32, 473-488.
- 1796 Lericolais, G., Bourget, J., Popescu, I., Jermannaud, P., Mulder, T., Jorry, S. and Panin, N. (2013)
1797 Late Quaternary deep-sea sedimentation in the western Black Sea: New insights from recent coring
1798 and seismic data in the deep basin. *Global and Planetary Change* 103, 232-247.
- 1799 Letouzey, J., Biju-Duval, B., Dorkel, A., Gonnard, R., Kristchev, K., Montadert, L. and Sungurlu, O.
1800 (1977) The Black Sea: A Marginal Basin, Geophysical and Geological Data, in: Biju-Duval, B.,
1801 Montadert, L. (Eds.), *International Symposium of the Mediterranean Basins*. Editions Technip, Paris,
1802 pp. 363-376.
- 1803 Liira, M., Noormets, R., Sepp, H., Kekišev, O., Maddison, M. and Olaussen, S. (2019) Sediment
1804 geochemical study of hydrocarbon seeps in Isfjorden and Mohnbukta: a comparison between western
1805 and eastern Spitsbergen, Svalbard. *Arctos* 1, 49-62.
- 1806 Loncke, L., Mascle, J. and Fanil Scientific, P. (2004) Mud volcanoes, gas chimneys, pockmarks and
1807 mounds in the Nile deep-sea fan (Eastern Mediterranean): geophysical evidences. *Marine and*
1808 *Petroleum Geology* 21, 669-689.
- 1809 López Pérez, A.E., Rey, D., Martins, V., Plaza-Morlote, M. and Rubio, B. (2019) Application of
1810 multivariate statistical analyses to Itrax (TM) core scanner data for the identification of deep-marine
1811 sedimentary facies: A case study in the Galician Continental Margin. *Quaternary International* 514,
1812 152-160.
- 1813 Lundin, E.R. and Doré, A.G. (1997) A tectonic model for the Norwegian passive margin with
1814 implications for the NE Atlantic: Early Cretaceous to break-up. *Journal of the Geological Society* 154,
1815 545-550.
- 1816 Lykousis, V., Alexandri, S., Woodside, J., de Lange, G., Dahlmann, A., Perissoratis, C., Heeschen,
1817 K., Ioakim, C., Sakellariou, D., Nomikou, P., Rousakis, G., Casas, D., Ballas, D. and Ercilla, G.
1818 (2009) Mud volcanoes and gas hydrates in the Anaximander mountains (Eastern Mediterranean Sea).
1819 *Marine and Petroleum Geology* 26, 854-872.

- 1820 Macgregor, D.S. (2012) The development of the Nile drainage system: integration of onshore and
1821 offshore evidence. *Petroleum Geoscience* 18, 417-431.
- 1822 Maestro, A., Jané, G., Llave, E., López-Martínez, J., Bohoyo, F. and Druet, M. (2018) The role of
1823 tectonic inheritance in the morphostructural evolution of the Galicia continental margin and adjacent
1824 abyssal plains from digital bathymetric model (DBM) analysis (NW Spain). *International Journal of*
1825 *Earth Sciences* 107, 1267-1286.
- 1826 Magalhaes, V.H., Pinheiro, L.M., Ivanov, M.K., Kozlova, E., Blinova, V., Kolganova, J.,
1827 Vasconcelos, C., McKenzie, J.A., Bernasconi, S.M., Kopf, A.J., Diaz-del-Rio, V., Gonzalez, F.J. and
1828 Somoza, L. (2012) Formation processes of methane-derived authigenic carbonates from the Gulf of
1829 Cadiz. *Sedimentary Geology* 243, 155-168.
- 1830 Majumdar, U., Cook, A.E., Shedd, W. and Frye, M. (2016) The connection between natural gas
1831 hydrate and bottom-simulating reflectors. *Geophysical Research Letters* 43, 7044-7051.
- 1832 Makris, J. and Stobbe, C. (1984) Physical properties and state of the crust and upper mantle of the
1833 Eastern Mediterranean Sea deduced from geophysical data. *Marine Geology* 55, 347-363.
- 1834 Maldonado, A., Somoza, L. and Pallares, L. (1999) The Betic orogen and the Iberian-African
1835 boundary in the Gulf of Cadiz: geological evolution (central North Atlantic). *Marine Geology* 155, 9-
1836 43.
- 1837 Marín-Moreno, H., Giustiniani, M., Tinivella, U. and Pinero, E. (2016) The challenges of quantifying
1838 the carbon stored in Arctic marine gas hydrate. *Marine and Petroleum Geology* 71, 76-82.
- 1839 Marín-Moreno, H., Sahoo, S.K. and Best, A.I. (2017) Theoretical modeling insights into elastic wave
1840 attenuation mechanisms in marine sediments with pore-filling methane hydrate. *Journal of*
1841 *Geophysical Research: Solid Earth* 122, 1835-1847.
- 1842 Martinez-Garcia, P., Comas, M., Lonergan, L. and Watts, A.B. (2017) From Extension to Shortening:
1843 Tectonic Inversion Distributed in Time and Space in the Alboran Sea, Western Mediterranean.
1844 *Tectonics* 36, 2777-2805.
- 1845 Mascle, J., Mary, F., Praeg, D., Brosolo, L., Camera, L., Ceramicola, S. and Dupre, S. (2014)
1846 Distribution and geological control of mud volcanoes and other fluid/free gas seepage features in the
1847 Mediterranean Sea and nearby Gulf of Cadiz. *Geo-Mar Lett* 34, 89-110.
- 1848 Mattingsdal, R., Knies, J., Andreassen, K., Fabian, K., Husum, K., Grøsfjeld, K. and De Schepper, S.
1849 (2014) A new 6 Myr stratigraphic framework for the Atlantic–Arctic Gateway. *Quaternary Science*
1850 *Reviews* 92, 170-178.
- 1851 Mau, S., Römer, M., Torres, M.E., Bussmann, I., Pape, T., Damm, E., Geprägs, P., Wintersteller, P.,
1852 Hsu, C.W., Loher, M. and Bohrmann, G. (2017) Widespread methane seepage along the continental
1853 margin off Svalbard - from Bjørnøya to Kongsfjorden. *Scientific Reports* 7, 42997.
- 1854 Max, M.D. and Johnson, A.H. (2014) Hydrate petroleum system approach to natural gas hydrate
1855 exploration. *Petroleum Geoscience* 20, 187-199.
- 1856 Max, M.D. and Johnson, A.H. (2016) Valuation of NGH deposits, *Exploration and Production of*
1857 *Oceanic Natural Gas Hydrate* Springer, New York, pp. 157-172.
- 1858 Mazurenko, L.L., Soloviev, V.A., Belenkaya, I., Ivanov, M.K. and Pinheiro, L.M. (2002) Mud
1859 volcano gas hydrates in the Gulf of Cadiz. *Terra Nova* 14, 321-329.

- 1860 Mazzini, A., Svensen, H., Hovland, M. and Planke, S. (2006) Comparison and implications from
1861 strikingly different authigenic carbonates in a Nyegga complex pockmark, G11, Norwegian Sea.
1862 *Marine Geology* 231, 89-102.
- 1863 McGlade, C. and Ekins, P. (2015) The geographical distribution of fossil fuels unused when limiting
1864 global warming to 2° C. *Nature* 517, 187-190.
- 1865 Medialdea, T., Somoza, L., Pinheiro, L.M., Fernandez-Puga, M.C., Vázquez, J.T., León, R., Ivanov,
1866 M.K., Magalhaes, V., Diaz-del-Rio, V. and Vegas, R. (2009) Tectonics and mud volcano
1867 development in the Gulf of Cadiz. *Marine Geology* 261, 48-63.
- 1868 Merey, S. and Longinos, S.N. (2018) Does the Mediterranean Sea have potential for producing gas
1869 hydrates? *Journal of Natural Gas Science and Engineering* 55, 113-134.
- 1870 Mienert, J., Vanneste, M., Bünz, S., Andreassen, K., Haflidason, H. and Sejrup, H.P. (2005) Ocean
1871 warming and gas hydrate stability on the mid-Norwegian margin at the Storegga slide. *Marine and*
1872 *Petroleum Geology* 22, 233-244.
- 1873 Minshull, T.A. and Keddie, A. (2010) Measuring the geotherm with gas hydrate bottom-simulating
1874 reflectors: a novel approach using three-dimensional seismic data from the eastern Black Sea. *Terra*
1875 *Nova* 22, 131-136.
- 1876 Mitchell, G., Mayer, L., Bell, K.L.C., Ballard, R.D., Raineault, N.A., Roman, C., Ballard, W.B.A.,
1877 Cornwell, K., Hine, A., Shinn, E., Dimitriadis, I. and Bogdan, O. (2013) Exploration of Eratosthenes
1878 Seamount-A Continental Fragment Being Forced Down an Oceanic Trench. *Oceanography* 26, 36-41.
- 1879 Moridis, G. (2003) Numerical studies of gas production from methane hydrates. *SPE Journal* 8, 359-
1880 370.
- 1881 Mork, M.B.E. (2013) Diagenesis and quartz cement distribution of low-permeability Upper Triassic-
1882 Middle Jurassic reservoir sandstones, Longyearbyen CO₂ lab well site in Svalbard, Norway. *AAPG*
1883 *Bulletin* 97, 577-596.
- 1884 Murillas, J., Mougnot, D., Boulot, G., Comas, M.C., Banda, E. and Mauffret, A. (1990) Structure
1885 and evolution of the Galicia Interior Basin (Atlantic western Iberian continental margin).
1886 *Tectonophysics* 184, 297-319.
- 1887 Naylor, D. and Shannon, P. (2011) *Petroleum Geology of Ireland*. Dunedin Academic Press Limited,
1888 Edinburgh, UK.
- 1889 Nielsen, T. and Jokat, W. (2009) Petroleum potential in southern Fram Strait?, AAPG 3-P Arctic
1890 Conference and Exhibition. AAPG, Moscow, Russia.
- 1891 Nielsen, T., Laier, T., Kuijpers, A., Rasmussen, T.L., Mikkelsen, N.E. and Norgard-Pedersen, N.
1892 (2014) Fluid flow and methane occurrences in the Disko Bugt area offshore West Greenland:
1893 indications for gas hydrates? *Geo-Mar Lett* 34, 511-523.
- 1894 Nielsen, T., Marcusses, C., Konradi, P., Kuijpers, A. and Christiansen, F.G. (2000) Geohazard desk
1895 study offshore West Greenland - Pilot project, GEUS Report 2000/21.
- 1896 Nikishin, A.M., Korotaev, M.V., Ershov, A.V. and Brunet, M.-F. (2003) The Black Sea basin:
1897 tectonic history and Neogene-Quaternary rapid subsidence modelling. *Sedimentary Geology* 156,
1898 149-168.

- 1899 Nikishin, A.M., Okay, A.I., Tuysuz, O., Demirer, A., Amelin, N. and Petrov, E. (2015) The Black Sea
1900 basins structure and history: New model based on new deep penetration regional seismic data. Part 1:
1901 Basins structure and fill. *Marine and Petroleum Geology* 59, 638-655.
- 1902 Norwegian Petroleum Directorate (2018) Resources for the future: Seabed minerals and gas hydrates,
1903 Resource Report Exploration 2018. Norwegian Petroleum Directorate, Stavanger, Norway, pp. 67-72.
- 1904 Nøttvedt, A., Berglund, L.T., Rasmussen, E. and Steel, R.J. (1988) Some aspects of Tertiary tectonics
1905 and sedimentation along the western Barents Shelf. *Geological Society, London, Special Publications*
1906 39, 421-425.
- 1907 Nøttvedt, A., Livbjerg, F., Midbøe, P.S. and Rasmussen, E. (1993) Hydrocarbon potential of the
1908 Central Spitsbergen Basin, in: Vorren, T.O., Bergsager, E., Dahl-Stammes, Ø.A., Holter, E., Johansen,
1909 B., Lie, E., Lund, T.B. (Eds.), *Norwegian Petroleum Society Special Publications*. Elsevier, pp. 333-
1910 361.
- 1911 Oakey, G.N. and Chalmers, J.A. (2012) A new model for the Paleogene motion of Greenland relative
1912 to North America: Plate reconstructions of the Davis Strait and Nares Strait regions between Canada
1913 and Greenland. *Journal of Geophysical Research: Solid Earth* 117,
1914 B10401, doi:10.1029/2011JB008942.
- 1915 Ogata, K., Senger, K., Braathen, A., Tveranger, J. and Olausson, S. (2012) The importance of natural
1916 fractures in a tight reservoir for potential CO₂ storage: case study of the upper Triassic to middle
1917 Jurassic Kapp Toscana Group (Spitsbergen, Arctic Norway), *Geological Society of London, Special*
1918 *Publications, London, UK*, pp. 395-415.
- 1919 Ohm, S.E., Larsen, L., Olausson, S., Senger, K., Birchall, T., Demchuk, T., Hodson, A., Johansen, I.,
1920 Titlestad, G.O. and Braathen, A. (2019) Discovery of shale gas in organic rich Jurassic successions,
1921 Adventdalen, Central Spitsbergen, Norway. *Norwegian Journal of Geology* in review.
- 1922 Ostanin, I., Anka, Z., di Primio, R. and Bernal, A. (2013) Hydrocarbon plumbing systems above the
1923 Snøhvit gas field: Structural control and implications for thermogenic methane leakage in the
1924 Hammerfest Basin, SW Barents Sea. *Marine and Petroleum Geology* 43, 127-146.
- 1925 Oyama, A. and Masutani, S.M. (2017) A Review of the Methane Hydrate Program in Japan. *Energies*
1926 10, 1447, doi:10.3390/en10101447.
- 1927 Özel, O. (2012) Investigation of gas and gas hydrate accumulations in the Western Black Sea
1928 continental slope, Master thesis, The Graduate School of Natural and Applied Sciences. Dokuz Eylül
1929 University.
- 1930 Palomino, D., Lopez-Gonzalez, N., Vázquez, J.T., Fernandez-Salas, L.M., Rueda, J.L., Sanchez-Leal,
1931 R. and Diaz-del-Rio, V. (2016) Multidisciplinary study of mud volcanoes and diapirs and their
1932 relationship to seepages and bottom currents in the Gulf of Cadiz continental slope (northeastern
1933 sector). *Marine Geology* 378, 196-212.
- 1934 Panieri, G., Bünz, S., Fornari, D.J., Escartin, J., Serov, P., Jansson, P., Torres, M.E., Johnson, J.E.,
1935 Hong, W., Sauer, S., Garcia, R. and Gracias, N. (2017) An integrated view of the methane system in
1936 the pockmarks at Vestnesa Ridge, 79°N. *Marine Geology* 390, 282-300.
- 1937 Pape, T., Kasten, S., Zabel, M., Bahr, A., Abegg, F., Hohnberg, H.J. and Bohrmann, G. (2010) Gas
1938 hydrates in shallow deposits of the Amsterdam mud volcano, Anaximander Mountains, Northeastern
1939 Mediterranean Sea. *Geo-Mar Lett* 30, 187-206.

- 1940 Pedersen, G.K., Andersen, L.A., Lundsteen, E.B., Petersen, H.I., Bojesen-Koefoed, J.A. and Nytoft,
1941 H.P. (2006) Depositional environments, organic maturity and petroleum potential of the Cretaceous
1942 coal-bearing Atane Formation at Qullissat, Nuussuaq Basin, West Greenland. *Journal of Petroleum*
1943 *Geology* 29, 3-25.
- 1944 Pérez-Belzuz, F., Alonso, B. and Ercilla, G. (1997) History of mud diapirism and trigger mechanisms
1945 in the Western Alboran Sea. *Tectonophysics* 282, 399-422.
- 1946 Pérez-Gussinyé, M., Ranero, C.R., Reston, T.J. and Sawyer, D. (2003) Mechanisms of extension at
1947 nonvolcanic margins: Evidence from the Galicia interior basin, west of Iberia. *Journal of Geophysical*
1948 *Research: Solid Earth* 108, 2245, doi:2210.1029/2001JB000901.
- 1949 Pérez-Gussinyé, M. and Reston, T.J. (2001) Rheological evolution during extension at nonvolcanic
1950 rifted margins: Onset of serpentinization and development of detachments leading to continental
1951 breakup. *Journal of Geophysical Research: Solid Earth* 106, 3961-3975.
- 1952 Perissoratis, C., Ioakim, C., Alexandri, S., Woodside, J., Nomikou, P., Dahlmann, A., Casas, D.,
1953 Heeschen, K., Amman, H., Rousakis, G. and Lykousis, V. (2011) Thessaloniki Mud Volcano, the
1954 shallowest gas hydrate-bearing mud volcano in the Anaximander Mountains, eastern Mediterranean.
1955 *Journal of Geological Research*, doi:10.1155/2011/247983.
- 1956 Petersen, C.J., Bünz, S., Hustoft, S., Mienert, J. and Klaeschen, D. (2010) High-resolution P-Cable 3D
1957 seismic imaging of gas chimney structures in gas hydrated sediments of an Arctic sediment drift.
1958 *Marine and Petroleum Geology* 27, 1981-1994.
- 1959 Pinheiro, L.M., Ivanov, M.K., Sautkin, A., Akhmanov, G., Magalhaes, V.H., Volkonskaya, A.,
1960 Monteiro, J.H., Somoza, L., Gardner, J., Hamouni, N. and Cunha, M.R. (2003) Mud volcanism in the
1961 Gulf of Cadiz: results from the TTR-10 cruise. *Marine Geology* 195, 131-151.
- 1962 Pinheiro, L.M., Wilson, R.C.L., Pena dos Reis, R., Whitmarsh, R.B. and Ribeiro, A. (1996) The
1963 western Iberia margin; a geophysical and geological overview. *Proceedings of the Ocean Drilling*
1964 *Program, Scientific Results* 149, 3-23.
- 1965 Platt, J.P., Whitehouse, M.J., Kelley, S.P., Carter, A. and Hollick, L. (2003) Simultaneous extensional
1966 exhumation across the Alboran Basin: Implications for the causes of late orogenic extension. *Geology*
1967 31, 251-254.
- 1968 Plaza-Faverola, A., Bünz, S., Johnson, J.E., Chand, S., Knies, J., Mienert, J. and Franek, P. (2015)
1969 Role of tectonic stress in seepage evolution along the gas hydrate charged Vestnesa Ridge, Fram
1970 Strait. *Geophysical Research Letters* 42, 733-742.
- 1971 Plaza-Faverola, A., Bünz, S. and Mienert, J. (2011) Repeated fluid expulsion through sub-seabed
1972 chimneys offshore Norway in response to glacial cycles. *Earth and Planetary Science Letters* 305,
1973 297-308.
- 1974 Plaza-Faverola, A., Vadakkepulyambatta, S., Hong, W.L., Mienert, J., Bünz, S., Chand, S. and
1975 Greinert, J. (2017) Bottom-simulating reflector dynamics at Arctic thermogenic gas provinces: An
1976 example from Vestnesa Ridge, offshore west Svalbard. *Journal of Geophysical Research: Solid Earth*
1977 122, 4089-4105.
- 1978 Plaza-Faverola, A., Westbrook, G.K., Ker, S., Exley, R.J.K., Gailler, A., Minshull, T.A. and Broto, K.
1979 (2010) Evidence from three-dimensional seismic tomography for a substantial accumulation of gas
1980 hydrate in a fluid-escape chimney in the Nyegga pockmark field, offshore Norway. *Journal of*
1981 *Geophysical Research: Solid Earth* 115, B08104, doi:08110.01029/02009JB007078.

- 1982 Popescu, I., De Batist, M., Lericolais, G., Nouzé, H., Poort, J., Panin, N., Versteeg, W. and Gillet, H.
 1983 (2006) Multiple bottom-simulating reflections in the Black Sea: Potential proxies of past climate
 1984 conditions. *Marine Geology* 227, 163-176.
- 1985 Popescu, I., Lericolais, G., Panin, N., De Batist, M. and Gillet, H. (2007) Seismic expression of gas
 1986 and gas hydrates across the western Black Sea. *Geo-Mar Lett* 27, 173-183.
- 1987 Popescu, I., Lericolais, G., Panin, N., Wong, H.K. and Droz, L. (2001) Late Quaternary channel
 1988 avulsions on the Danube deep-sea fan, Black Sea. *Marine Geology* 179, 25-37.
- 1989 Posewang, J. and Mienert, J. (1999) The enigma of double BSRs: indicators for changes in the
 1990 hydrate stability field? *Geo-Mar Lett* 19, 157-163.
- 1991 Praeg, D., Geletti, R., Mascle, J., Unnithan, V. and Harmegnies, F. (2008) Exploration for gas
 1992 hydrates in the Mediterranean Sea and a bottom simulating reflection on the Nile Fan, GNGTS,
 1993 Trieste, Italy.
- 1994 Praeg, D., Geletti, R., Wardell, N., Unnithan, V., Mascle, J., Migeon, S. and Camerlenghi, A. (2011)
 1995 The Mediterranean Sea: a natural laboratory to study gas hydrate dynamics?, 7th International
 1996 Conference on Gas Hydrates, Edinburgh, UK.
- 1997 Praeg, D., Migeon, S., Mascle, J., Unnithan, V., Wardell, N., Geletti, R. and Ketzer, J.M. (2017)
 1998 Geophysical Evidence of Gas Hydrates Associated with Widespread Gas Venting on the Central Nile
 1999 Deep-Sea Fan, Offshore Egypt, 9th International Conference on Gas Hydrates, Denver, Colorado,
 2000 USA.
- 2001 Priest, J.A., Best, A.I. and Clayton, C.R.I. (2005) A laboratory investigation into the seismic
 2002 velocities of methane gas hydrate-bearing sand. *Journal of Geophysical Research: Solid Earth* 110,
 2003 B04102, doi:04110.01029/02004JB003259.
- 2004 Przybylak, R., Arażny, A., Nordli, Ø., Finkelnburg, R., Kejna, M., Budzik, T., Migala, K., Sikora, S.,
 2005 Puczko, D., Rymer, K. and Rachlewicz, G. (2014) Spatial distribution of air temperature on Svalbard
 2006 during 1 year with campaign measurements. *International Journal of Climatology* 34, 3702-3719.
- 2007 Rangin, C., Demirbag, E., Imren, C., Crusson, A., Le Pichon, X. and Sengor, A.M.C. (2001) Marine
 2008 atlas of the Sea of Marmara (Turkey): data collected on board R.V. le Suroit, September 2000.
 2009 Ifremer, Plouzane, France.
- 2010 Reston, T.J. (2005) Polyphase faulting during the development of the west Galicia rifted margin.
 2011 *Earth and Planetary Science Letters* 237, 561-576.
- 2012 Rey, D. and Gran Burato Science Team (2010) GB4240 Cruise Technical Report. University of Vigo,
 2013 Vigo, Spain.
- 2014 Rey, D. and Gran Burato Science Team (2011) GRAN BURATO 2011 Cruise Technical Report.
 2015 University of Vigo, Vigo, Spain.
- 2016 Ribeiro, T. (2011) Multichannel Seismic Investigation of the Gran Burato area, off W Galicia. MSc
 2017 thesis, University of Aveiro.
- 2018 Riboulot, V., Ker, S., Sultan, N., Thomas, Y., Marsset, B., Scalabrin, C., Ruffine, L., Boulart, C. and
 2019 Ion, G. (2018) Freshwater lake to salt-water sea causing widespread hydrate dissociation in the Black
 2020 Sea. *Nature Communications* 9, 117, doi:110.1038/s41467-41017-02271-z.

- 2021 Riedel, M., Spence, G.D., Chapman, N.R. and Hyndman, R.D. (2002) Seismic investigations of a vent
 2022 field associated with gas hydrates, offshore Vancouver Island. *Journal of Geophysical Research: Solid*
 2023 *Earth* 107, 2200, doi:2210.1029/2001JB000269.
- 2024 Riedel, M., Wallmann, K., Berndt, C., Pape, T., Freudenthal, T., Bergenthal, M., Bünz, S. and
 2025 Bohrmann, G. (2018) In Situ Temperature Measurements at the Svalbard Continental Margin:
 2026 Implications for Gas Hydrate Dynamics. *Geochemistry, Geophysics, Geosystems* 19, 1165-1177.
- 2027 Rise, L., Bellec, V., Chand, S. and Bøe, R. (2015) Pockmarks in the southwestern Barents Sea and
 2028 Finnmark fjords. *Norwegian Journal of Geology* 94, 163-282.
- 2029 Rise, L., Ottesen, D., Berg, K. and Lundin, E. (2005) Large-scale development of the mid-Norwegian
 2030 margin during the last 3 million years. *Marine and Petroleum Geology* 22, 33-44.
- 2031 Ritzmann, O. and Jokat, W. (2003) Crustal structure of northwestern Svalbard and the adjacent
 2032 Yermak Plateau: evidence for Oligocene detachment tectonics and non-volcanic breakup.
 2033 *Geophysical Journal International* 152, 139-159.
- 2034 Römer, M., Sahling, H., Pape, T., Ferreira, C.D., Wenzhofer, F., Boetius, A. and Bohrmann, G.
 2035 (2014) Methane fluxes and carbonate deposits at a cold seep area of the Central Nile Deep Sea Fan,
 2036 Eastern Mediterranean Sea. *Marine Geology* 347, 27-42.
- 2037 Roy, S., Marin-Moreno, H. and max, M.D. (2017) Natural Gas Hydrates and fluid flow: implications
 2038 from Irish offshore, 9th International Conference on Gas Hydrates, Denver, Colorado, USA.
- 2039 Roy, S. and Max, M. (2017) Acoustic Evidence of Fluid Flow in Ireland Offshore and Physical
 2040 Property Measurements on Methane Gas Hydrate in Sediment Cores from the Irish GHSZ, AAPG
 2041 International Conference, London, U.K.
- 2042 Roy, S. and Max, M. (2018) Assessment of Natural Gas Hydrate Petroleum System in western Irish
 2043 offshore, American Geophysical Union - Fall Meeting, Washington, D.C.
- 2044 Roy, S., Senger, K., Hovland, M. and Noormets, R. (2012) Gas Hydrate formation potential in the
 2045 fjords of Svalbard, Arctic Frontiers Conference-Energies of the High North, Tromsø, Norway.
- 2046 Roy, S., Senger, K., Hovland, M., Römer, M. and Braathen, A. (2019) Geological controls on shallow
 2047 gas distribution and seafloor seepage in an Arctic fjord of Spitsbergen, Norway. *Marine and*
 2048 *Petroleum Geology* 107, 237-254.
- 2049 Rubin-Blum, M., Antler, G., Turchyn, A.V., Tsadok, R., Goodman-Tchernov, B.N., Shemesh, E.,
 2050 Austin, J.A., Coleman, D.F., Makovsky, Y., Sivan, O. and Tchernov, D. (2014) Hydrocarbon- related
 2051 microbial processes in the deep sediments of the Eastern Mediterranean Levantine Basin. *Fems*
 2052 *Microbiology Ecology* 87, 780-796.
- 2053 Ruffine, L., Donval, J.P., Croguennec, C., Bignon, L., Birot, D., Battani, A., Bayon, G., Caprais, J.C.,
 2054 Lanteri, N., Levache, D. and Dupre, S. (2017) Gas Seepage along the Edge of the Aquitaine Shelf
 2055 (France): Origin and Local Fluxes. *Geofluids* 2017, doi:10.1155/2017/4240818.
- 2056 Ruppel, C.D. and Kessler, J.D. (2017) The interaction of climate change and methane hydrates.
 2057 *Reviews of Geophysics* 55, 126-168.
- 2058 Ryan, W.B.F., Pitman Iii, W.C., Major, C.O., Shimkus, K., Moskalenko, V., Jones, G.A., Dimitrov,
 2059 P., Gorür, N., Sakiñç, M. and Yüce, H. (1997) An abrupt drowning of the Black Sea shelf. *Marine*
 2060 *Geology* 138, 119-126.

- 2061 Santamarina, J.C., Dai, S., Terzariol, M., Jang, J., Waite, W.F., Winters, W.J., Nagao, J., Yoneda, J.,
2062 Konno, Y., Fujii, T. and Suzuki, K. (2015) Hydro-bio-geomechanical properties of hydrate-bearing
2063 sediments from Nankai Trough. *Marine and Petroleum Geology* 66, 434-450.
- 2064 Saritas, H. (2013) Mapping and exploration of gas and possibly gas hydrate accumulation in Western
2065 High, Sea of Marmara in light of 2D-3D high resolution seismic data, Masters thesis, Institute of
2066 Marine Sciences and Technology. Dokuz Eylul University.
- 2067 Saritaş, H., Çifçi, G., Géli, L., Thomas, Y., Marsset, B., Henry, P., Grall, C. and Rochat, A. (2018)
2068 Gas occurrence and shallow conduit systems in the Western Sea of Marmara: a review and new
2069 acoustic evidence. *Geo-Mar Lett* 38, 385-402.
- 2070 Sarkar, S., Berndt, C., Minshull, T.A., Westbrook, G.K., Klaeschen, D., Masson, D.G., Chabert, A.
2071 and Thatcher, K.E. (2012) Seismic evidence for shallow gas-escape features associated with a
2072 retreating gas hydrate zone offshore west Svalbard. *Journal of Geophysical Research* 117, B09102,
2073 doi:09110.01029/02011JB009126.
- 2074 Sassen, R. and MacDonald, I.R. (1994) Evidence of structure H hydrate, Gulf of Mexico continental
2075 slope. *Organic Geochemistry* 22, 1029-1032.
- 2076 Senger, K., Betlem, P., Liira, M., Roy, S., Midttømme, K., Wheeler, W., Beka, T., Olausen, S. and
2077 Ohm, S. (2017) Integrated thermo-baric modelling of the gas hydrate stability zone onshore Svalbard,
2078 Arctic Norway, 9th International Conference on Gas Hydrates, Denver, USA.
- 2079 Senger, K., Brugmans, P., Grundvåg, S.-A., Jochmann, M., Nøttvedt, A., Olausen, S., Skotte, A. and
2080 Smyrak-Sikora, A. (2019) Petroleum, coal and research drilling onshore Svalbard: a historical
2081 perspective. *Norwegian Journal of Geology* 99, in press.
- 2082 Senger, K., Bünz, S. and Mienert, J. (2010) First-Order Estimation of In-Place Gas Resources at the
2083 Nyegga Gas Hydrate Prospect, Norwegian Sea. *Energies* 3, 2001-2026.
- 2084 Serov, P., Vadakkepuliymbatta, S., Mienert, J., Patton, H., Portnov, A., Silyakova, A., Panieri, G.,
2085 Carroll, M.L., Carroll, J., Andreassen, K. and Hubbard, A. (2017) Postglacial response of Arctic
2086 Ocean gas hydrates to climatic amelioration. *Proceedings of the National Academy of Sciences* 114,
2087 6215-6220.
- 2088 Shannon, P.M., Moore, J.G., Jacob, A.W.B. and Makris, J. (1993) Cretaceous and Tertiary basin
2089 development west of Ireland. *Geological Society, London, Petroleum Geology Conference series* 4,
2090 1057-1066.
- 2091 Shillington, D.J., White, N., Minshull, T.A., Edwards, G.R.H., Jones, S., Edwards, R.A. and Scott,
2092 C.L. (2008) Cenozoic evolution of the eastern Black Sea: a test of depth-dependent stretching models.
2093 *Earth and Planetary Science Letters* 265, 360-378.
- 2094 Singhroha, S., Chand, S. and Buenz, S. (2019) Constraints on gas hydrate distribution and
2095 morphology in Vestnesa Ridge, western Svalbard margin, using multicomponent ocean-bottom
2096 seismic data. *Journal of Geophysical Research: Solid Earth* 124, 4343-4364.
- 2097 Sloan, E.D. and Koh, C.A. (2008) *Clathrate Hydrates of Natural Gases*, Third Edition. CRC Press-
2098 Taylor & Francis Group, Boca Raton, Florida.
- 2099 Smith, A.J., Mienert, J., Bünz, S. and Greinert, J. (2014) Thermogenic methane injection via bubble
2100 transport into the upper Arctic Ocean from the hydrate-charged Vestnesa Ridge, Svalbard.
2101 *Geochemistry, Geophysics, Geosystems* 15, 1945-1959.

- 2102 Smith, W.H.F. and Sandwell, D.T. (1997) Global Sea Floor Topography from Satellite Altimetry and
2103 Ship Depth Soundings. *Science* 277, 1956-1962.
- 2104 Somoza, L., Diaz-del-Rio, V., León, R., Ivanov, M., Fernandez-Puga, M.C., Gardner, J.M.,
2105 Hernandez-Molina, F.J., Pinheiro, L.M., Rodero, J., Lobato, A., Maestro, A., Vazquez, J.T.,
2106 Medialdea, T. and Fernandez-Salas, L.M. (2003) Seabed morphology and hydrocarbon seepage in the
2107 Gulf of Cadiz mud volcano area: Acoustic imagery, multibeam and ultra-high resolution seismic data.
2108 *Marine Geology* 195, 153-176.
- 2109 Somoza, L., Ercilla, G., Urgorri, V., León, R., Medialdea, T., Paredes, M., Gonzalez, F.J. and
2110 Nombela, M.A. (2014) Detection and mapping of cold-water coral mounds and living *Lophelia* reefs
2111 in the Galicia Bank, Atlantic NW Iberia margin. *Marine Geology* 349, 73-90.
- 2112 Somoza, L., Medialdea, T., León, R., Ercilla, G., Vázquez, J.T., Farran, M.L., Hernandez-Molina, J.,
2113 Gonzalez, J., Juan, C. and Fernandez-Puga, M.C. (2012) Structure of mud volcano systems and
2114 pockmarks in the region of the Ceuta Contourite Depositional System (Western Alboran Sea). *Marine*
2115 *Geology* 332, 4-26.
- 2116 Song, Y.C., Yang, L., Zhao, J.F., Liu, W.G., Yang, M.J., Li, Y.H., Liu, Y. and Li, Q.P. (2014) The
2117 status of natural gas hydrate research in China: A review. *Renewable & Sustainable Energy Reviews*
2118 31, 778-791.
- 2119 Sorlien, C.C., Akhun, S.D., Seeber, L., Steckler, M.S., Shillington, D.J., Kurt, H., Cifci, G., Poyraz,
2120 D.T., Gurcay, S., Dondurur, D., Imren, C., Perincek, E., Okay, S., Kucuk, H.M. and Diebold, J.B.
2121 (2012) Uniform basin growth over the last 500 ka, North Anatolian Fault, Marmara Sea, Turkey.
2122 *Tectonophysics* 518, 1-16.
- 2123 Spangenberg, E. and Kulenkampff, J. (2006) Influence of methane hydrate content on electrical
2124 sediment properties. *Geophysical Research Letters* 33, L24315, doi:24310.21029/22006GL028188.
- 2125 Stadnitskaia, A., Ivanov, M.K., Blinova, V., Kreulen, R. and van Weering, T.C.E. (2006) Molecular
2126 and carbon isotopic variability of hydrocarbon gases from mud volcanoes in the Gulf of Cadiz, NE
2127 Atlantic. *Marine and Petroleum Geology* 23, 281-296.
- 2128 Stoffers, P., Degens, E.T. and Trimonis, E.S. (1978) Stratigraphy and suggested ages of Black Sea
2129 sediments cored during Leg 42B. *Initial Reports of the Deep Sea Drilling Project* 42, 483-487.
- 2130 Stuevold, L.M. and Eldholm, O. (1996) Cenozoic uplift of Fennoscandia inferred from a study of the
2131 mid-Norwegian margin. *Global and Planetary Change* 12, 359-386.
- 2132 Tayber, Z., Meilijson, A., Ben-Avraham, Z. and Makovsky, Y. (2019) Methane Hydrate Stability and
2133 Potential Resource in the Levant Basin, Southeastern Mediterranean Sea. *Geosciences* 9, 306.
- 2134 Thomas, Y., Marsset, B., Westbrook, G.K., Grail, C., Géli, L., Henry, R., Çifçi, G., Rochat, A. and
2135 Saritas, H. (2012) Contribution of high-resolution 3D seismic near-seafloor imaging to reservoir-scale
2136 studies: Application to the active North Anatolian Fault, Sea of Marmara. *Near Surface Geophysics*
2137 10, 291-301.
- 2138 Toyos, M.H., Medialdea, T., León, R., Somoza, L., Gonzalez, F.J. and Melendez, N. (2016) Evidence
2139 of episodic long-lived eruptions in the Yuma, Ginsburg, JesA(0)s Baraza and Tasyo mud volcanoes,
2140 Gulf of Cadiz. *Geo-Mar Lett* 36, 197-214.
- 2141 Uchida, S., Soga, K. and Yamamoto, K. (2012) Critical state soil constitutive model for methane
2142 hydrate soil. *Journal of Geophysical Research* 117, B03209, doi:03210.01029/02011JB008661,.

- 2143 Unnithan, V., Shannon, P.M., McGrane, K., Readman, P.W., Jacob, A.W.B., Keary, R. and Kenyon,
2144 N.H. (2001) Slope instability and sediment redistribution in the Rockall Trough: constraints from
2145 GLORIA. Geological Society, London, Special Publications 188, 439-454.
- 2146 Vadakkepuliambatta, S., Bünz, S., Mienert, J. and Chand, S. (2013) Distribution of subsurface fluid-
2147 flow systems in the SW Barents Sea. *Marine and Petroleum Geology* 43, 208-221.
- 2148 Vadakkepuliambatta, S., Chand, S. and Bünz, S. (2017) The history and future trends of ocean
2149 warming-induced gas hydrate dissociation in the SW Barents Sea. *Geophysical Research Letters* 44,
2150 835-844.
- 2151 Vadakkepuliambatta, S., Hornbach, M.J., Bünz, S. and Phrampus, B.J. (2015) Controls on gas
2152 hydrate system evolution in a region of active fluid flow in the SW Barents Sea. *Marine and*
2153 *Petroleum Geology* 66, 861-872.
- 2154 Van Rensbergen, P., Depreiter, D., Pannemans, B., Moerkerke, G., Van Rooij, D., Marsset, B.,
2155 Akhmanov, G., Blinova, V., Ivanov, M., Rachidi, M., Magalhaes, V., Pinheiro, L., Cunha, M. and
2156 Henriët, J.P. (2005a) The El arraiche mud volcano field at the Moroccan Atlantic slope, Gulf of
2157 Cadiz. *Marine Geology* 219, 1-17.
- 2158 Van Rensbergen, P., Rabaute, A., Colpaert, A., Ghislain, T.S., Mathijs, M. and Bruggeman, A.
2159 (2005b) Fluid migration and fluid seepage in the Connemara Field, Porcupine Basin interpreted from
2160 industrial 3D seismic and well data combined with high-resolution site survey data. *International*
2161 *Journal of Earth Sciences* 96, 185-197.
- 2162 Vanneste, M., Guidard, S. and Mienert, J. (2005) Bottom-simulating reflections and geothermal
2163 gradients across the western Svalbard margin. *Terra Nova* 17, 510-516.
- 2164 Vassilev, A. and Dimitrov, L. (2002) Spatial and quantity evaluation of the Black Sea gas hydrates.
2165 *Russian Geology and Geophysics* 43, 672-684.
- 2166 Vaular, E.N., Barth, T. and Haflidason, H. (2010) The geochemical characteristics of the hydrate-
2167 bound gases from the Nyegga pockmark field, Norwegian Sea. *Organic Geochemistry* 41, 437-444.
- 2168 Vázquez, J.T., Medialdea, T., Ercilla, G., Somoza, L., Estrada, F., Puga, M.C.F., Gallart, J., Gracia,
2169 E., Maestro, A. and Sayago, M. (2008) Cenozoic deformational structures on the Galicia Bank Region
2170 (NW Iberian continental margin). *Marine Geology* 249, 128-149.
- 2171 Vorren, T.O. and Laberg, J.S. (1997) Trough mouth fans — palaeoclimate and ice-sheet monitors.
2172 *Quaternary Science Reviews* 16, 865-881.
- 2173 Vorren, T.O., Laberg, J.S., Blaume, F., Dowdeswell, J.A., Kenyon, N.H., Mienert, J., Rumohr, J.A.N.
2174 and Werner, F. (1998) The Norwegian-Greenland Sea Continental Margins: Morphology and Late
2175 Quaternary Sedimentary Processes and Environment. *Quaternary Science Reviews* 17, 273-302.
- 2176 Vorren, T.O., Richardsen, G., Knutsen, S.M. and Henriksen, E. (1991) Cenozoic erosion and
2177 sedimentation in the western Barents Sea. *Marine and Petroleum Geology* 8, 317-340.
- 2178 Waghorn, K.A., Bünz, S., Plaza-Faverola, A. and Johnson, J.E. (2018) 3D Seismic Investigation of a
2179 Gas Hydrate and Fluid Flow System on an Active Mid-Ocean Ridge; Svyatogor Ridge, Fram Strait.
2180 *Geochemistry, Geophysics, Geosystems* 19, 2325-2341.
- 2181 Wallmann, K., Pinero, E., Burwicz, E., Haeckel, M., Hensen, C., Dale, A. and Rüpke, L. (2012) The
2182 Global Inventory of Methane Hydrate in Marine Sediments: A Theoretical Approach. *Energies* 5,
2183 2449-2498.

- 2184 Wallmann, K., Riedel, M., Hong, W.L., Patton, H., Hubbard, A., Pape, T., Hsu, C.W., Schmidt, C.,
2185 Johnson, J.E., Torres, M.E., Andreassen, K., Berndt, C. and Bohrmann, G. (2018) Gas hydrate
2186 dissociation off Svalbard induced by isostatic rebound rather than global warming. *Nature*
2187 *Communications* 83, doi:10.1038/s41467-017-02550-9, 9.
- 2188 Weitemeyer, K.A., Constable, S.C., Key, K.W. and Behrens, J.P. (2006) First results from a marine
2189 controlled-source electromagnetic survey to detect gas hydrates offshore Oregon. *Geophysical*
2190 *Research Letters* 33, L03304, doi:03310.01029/02005GL024896.
- 2191 Westbrook, G.K., Chand, S., Rossi, G., Long, C., Bünz, S., Camerlenghi, A., Carcione, J.M., Dean,
2192 S., Foucher, J.P., Flueh, E., Gei, D., Haacke, R.R., Madrussani, G., Mienert, J., Minshull, T.A.,
2193 Nouzé, H., Peacock, S., Reston, T.J., Vanneste, M. and Zillmer, M. (2008) Estimation of gas hydrate
2194 concentration from multi-component seismic data at sites on the continental margins of NW Svalbard
2195 and the Storegga region of Norway. *Marine and Petroleum Geology* 25, 744-758.
- 2196 Westbrook, G.K., Thatcher, K.E., Rohling, E.J., Piotrowski, A.M., Palike, H., Osborne, A.H., Nisbet,
2197 E.G., Minshull, T.A., Lanoiselle, M., James, R.H., Huhnerbach, V., Green, D., Fisher, R.E., Crocker,
2198 A.J., Chabert, A., Bolton, C., Beszczynska-Moller, A., Berndt, C. and Aquilina, A. (2009) Escape of
2199 methane gas from the seabed along the West Spitsbergen continental margin. *Geophysical Research*
2200 *Letters* 36, L15608, doi:15610.11029/12009GL039191.
- 2201 Wilson, R.C.L., Hiscott, R.N., Willis, M.G. and Gradstein, F.M. (1989) The Lusitanian Basin of
2202 West-Central Portugal: Mesozoic and Tertiary Tectonic, Stratigraphic, and Subsidence History, in:
2203 Tankard, A.J., Balkwill, H.R. (Eds.), *Extensional Tectonics and Stratigraphy of the North Atlantic*
2204 *Margins*. American Association of Petroleum Geologists, pp. 341-361.
- 2205 Winguth, C., Wong, H.K., Panin, N., Dinu, C., Georgescu, P., Ungureanu, G., Krugliakov, V.V. and
2206 Podshuveit, V. (2000) Upper Quaternary water level history and sedimentation in the northwestern
2207 Black Sea. *Marine Geology* 167, 127-146.
- 2208 Woodside, J.M., Ivanov, M.K. and Limonov, A.F. (1997) Neotectonics and fluid flow through the
2209 seafloor sediments in the Eastern Mediterranean and Black Seas. Part I: eastern Mediterranean Sea,
2210 IOC Technical Series, pp. 1-128.
- 2211 Worsley, D. (2008) The post-Caledonian development of Svalbard and the western Barents Sea. *Polar*
2212 *Res* 27, 298-317.
- 2213 Yefremova, A.G. and Zhizchenko, B.P. (1974) Occurrence of crystal hydrates of gases in the
2214 sediments of modern marine basins. *Akademii Nauk SSSR* 214, 1179-1181.
- 2215 Zander, T., Haeckel, M., Berndt, C., Chi, W.-C., Klaucke, I., Bialas, J., Klaeschen, D., Koch, S. and
2216 Atgin, O. (2017) On the origin of multiple BSRs in the Danube deep-sea fan, Black Sea. *Earth and*
2217 *Planetary Science Letters* 462, 15-25.
- 2218 Zavatarelli, M. and Mellor, G.L. (1995) A numerical study of the Mediterranean Sea circulation.
2219 *Journal of Physical Oceanography* 25, 1384-1414.
- 2220 Zillmer, M., Flueh, E.R. and Petersen, J. (2005) Seismic investigation of a bottom simulating reflector
2221 and quantification of gas hydrate in the Black Sea. *Geophysical Journal International* 161, 662-678.
- 2222 Zitter, T.A.C., Huguen, C. and Woodside, J.M. (2005) Geology of mud volcanoes in the eastern
2223 Mediterranean from combined sidescan sonar and submersible surveys. *Deep-Sea Research Part I-*
2224 *Oceanographic Research Papers* 52, 457-475.

- 2225 Zonenshain, L.P. and Le Pichon, X. (1986) Deep Basins of the Black Sea and Caspian Sea as
2226 Remnants of Mesozoic Back-Arc Basins. *Tectonophysics* 123, 181-211.
- 2227